The Alpha Particle X-Ray Spectrometer (APXS): Results from Gusev Crater and Calibration Report.

R. Gellert[1,2], R. Rieder[1], J. Brückner[1], B. Clark[3], G. Dreibus[1], G. Klingelhöfer[4], G. Lugmair[1], D. Ming[5], H. Wänke[1], A. Yen[6], J. Zipfel[1], and S. Squyres[7]

[1] Max-Planck-Institut für Chemie, Postfach 3060, D-55020 Mainz, Germany, brueckner@mpch-mainz.mpg.de
[2] Department of Physics, University of Guelph, N1G2W1 Guelph, On, Canada
[3] Lockheed Martin Corporation, Littleton, Colorado, USA
[4] Institut für Inorganische & Analytische Chemie, Johannes Gutenberg-Universität, D-55099 Mainz, Germany
[5] NASA Johnson Space Center, Houston, Texas, USA
[6] Jet Propulsion Laboratory, Pasadena, California, USA
[7] Center for Radiophysics and Space Research, Cornell University, Ithaca, New York, USA

Abstract

The chemical composition of rocks and soils on Mars analyzed during the Mars Exploration Rover Spirit Mission was determined by X-ray analyses with the Alpha Particle X-Ray Spectrometer (APXS). Details of the data analysis method and the instrument calibration are presented. Measurements performed on Mars to address geometry effects and background contributions are shown. Cross calibration measurements among several instrument sensors and sources are discussed. An unintentional swap of the two flight instruments is evaluated. New concentration data acquired during the first 470 sols of rover Spirit in Gusev Crater are presented. There are two geological regions, the Gusev plains and the Columbia Hills. The plains contain soils that are very similar to previous landing sites on Mars. A meteoritic component in the soil is identified. Rocks in the plains revealed thin weathering rinds. The underlying abraded rock was classified as primitive basalt. One of these rocks contained significant Br that is probably associated with vein-filling material of different composition. One of the trenches showed large subsurface enrichments of Mg, S, and Br. Disturbed soils and rocks in the Columbia Hills revealed different elemental compositions. These rocks are significantly weathered and enriched in mobile elements, such as P, S, Cl, or Br. Even abraded rock surfaces have high Br concentrations. Thus, in contrast to the rocks and soils in the Gusev Plains, the Columbia Hills material shows more significant evidence of ancient aqueous alteration.

Introduction

The Alpha Particle X-ray Spectrometer (APXS) is part of the Athena instrument suite carried on both Mars Exploration Rovers (MER) [*Squyres et al.,* 2003]. It determines the chemical composition of rocks and soils by x-ray spectroscopy. Since their successful landing in January of 2004 both rovers have performed extremely well. Each rover drove several kilometers, which allowed investigation of many targets of interest along the traverse with the instrument suite mounted on the IDD (Instrument Deployment Device). A total of nearly 100 APXS measurements were taken in Gusev crater during the first 470 sols of operation. The objectives of this paper are to 1) present the methods used to calibrate the APXS, including cross calibration of flight and laboratory instruments and 2) describe the APXS results obtained during the first 470 soils of Spirit's traverse in Gusev crater.

We have previously shown that rocks around Spirit's landing site are primitive basalts [*Gellert et al.,* 2004, *McSween et al.,* 2004]. The Rock Abrasion Tool (RAT) has enhanced the analyses of rocks because it removed dust and weathered surfaces of rocks to expose "fresh" rock surfaces by grinding operations. The ability of the RAT to mechanically brush and abrade a surface in several steps has revealed one or several layers of alteration rinds on these rocks [*McSween at al*., 2004; *Haskin et al*., 2005]. The combined data enable deciphering of potential elemental correlations that reveal probably formed weathered products, as inferred from minerals.

Instrument description

The Alpha Particle X-ray Spectrometer (APXS) is an x-ray spectrometer using radioactive Curium-244 sources for x-ray excitation [*Rieder et al.,* 2003]. It consists of a sensor head mounted on the IDD and main electronics located in the Warm Electronics Box (WEB) of the rover's body. Figure 1 shows schematics of the sensor head. A picture of the sensor head mounted on the IDD is presented in Figure 2.

The sensor head is brought into contact with the sample whose surface is bombarded with energetic alpha particles and x-ray radiation. The x-ray detector, located inside the sensor head, registers the emitted x-rays, which are accumulated in a histogram, i.e. x-ray energy spectrum. Each element present has peaks at characteristic energies. Element abundances are derived from the peak areas. The emission of x-rays by both incident x-rays and alpha particles are combined in this instrument from two well-known excitation mechanisms: x-ray fluorescence (XRF) and particle induced x-ray emission (PIXE). This combination of excitation modes results in good sensitivities for the elements ranging from sodium (atomic mass = 23) up to bromine (atomic mass = 79.9).

Compared to an earlier generation of APXS that flew on the Mars Pathfinder mission [*Rieder et al.,* 1997] important improvements were made. Especially the new room-temperature x-ray detector [*Rieder et al.,* 2003] of the MER APXS provided better energy resolution and higher sensitivity. At low temperatures (i.e. nighttime temperatures) the energy resolution on both MER APXS was typically ~160 eV at the 6.4-keV Kα line of iron compared to the energy resolution of 250 eV of the Pathfinder APXS. This improved energy resolution minimizes peak overlaps and allows low Z element peaks to be resolved (Figure 3). An increase in sensitivity by

a factor of approximately 20 was obtained mainly due to geometrical changes in the assembly of the sensor head [see *Rieder et al.,* 2003, for details].

The main electronics located in the WEB is connected with the sensor head through a 4 meter long cable that is fed through the IDD. The main electronics contains the main amplifier for the detector signals and the analog to digital converter. The non-volatile 32 Kbyte RAM allows storage of 12 spectra. During data acquisition the internal APXS firmware records consecutive spectra according to the preset integration time intervals. The APXS Central Processing Unit (CPU) collects and stores the spectra and handles the communication with the rover CPU. The APXS command set includes commands that start, stop and transmit the data to the rover CPU. Other commands allow adjusting instrument parameters like temperature-dependent gain and integration time intervals for individual spectra.

In addition to the x-ray detector, the APXS also contains alpha detectors to record backscattered alpha particles. This alpha mode is similar to Rutherford Back Scattering (RBS). It is mainly sensitive to low Z elements like carbon and oxygen. However, under martian conditions the sensitivity is limited by the CO_2 atmosphere that interferes with signals stemming from the same elements in the sample. Thus, compared to the Pathfinder APXS, the MER source-sample geometry was optimized for the x-ray channel. Also, the source was covered with a 3 μm thin Ti foil to retain sputtered fragments resulting from the alpha decay of curium. Using these Ti foils, a significant advantage for the calibration work of the MER APXS compared to the Pathfinder APXS was achieved as the risk of sample contamination by sputtering was completely eliminated. The disadvantage of the MER APXS design for the alpha mode was that the Ti foils lowered the primary alpha energy below a (α,α) resonance of carbon. The sensitivity for carbon detection decreased significantly compared to the Pathfinder APXS as a result of the foils. The

different source-sample geometry of the MER APXS design also reduced the detection sensitivity of oxygen and the other high-Z elements in the alpha mode compared to the Pathfinder APXS. In addition, uncertainties in source-sample distances cannot be as easily taken into account as for the x-ray mode since backscattered alpha spectra are very angle dependent. Given these issues, the data obtained from the alpha channel has not yet been fully evaluated. An alpha mode optimized instrument would have provided oxygen contents (and a detection limit for C) as demonstrated for the Pathfinder data [Foley at al., 2003]. However, the improvements of the MER x-ray mode compared to the Pathfinder x-ray mode mostly compensated the deficiency of C and O detection.

Operation of the APXS on Mars

The application of the APXS on Mars is constrained by available power and operation time. For the in-situ instruments mounted on the IDD, an additional limitation is the ability to deploy the IDD since gears and motors can only be operated at temperatures above -55 °C. IDD deployments were limited to operational scenarios with complete image coverage (i.e., front hazard avoidance images) of the working volume in front and below the rover chassis. These images had to be transmitted to earth and assessed for any hazards (e.g., rocks) before deploying the arm.

Early in the mission the usual operational scenario was to deploy the Mössbauer Spectrometer (MB) in order to sense the target by using its contact plate; the MB touch was typically done in the afternoon. Usually at around 4:00 AM the rover would ‘wake up’ for communication with Earth at which time the IDD heaters were turned on to enable IDD movement for a tool change from MB to APXS. Autonomous APXS integration was started

before the rover was allowed to 'fall asleep' again. APXS acquisition lasted about 4 hours until rover 'wake up' for daily activities in the morning. Later in the mission the decrease in available power and the decay of the MB radioactive source made it necessary to extend IDD campaigns to at least 2 sols. IDD tool changes at night were eliminated due to engineering constraints. The APXS was placed on the desired target near the end of the afternoon operations and not turned on until the morning communication pass at around 4:00 AM as described above. Complete overnight APXS integrations (i.e., turned on late in the afternoon and integrated until rover wake up the next morning) were conducted only when sufficient power was available or significant improvement of statistics was needed for trace element determination.

The instrument performance during martian night was found to be comparable to spectra taken in the laboratory at temperatures below -40 ºC. But soon after landing, it was discovered that the IDD signal cable degenerated the APXS signal performance at higher temperatures. This is caused by a very high capacity against ground of the shielded IDD cable, a parameter unknown at time of instrument design and delivery. This capacitance added a significant filter element in the signal path that decreased the steepness of the detector signals. Since the filter times of the main amplifiers were hard wired, they could not be adapted prior to launch. At low temperatures, the signals from the detector were steep enough to be properly shaped by the electronics as tests prior to launch revealed. The signal heights were approximately 5 % lower compared to ground support setup, as the signal timing was slightly misaligned. Therefore, the low energy side of the 1.04 keV Na peak was partly cut off without affecting the fit of the spectral background. The truncated Na peak area was taken into account in the data analysis.

The impact of the IDD cable at higher temperatures led to procedures where the APXS was mainly operated during the night, when the temperatures were below -40 °C. Short

acquisitions of 15 to 30 minutes or so called “Touch and Go (T&G)” measurements during the martian day were performed early in the morning prior to driving only if the operational scenario did not allow the rover to remain at a sample of interest for a complete sol (i.e., overnight). This strategy (i.e., T&G) was used for systematic soil measurements along the traverse on the plains towards the Columbia Hills. Such short measurements produced APXS spectra with degraded energy resolution and limited counting statistics. Despite the lower quality, these spectra provided vital information about major elements, e.g., Ca, Fe and S, and their relative proportions to Si. Several times, T&G spectra were also acquired in order to evaluate whether longer night integrations were necessary to acquire better statistics. Comparing spectra of T&G measurements with their corresponding night integrations proved the value of the T&G datasets. But there are limitations of the T&G measurements. In particular, typically major element peaks of T&G and long nighttime measurements overlap within error bars, while minor elements can show large enough errors that they fall statistically within their detection limit.

A further operational constraint of T&G measurements is the rather late wakeup time (and therefore increased ambient temperature) of the rover, since the rover CPU needs approximately 40 Watts for operation and solar power is not sufficiently available in early morning hours. Therefore, APXS integrations that occurred after 10:00 AM (i.e., temperatures > -40 °C) lead to spectra of degraded quality. All spectra stored in the internal memory of the APXS are transmitted to Earth, where data are screened by the acting APXS operator. Only those spectra with good energy resolution are used for final data reduction.

Data analysis procedure

Analysis of the APXS raw data obtained from Mars is performed in several steps. First, the raw data from the APXS memory (RAM) have to be assessed with respect to successful deployment and health of the instrument. In rare cases, the data acquisition was not successful due to an IDD fault, a failed door opening, or a sequencing error. Here, a fast request to the Science Operation Working Group (SOWG) for a repeat of the data acquisition was required.

The transmitted raw data are a mirror of the 32 Kbyte APXS memory. Besides the scientific data, a section with engineering information and a logbook of received commands are accessible. The science data consist of 12 separate spectra (either only new spectra or a mixture of new and old ones) including a temperature record measured every 30 seconds during acquisition. Each spectrum has a unique identification number, which allows discarding old spectra obtained during the preceding acquisition. Spectra showing a peak broadening due to higher temperatures can be discarded before summing all high-quality spectra for a specific target. Also, individual spectra with good energy resolution might show a small peak position drift due to imperfect temperature compensation of the overall gain. Such a drift can easily be corrected by adjusting each spectrum to a common gain. Typically, a drift below half a percent was found in a temperature range from -85 to -40 °C.

Summed spectra with good energy resolution are fed into a non-linear least squares fit computer routine. The fitting model used was developed during instrument calibration and is described in detail below. The main results of the fitting procedure are peak areas of the characteristic element lines. In the subsequent analysis routine, peak areas are converted into element and then into oxide concentrations using look-up calibration tables for each instrument. This step assumes a water and carbon free sample matrix. The sum of the oxides, also referred to

as geometric norm, is a relative indicator for the unknown distance of the sensor head to the sample surface. Re-normalizing the oxide sum to 100 % compensates for the distance and allows correcting for distance dependent elemental background contributions.

The matrix correction described below is applied in an iterative procedure. First the average matrix of all calibration samples is assumed. Each new matrix is calculated iteratively until the composition converges. The final output of the analysis routine consists of elemental concentrations in weight percent and their 2-sigma statistical error. These errors are derived from the peak area errors, which do not include calibration uncertainties. Therefore, the statistical errors given with the concentrations represent the precision and not the accuracy of the data analysis.

Individual spectra were analyzed in addition to the sum of the spectra for a specific target. These spectra allow to judge repeatability and statistical significance of the full analysis. The assessment of individual spectra includes any temporary effects on the quality of the measurements, like electronic noise, impact of sun light on leakage currents, or temperature shifts. Also, the reliability of the statistical errors was checked using single spectra of the same sample.

Calibration

The calibration of the flight sensors consists of two parts. First, the method has to be calibrated. The abundance of the identified element is hereby correlated with the peak area. This step includes a deconvolution procedure of the characteristic peaks from the spectrum. The peak fit procedure includes the determination of the detector properties such as energy calibration, peak form, and full-width-at-half-maximum (FWHM). These parameters are fitted parameters,

which are used to retrieve the peak areas. This method calibration is done in the laboratory with a given instrument. Therefore, in a second step the influence of the individual setup and instrument has to be taken into account. Properties that influence the measurements are the energy dependent detector efficiency, the source strength, the measurement geometry, and the radiation environment. These properties have to be accounted for to retrieve the results for a given setup. This second step is called cross calibration.

Peak Fit Analysis

Although commercial peak fit programs are available for XRF and PIXE spectra, a special fit routine was developed to extract the elemental peak areas from an APXS spectrum. This step was made to tailor the theoretical fitting model to the APXS measuring method. Background contributions, escape peaks, and scatter peaks were investigated and included in the analyses.

The non-linear least-squares fit program is based on the minimization routine of MINUIT [*James and Ross,* 1989]. A typical result from the deconvolution of a spectrum obtained on Mars is shown in Figure 3 and shows all components that are used to fit the spectra. Spectral components are described below and examples are provided for the spectrum in Figure 3.

- Element peaks from sodium up to bromine with up to five satellite peaks per element: Except for iron all Kα to Kβ ratios were determined with the corresponding oxide sample and fixed. For iron the Kα and Kβ lines have high count rates and don't overlap with other elements, except for Co, which is a trace element. The main elements are labeled in Figure 3. The peaks are assumed to be of Gaussian shape, whereby the data points are calculated using the error function to improve the fit of the peak shape. The

low-energy sides of the peaks have an exponential tailing, best visible at the Fe peak at 6.4 keV. The tailing is a known effect in x-ray spectroscopy caused by incomplete charge collection in the detector. The ratio of the tailing area to the Gaussian part of the peak area is very low but it has to be taken into account for the correct fit of overlapping peaks, such as the manganese peak adjacent to the iron peak.

- Elastic and inelastic scatter peaks of the primary plutonium x-ray radiation: The elastic peaks (E1 and E2 in Figure 3) are the Lα and Lβ lines of Pu in the energy range of our detector. They are assumed to have the same Gaussian peak shape like elemental peaks. The inelastic scatter peaks (I1, I2 and I3) are fitted with a model similar to that of *Van Gysel et al.,* [2003]. It assumes two different peak shape parameters on the lower and the higher energy side.
- The spectrometer response: The Energy resolution and calibration is fitted with four parameters: FWHM (0), F, E0, k, where FWHM (0) is the full-width-at-half-maximum (energy resolution) at channel zero, F contains the Fano factor, E0 is the energy at channel zero, and k is energy per channel.

$$FWHM(E) = \sqrt{FWHM^2(0) + F \cdot E} \quad \text{and} \quad E = E0 + k * channel \qquad (1)$$

An additional parameter takes into account the energy dependence of the exponential tailing (parameter not shown in the above formula). The tailing was found to increase with energy. This characteristic was determined with oxide standards. Each peak has an assigned escape peak, for example the Fe-escape peak that nearly overlaps with the Ti peak.

- Spectral background: The shape of the background consists of a step function that rises behind every elemental K-shell edge energy. Background is produced by Compton

scattering in the sample and the detector. This step function background is marked with **1** in Figure 3 for the elements Fe, Ca and Si. A constant background, marked with **0** completes the background. An additional background arises at lower energies starting at approximately 2 keV. It is marked with **2** in Figure 3 and will be described later in the discussion on background.

The energies for the elemental peaks are taken from Thompson et al., [2001]. The energy range from potassium to bromine have discrete Kα1 and Kα2 lines with an intensity ratio of 2 to 1 that are taken for the model spectra. The peak area used for the calibration is the sum of these main Kα lines. The linearity of the energy scale in the lab as well as on Mars was checked with the χ^2 (chi squared) residual of the fit since any deviations of the linearity show a big effect in the χ^2. The largest deviations were found for Ca. Instead of the published value of 3.692 keV a peak position of 3.697 keV was derived for the Kα1 line. This small deviation seems to be an overlap with backscattered Pu M lines rather than a non-linearity of the energy scale. Published values were used for all other elements.

The spectrum is fitted between a lower and an upper energy limit. The lower limit was taken as 1.020 keV, which cuts off a portion of the Na peak. This is taken into account as the peak area is determined by the theoretical peak form, which is not limited by the assumed lower threshold. Thus, as long as the main position of the peak is within the energy range, the cut of the Na peak only limits the statistics and does not influence the peak area.

The excellent peak to background ratio of this type of x-ray detector reveals a statistical problem during the fit procedure. The very high counts in peaks like silicon or iron cause the minimization routine to overemphasize the top of these peaks. This can have negative effects on

the tailing of the peaks. Therefore, the statistics of the measured peaks are limited artificially to 1% in the fit routine. This especially influences the calibration spectra, which were measured with extremely high statistics.

The fit routine was tested with various spectra obtained from the laboratory and from Mars. It was found that the degraded Touch & Go spectra taken at elevated temperatures can be fitted very well with the model. The tailing parameter as well as the energy dependent FWHM can be used to model the degraded spectra very well. This was tested on many samples using the full data set from the same sample for comparison. The model was tailored to retrieve the best possible fit with a minimum number of free parameters.

Method Calibration

The APXS method calibration was performed after launch with a bread board similar to the flight instruments. The term "method calibration" is used because it comprises all physical processes that make up the APXS method. It includes the excitation with alpha particles and x-rays as well as the resulting matrix effects.

All calibration work was carried out in a martian simulation chamber, where the sensor head was cooled to temperatures below -40 ºC and the atmospheric pressure could be regulated between several tens of mbar of CO_2 gas or a vacuum below 0.01 mbar. Approximately 100 different samples were used for calibration that included certified powdered geological samples and various chemical compounds. A list of samples can be found in the on-line support material. This work substantially extended the initial calibration of the actual flight instruments as reported in [*Rieder et al*., 2003]. The flight assemblies of main electronics, ground support cable, sensor head, and source were calibrated with a set of 11 certified powdered samples as

well as a limited set of chemical compounds. Prior to flight instrument integration on the rovers, this set of data was assumed to be the basic main library for the calibration. However, an augmentation of the calibration work by using a duplicate instrument was required, particularly because 'new' elements like bromine were identified on Mars that had not been taken into account during initial calibration. All calibrations were performed under standardized environmental conditions, which included the distance between sensor and sample, atmospheric pressure, and operation temperature. All deviations of this APXS method calibration setup (instrument, source, environment) can be taken into account by the cross calibration.

The APXS method calibration correlates the peak areas with the certified elemental abundance of the samples. This procedure is commonly used in the lab for methods like XRF or PIXE. However, on Earth special precautions are taken in sample preparation to obtain a homogeneous sample. For XRF the powdered sample is homogenized and diluted by melting it into a borated glass pellet. These measures were not considered feasible for the APXS calibration since powdered samples are much more similar to samples expected on Mars, where sample preparation is limited. Most laboratory samples were ground to grain sizes of less than 50 µm and filled into a shallow depression of a sample holder. The sample material was assumed to be homogeneous within a sample diameter of about 2.5 cm and to a depth of more than 1 mm.

All calibration spectra were analyzed to retrieve the peak areas of the identified elements. The following formula was used to correlate the peak area with the elemental abundance for every element and every calibration sample.

$$CPS = offset + const \cdot response \cdot Weight + (1 - const) \cdot response \cdot Weight \cdot \frac{\mu mean}{\mu} \qquad (2)$$

Where *CPS*: counts per second of the main elemental peak

Offset: parameter that indicates a background offset

Const: parameter that allows the influence of the cross section

Response: peak area per weight percent of the element

Weight: fractional concentration of element in sample

μ*mean:* average attenuation cross section for the characteristic x-ray line averaged over all used samples

μ: calculated attenuation cross section of the characteristic elemental x-ray line for the sample

A lower limit of abundance was adopted for some elements; abundances below this limit were not used for the calibration. Some samples that were used for the initial calibration were discarded from the final calibration as they produced data that deviated largely from the derived mean response. Those samples were mostly meteorites that provided extraterrestrial material but turned out to have a rather inhomogeneous matrix for the purpose of APXS calibration.

For all elements the above formula is fitted in the beginning with the three free parameters: *offset*, *const*, and *response*. The resulting matrix is used to calculate the attenuation cross section for the excitation and emission of radiation for each element. These values are calculated on the basis of the results of the calibration.

The rational for this calibration approach is the following: For XRF it is well known that self absorption takes place. The source radiation has to penetrate the sample and the excited radiation is attenuated on its path to the sample surface. This provides a dependence of the resulting peak area on the sample composition that is usually called matrix effect.

The parameter *const* in the formula allows the high Z element spectra that are mainly obtained due to the XRF mode to be corrected for this matrix effect. For low Z elements this approach does not have to work per se, as here the excitation is made with the alpha particles and not with x-ray radiation. The fitted parameter *const* shows that the best results for low Z elements are obtained by a mixture of cross section correction and no correction. For higher Z the parameter *const* decreases to lower values indicating an XRF type of matrix effect.

The results for the APXS method calibration are given in Table 1. The retrieved parameters for the calibration table are given together with information about the typical accuracy and lowest concentration used for all elements.

There are two approaches to improve the calibration accuracy. First, the physics of the excitation and absorption process could be described in a more detailed model. Work done by *Omand et al.* [2005] applied a combination of PIXE and XRF excitation and radiation absorption using their existing computer routine GUPIX, developed for PIXE, and combined it with a newly developed XRF excitation routine. Computations by *Omand et al.* [2005] used the concentrations of a set of certified samples that we also used for our calibration in the laboratory. Their response of each element calculated with a theoretically proper model showed similar values as our simple approach (formula 2). Large deviations of some samples do not result from an erroneous model; rather, they could result from the heterogeneity of the sample matrix.

A second way to increase the accuracy of the calibration is to directly take into account the heterogeneity of the sample. Although the samples we used are powdered, the mineral grains might still be larger than the penetration depth of the low-energy radiation. This means that the matrix should not be assumed as an ‘infinitely fine’ powder, but rather as an assemblage of

macroscopically large mineral grains. Corrections for the radiation attenuation should therefore use the composition of the single mineral grains and not the average composition of the bulk sample. The surface of the sample could be composed of a mixture of different mineral grains with different areal coverage. This work is currently in progress and might yield better accuracy for certain samples used in the calibration. An obvious problem of this approach is that assumptions have to be made on the mineral composition (and areal coverage) or additional information on the mineralogical composition is needed.

Simulations by *Omand et al.* [2005] indicate that for low Z elements up to silicon their spectral yields versus concentrations better fit a parabolic than a linear curve. Nevertheless, the linear approach is maintained in our model since it offers the big advantage that the response can be continuously compared from sodium to bromine.

In the beginning of the calibration fit, all parameters for all elements can change freely. A non-zero offset indicates either a background contribution or a problem with the linear response approach. In the laboratory significant positive background offsets were identified for phosphorus, potassium and titanium (all Kα-lines). For phosphorus the background is caused by the Zr L-line of the x-ray detector's zirconium collimator, which can be directly absorbed by the detector. Titanium foils covering the curium sources are excited by the emitted radiation of the Cm source. This Ti radiation is elastically backscattered by the sample surface into the detector. The K background is generated by a similar process from the Pu M lines of the Cm source. Potassium and Ti backgrounds therefore depend on the distance to the sample (in contrast to the P background). The approach for these elements was to scale the elemental background with the geometric norm of the spectrum. The element background was determined at standard geometry, which corresponds to 100 % norm, and in atmospheric calibration measurements (0 % norm).

This approach was tested with a distance dependent measurement on Mars and seems to be appropriate (see below).

Copper and zirconium K-line peaks are also detected in the spectra. Their contributions are inferred to be background from the instrument because non-sample facing (sky-facing) measurements reveal their presence. Since their background signals are higher than the ones from expected concentrations in geologic samples they mask the detection of possible low concentrations in the martian samples. On Mars, the Zr K-line peak is below the upper energy threshold and, therefore, the K to L ratio could be determined in atmospheric measurements. Compared to the laboratory, the Zr K line is increased by a factor of ~ 3. This is likely due to the additional MB radiation. The determined K to L ratio assures the correct compensation of the P background. In contrast, the Cu signal does not interfere with the measurement of any element.

For all other elements the offset can also be non-zero without obvious reason. Especially for Si this offset represents a non-linear response that is clearly visible where the response is parabolic.

Figure 4 shows the result of the newly refined calibration compared to previous calibration curve [*Rieder et al.,* 2003]. The main differences are found for chlorine and bromine. Very few certified geological standards were available for both elements during the initial calibration. For chlorine, the previous calibration already showed a non-systematic increase of the Cl response value. The refined Cl calibration was obtained by using a newly available standard, MAG-1, and some additional chlorine salts. The new response value increases the concentration of chlorine by 40 % compared to previously reported results. As a good sign of improvement, the new Cl response value matches much better the Z systematic in the region between sulfur and potassium (Figure 4).

For bromine, a refined response curve was obtained by discarding certain previously used chemical compounds because their attenuation cross sections exceeded by a factor of 4 those of normal geological samples. The refinement resulted in a ~15 % lower concentration in martian samples.

The uncertainties in Cl and Br seem to be an indicator for the influence of microscopic heterogeneity on the calibration result. Both elements form salts without oxygen. Therefore the averaging influence of oxygen in the grains is missing. Because of these uncertainties the accuracy in table 1 is marked with a star. All other elements show only minor changes of a few percent compared to the calibration published earlier.

Cross Calibration

Figure 5 shows an overview of the various hardware configurations that were used for cross calibration. The instruments used are the flight modules FM1 and FM2 and the laboratory bread board BB10 with their corresponding sources S1, S2 and S10. The comparison of measurements carried out with the different configurations will clearly show that an unintentional swap of the two flight modules happened during a rework prior to their delivery to the flight rovers before launch. The source holder that contains the curium pellets is easily attached to the sensor head with a spring loaded bayonet mechanism. The source holder was removed for rework of the sensor heads. Because the swap of the flight modules was not initially recognized, the measurements using configurations E and G, see Figure 5, were done with crossed sources compared to the original calibration. Unfortunately, this swap was not recognized immediately because both sensor heads do not have any visual differences. The electrical interfaces, amplification gain and other properties are almost identical. The only difference is the small

variation in the thickness of the beryllium window that seals the x-ray detector. The different attenuation of x-rays in the windows mainly affects the peak heights of the low Z elements Na and Mg in the spectra. Even the usage of the built-in calibration target located on the backside of the protective doors, a gold covered copper-beryllium surface, did not reveal the small difference in window thickness. The ratio of the low energy gold M line at 2.1 keV to the L lines at about 10 keV is too small to be diagnostic as the 2-keV line is already rather penetrating.

An initial sign for the possibility of an unintended swap was the homogeneity of the martian soil on each landing site along the traverse. Nevertheless, there were characteristic differences between the soil of Gusev and Meridiani that could be easily explained by a swap of the instruments.

Peak areas of all elements contained in the same samples were determined for a cross calibration of the different configurations. The influence of the instrument response, such as peak shape, energy resolution, gain, and background, can be neglected, because the fitting routine determines these parameters during the deconvolution procedure and the calculated peak areas are independent of these parameters. One important parameter of the instrument response is the attenuation of x-rays by the beryllium window that seals the x-ray detector. Since these windows have small differences in their thicknesses, the attenuation of low Z elements with their low x-ray energies is a strong function of the window thickness.

Measurements that were carried out in a certain configuration will be labeled with the corresponding letter in the following discussion (Figure 5). The ratio of these measurements proved that the two flight instruments had been swapped during integration into the rovers. Measurements E and G shown in Figure 5 were taken with swapped sources and then compared to the previous calibration measurements D and F. The ratios E/D and F/G as illustrated in

Figure 6 clearly show that in both cases the instruments have been swapped from D to E and F to G by showing the effect of a thicker detector window of FM2 for low-Z elements: the ratios decrease from one with decreasing Z below Cl.

Final proof that a swap occurred is illustrated in Figure 7, which shows that the influence of different sources is small compared to that of different instruments. The ratio E/F has large error bars as it is based only on one measurement that had to be corrected for vacuum conditions. The ratio D/G has smaller error bars as it is based on three measurements. The sources S1 and S2 are comparable in strength. Sodium measurements taken with S1 decrease by 10 %. It is unlikely that the source had an influence on the ratio. The alpha spectra of both sources S1 and S2 showed a similar energy spectrum. Source 1 emitted alpha particles with a slightly higher energy as their titanium foils were somewhat thinner compared to those of S2. Therefore, it is unlikely that Na is enhanced when excited with S2. The deviation of the response in Na appears to have been caused by some factor other than the source. A factor that may have caused the difference in Na content is a different CO2 -pressure in both setups. For example, Figure 8 shows the ratio of long term measurements carried out with S1 and S10. There is no significant deviation from a horizontal line, except for very low-Z elements, indicating that the excitations of both sources are equivalent.

The PIXE mode results from excitation with alpha particles while the XRF mode is due to excitation with x-rays. Energetic alpha particles have a much shorter emission depth out of the source compared to x-rays from plutonium. If the curium depth distribution inside the source is not homogeneous, there should be variations of the XRF part to the PIXE part of the spectrum. Variations in the silicon to iron ratios were not observed for different sources, as both elements

are excited by different modes. The influence of individual sources was neglected in this work because of these observations.

The cross calibration of the bread board 10 to the flight sensors is shown in Figure 9, which shows the ratio of the peak areas measured with the bread board and the flight instruments. The curve has three distinct energy regions that are influenced by different properties of the instrument. The thickness of the beryllium window provides a different absorption of the lower Z elements for energies below 3 keV. Both flight instruments have thicker windows than the bread board. For energies higher than 6 keV, the detector efficiency decreases as the detector thickness is no longer sufficient for complete absorption of x-rays. The detector thickness is lower for both flight instruments compared to the bread board (about 5 percent). The absolute count rate is defined by the area size of each detector. The 'active' area for FM1 is 5 % lower than FM2 and the bread board.

Measurements of peak area ratios that define the curves in Figure 9 were used for cross calibration of the calibration method and the flight instrument calibration on Mars. Whenever measured data points in Figure 9 resulted from strong background contributions or insufficient counting statistics, these data points were omitted from the fitting and replaced by interpolation of adjacent data points. The 'smoothed' peak area ratios were used to transform the peak areas measured on Mars into comparable peak areas measured with bread board BB10, which was calibrated extensively.

Geometry Effects

Data acquired by the APXS on Mars showed that the positioning of the APXS sensor head with the IDD had a large standoff uncertainty for soil samples (i.e., distance from the

surface of the soil target), whereas the reproducibility on the spot itself was excellent (i.e., x-y positioning of the IDD). The APXS contact ring requires a solid rock sample to trigger contact and hence, cannot be triggered on a soil target. Therefore, the contact ring of the MB was used as an IDD reference point to sense contact with soils and the APXS was positioned to the target based upon the MB touch. Larger unintentional standoffs of the APXS seemed to have occurred early in the mission; however, the distance of placement of the APXS from a target became more certain due to experience gained by the rover planners as the mission progressed. Larger standoff distances for the APXS were also experienced for targets that occurred at the bottom of a 'deep' RAT hole. The MB and APXS contact plates would come into contact with the sides of the RAT hole and hence, the APXS would be positioned a larger distance away from the target compared to a flat surface target. The data reduction program calculates the sum of all oxides using the calibration table. Calibration was performed in the laboratory at a distance of 2 mm between the contact ring of the APXS and the surface of the sample. This distance was chosen to prevent physical cross contamination of powered samples between targets. The sum of all the oxides - assumed to be free of any x-ray invisible components, such as water or carbon – is called geometric norm, which is provided in the results table for each measurement. A sum less than 100 percent indicates a larger APXS standoff distance to the sample assuming lack of volatile elements. To quantify the influence of the standoff, measurements at different distances from the target surface were done in the simulation chamber. A similar experiment was conducted on the Spirit rover at Gusev. The rock dubbed 'Temples Dwarf' in the Columbia Hills was measured four times with standoff distances of 3.1, 6.1, 11.5, and 16.5 mm. This experiment was designed to determine the influence of sample-detector distance on background corrections and the effects of the APXS geometry on calibration.

The influence of the sample-detector distance on the results was evaluated with the assumption that the target was a homogeneous rock surface. Figure 10 shows the elemental concentrations for different standoffs normalized to the results obtained with 3.1 mm standoff distance. No significant effect of distance was observed on the derived chemical composition of 'Temples Dwarf', even for elements that have interference from background signals, such as P, K, and Ti. Phosphorus concentrations are well corrected, in spite of the interference of Zr L-lines, which make up about 10 % of the phosphorus peak. The interferences at Ti and K result from backscattered x-rays by the sample surface and are therefore distance dependent. The approach to scale the interfering background with the geometric norm works well. The K and Ti results vary within 10 % for different distances. Nevertheless, their uncertainties increased, especially for samples with a low content of one of these elements.

The various measurements on the rock 'Temples Dwarf' were also used to compare the defined APXS standoff distances on Mars with the geometry calibration performed in the laboratory. In addition, we also examined the attenuation of lower Z elements by increased atmospheric thickness for measurements made at larger standoff distances. Figure 11 shows the comparison of the laboratory calibration with the measurements on Mars. In the laboratory one of our standard samples, named SSK, was measured at various distances in 10 mbar CO_2. The peak areas for Na, Al, Si, and Ca were normalized to those taken at standard geometry of 2 mm in 10 mbar CO_2. Magnesium was not in this calibration because SSK has a low Mg content that would result in very large error bars. For elements above Al, peak areas are independent of the distance within a couple of percent. Sodium decreases by approximately 10 % at larger distances, which can be explained by the attenuation of the thicker atmosphere. The attenuation of Na was not observed in the 'Temples Dwarf' results.

Data Acquisition on Mars

Systematic measurements were made before launch with the intent of understanding the additional background induced by the high intensity Mössbauer gamma-ray source. Figure 12 shows a comparison of spectra taken with the same instrument (FM1) on Mars and during calibration. The Mössbauer induced background was doubled compared to measurements without the MB, which is in good agreement with tests in the laboratory. Reduction of the MB background was achieved by positioning tantalum plates in the radiation path between both instruments. Without any shielding the MB induced background was higher by a factor of ten. On Mars, such a high background would have significantly decreased the sensitivity for minor elements.

Spectra taken on Mars show the same energy resolution as observed in the laboratory. However, the high capacitance of the IDD signal cable decreased the overall gain by approx. 5 %. This shifts the Zr K-line below the upper energy threshold.

Periodically, the instrument was checked on Mars for background and possible contamination by looking into the atmosphere with open doors (Figure 13). Long measurements show small peaks of Ni, Au, and Pb, elements contained in the instrument hardware. These backgrounds are corrected during the fitting process (e.g. the Ni background would correspond to about 40 ppm). In addition, the Zr K to L ratio can be determined. At energies below 2 keV a broad structure is visible in the atmosphere spectra. It was modeled and added to the background components used for fitting the spectra.

The height of the MB background depends on the source strength of the radioactive Co-57 sources, which have a half-life of 271 days. It can be estimated by observing the spectra

recorded throughout the duration of the mission. Figure 14 shows the Zr peak areas as function of time (sol). These data were used to remove the interfering Zr L-lines on the P K-line by using the Zr L to K ratio (see above). The Zr peak is excited by the MB source as well as by the APXS source itself. Furthermore, whenever a measurement was taken in a soil trench, the Zr peak area was higher by a factor of about two because of backscattered high energy radiation from the trench walls. Based on a Zr response of about 2 cps per weight percent, a Zr detection limit of about 500 ppm can be derived.

Discussion

Samples

Compositional data acquired by the APXS have characterized a wide variety of samples found on the martian surface, e.g., soil surfaces and trenches to undisturbed and abraded (RAT grind) surfaces of rocks and outcrops. Here, we provide a brief overview of the compositional results of the APXS measurements. Further aspects of rock and soil compositions obtained by APXS and other instruments are discussed in greater detail in this volume [*McSween et al., Ming et al., Morris et al., Wang et al, Hurowitz et al.,* this issue].

The mobility of rover Spirit allowed in-situ studies of rocks and soils over a larger area on Mars than has been previously done. Within the first 160 sols of the mission, the rover Spirit explored the surroundings of the Columbia Memorial Station (landing site), drove over Gusev plains while passing several impact craters (e.g., Bonneville Crater) and finally reached the Columbia Hills. For the last approximately 310 sols, the rover has investigated samples in the Columbia Hills. Names have been assigned to geographic features, soils, and rocks by the Athena Science Team for planning and operations purposes. They are not formally recognized by the International Astronomical Union.

Samples measured by the APXS can be generally classified as soils or rocks. The term soil is used here to denote any loose, unconsolidated material that can be distinguished from rocks, bedrock or strongly cohesive sediments. No implication of the presence or absence of organic materials or living matter is intended.

To specify the samples in table 2 they are labeled with an acronym as described in the following. ‘Soil’ is subdivided into ‘soil undisturbed (SU)’, ‘soil disturbed (SD)’, and ‘soil trenched (ST)’. Undisturbed soil is a target location at the surface that was never touched or disturbed by the rover wheels. Disturbed soil was usually a spot on the wheel tracks, where the

top most soil layer (about 1 mm) was more or less removed or mixed with subsurface material. Trenches were deliberately dug by rover wheel motion sequences resulting in depressions several centimeters in depth (usually 5 to 10 cm). Rocks are subdivided into 'rock as is' or undisturbed rock (RU), which means a natural surface that may be variably covered with airborne soil, 'rock brushed (RB)', which is a surface, where the brushes of the RAT removed any loose material, and 'rock abraded (RR)', where the RAT ground a circular borehole of several millimeters depth (typically 3 to 10 mm), which provided access to subsurface material. In cases where the rock was abraded in several steps the samples are noted with RR1 and RR2. In one instance a pile of the abraded fines was chosen as a sample. These RAT fines are marked as RF in table 2.

Three basaltic rocks, 'Adirondack', 'Humphrey', and 'Mazatzal', were analyzed in the first 100 sols of the mission. Concentrations of S and Cl are high in their undisturbed rock surfaces (1.3 - 3.1 wt.-% S and 0.4 - 1.1 wt.-% Cl), and even their abraded surfaces contain some S and Cl; i.e., ~ 0.5 wt.-% S and ~ 0.3 wt.-% Cl. These values are high for basaltic rocks and suggest that the surfaces were contaminated by debris left behind by the RAT brushes during the grinding operation or that S and Cl are present in this material as the result of aqueous alteration. Since all three abraded surfaces are rather vertical in orientation, the likelihood for similarly high contamination appears to be small.

For the Mars Pathfinder mission, a similar Cl content was found for the derived soil-free rock composition of Ares Vallis [Brückner et al., 2003, Foley et al., 2003b]. Most of the Pathfinder rocks appeared to be weathered basalts because they are inferred to contain some mineral-bound water, above the level which is expected in basalt [Foley et al., 2003b]. This conclusion was derived from the alpha mode of the Pathfinder APXS that revealed excess amounts of oxygen in some samples [Foley et al., 2003b].

Basaltic Shergottites (martian meteorites) contain up to 0.3 wt.-% S but only <0.013 % Cl [*Dreibus*, priv. com.]. Therefore, although the measured concentrations of S in abraded Gusev basalts may be considered as intrinsic values, the higher Cl could indicate the presence of trace amounts of salts. In general, the concentration patterns of all elements of the three primitive basalts at Gusev are very similar with exception for K and Br, which are higher in 'Mazatzal'. Based on this observation and the assumption that these materials are rather 'clean' basaltic rocks, the composition of other rocks was normalized using rock 'Humphrey RAT2'.

Undisturbed Soils

Undisturbed soil surfaces were measured occasionally along the rover traverse from the Columbia Memorial Station up into the Columbia Hills. Most soil surfaces have similar chemical compositions. Undisturbed soils on the plains of Gusev crater have enrichments in P, S, Cl, K, Ti, Ni, and Zn and depletions in Mg, Cr, Mn, and Fe when normalized to typical Gusev plains basalts such as the rock 'Humphrey' (Figure 15). Larger compositional variations are observed for several undisturbed soil surfaces in the Columbia Hills (Figure 16). A soil target dubbed 'Crumble', deviates more from the Gusev plains soils by having larger compositional variations in P, S, Ti, Cr, Ni, and Zn, and have higher Al/Si and lower Fe/Si ratios. Lithic fragments observed in the 'Crumble' soil target indicate that this soil that is a mixture of local rock and windblown soil.

The Mg/Si ratio of almost all soils is very constant. For undisturbed soils the mean ratio was 0.24 ± 0.01 wt.-% and 0.25 ± 0.02 wt.-% for disturbed surfaces with exception of two disturbed soil targets called 'Paso Robles' and 'Paso Robles Light', which are described below and by *Ming et al.* (this issue). Higher Mg/Si ratios of 0.31 and 0.34 due to higher fractions of

Mg-salts were measured in the floor ('The Boroughs Mills') and wall ('The Boroughs Hells Kitchen') of the soil trench ('The Boroughs'), respectively, as discussed later.

The mean Fe/Mn weight percent ratio of all undisturbed soils is 50 ± 3, The mean Fe/Mn ratio of basaltic Gusev rocks is 46 ± 3 indicating that the source material for the soil has not had Fe and Mn substantially altered by oxidation-reduction weathering processes. Furthermore, this ratio matches the Fe/Mn ratio for the estimated Mars mantle composition by *Wänke and. Dreibus* (1988) confirming that during magmatic processes FeO was not fractionated from MnO.

An additional sign of soil composition homogeneity is the nearly constant Cl/S ratio of 0.28 (Figure 17), except for one trench on the Gusev plains and soils in the disturbed soil measurements in the Paso Robles area. Elemental variations for undisturbed soil surfaces are small except for the trace elements Ni, Zn, and Br, where variations by a factor of two and more have been observed. Global dust storms and local dust devils could be effective soil homogenization processes that have occurred over millions of years [e.g., *Gellert et al.,* 2004].

Furthermore, P concentrations of undisturbed soils have a well defined mean value of 0.36 ± 0.02 wt.-%, which is also observed for many disturbed soil samples (Figure 18). As the small error of the mean P concentration of undisturbed soils indicates, P is an element with a very small overall compositional variation along the rover's traverse. Assuming that most P is hosted in the Ca-phosphate minerals, the easy dissolution of these phosphates from rocks in weak acidic water but also the sorption of dissolved Ca-phosphates by rocks could be the reason for an even distribution on a once wet martian surface [*Dreibus et al*., 1996, *Dreibus and Haubold*, 2004]. Only one undisturbed soil, Crumble that exhibited a lot of lithic fragments had a higher P concentration of 0.6 wt.-%, which likely resulted from the composition of the fragments.

Disturbed Soils

Several disturbed soils show only small composition variations when normalized to the undisturbed soil 'Gusev Soil' near the landing site (sol 14), see Figure 19. This soil was selected for normalization because its APXS integration time was longer compared to other undisturbed soils and hence, its counting statistics were very good.

The largest concentration variations are revealed by two nearby soil locations in the Columbia Hills: Paso Robles and Paso Light (Figure 20). These disturbed soil targets had a S content that was nearly 5 times higher compared to the 'Gusev Soil' (sol 14); however, most elements were lower in Paso Robles except for P, Ca, Fe and Br (Figure 20). The concentrations of S in the Paso Robles soils are up to 12.7 wt.-%, which are even higher than those of the 'dirty' evaporite outcrops in Meridiani Planum [*Rieder et al.*, 2004]. The high S content of Paso Light is accompanied by a high Fe content (Figure 21), consistent with the identification of ferric sulfate as the main iron-bearing mineral by the MB spectrometer [*Morris et al.*, this issue].

The highest P abundance of 2.4 wt.-% was observed in Paso Robles disturbed soil, in contrast to the average concentration of about 0.36 wt.-% for undisturbed soil surfaces. Similarly, the Br concentrations of about 500 ppm of the two Paso Robles soil measurements are remarkably high. Based on these high S, P, and Br concentrations, these elements appear to have been transported by water to this area and then concentrated by evaporative processes (see *Ming et al*., this issue, for more details).

Soil Trenches

Trenches are artificial depressions excavated by the rover wheels. They have a depth of several centimeters (e.g. up to 10 cm) providing unique subsurface samples for analyses by the Athena science instruments. Only three trenches have been excavated by the rover wheels at the times of this writing. Usually, the top-most undisturbed soil close to the trench was measured first; then measurements were made on either one or two floor targets and/or one wall target within the trench. The subtle and apparent differences in elemental compositions are shown in Figures 22 and 23 where the elemental compositions are normalized to the composition of the Gusev Soil target (sol 14). Measurements of the 'Road Cut' Trench (sols 47 to 50), which is located within a depression called 'Laguna Hollow', consisted of surface, floor, and wall targets. Their chemical compositions are very similar, except for floor and wall measurements, where Cr and Br are enriched over the surface measurement (i.e., 'Grande Flats') and the measurement of the Gusev Soil target.

Measurements of 'Big Hole' trench (sols 113 to 115), which was located about 600 meters southeast of 'Bonneville' crater and between 'Missoula' and 'Lahontan' craters, consisted of one undisturbed surface target and two floor targets. The first substantial enrichments of S, Cl, Cr, and Br were discovered in the materials analyzed on the trench floor; K and P contents were depleted in the trench floor materials.

The third trench, which was called 'The Boroughs', is located about two thirds of the way from Bonneville Crater to the Columbia Hills. Surface, floor, and wall targets were measured on sols 135 to 141. The most striking feature was the higher content of S and Br in the wall target compared to floor and surface targets (Figure 23), while all three Cl measurements are lower than the Cl content of the Gusev Soil target. The composition of the other elements is very

similar for the wall and floor targets and the undisturbed soil surface. The wall target revealed the highest S content measured up to sol 141 (i.e., 14 wt.-% SO_3). Here, correlated increase of Mg and S and an enrichment of Br have occurred in a several centimeters thick subsurface layer that points to salts probably deposited by ground water [*Haskin et al.,* 2005]. This discovery of a subsurface layer enriched in salts provides strong evidence that water activity had once occurred in Gusev Crater.

Based on orbital imaging Gusev is a flat-floored crater of Noachian age. Its southern rim is breached by Ma'adim Vallis, a very large and long valley. Assuming the valley was cut by running water, Gusev would have acted as a settling pool [*Golombek et al*., 2003]. Traces of water based on data from APXS and MB point to water events of an unknown epoch, probably not to the Noachian flooding.

To estimate which elements are correlated with the large amounts of SO_3 observed in the subsurface samples of The Boroughs trench, the bulk compositions of all three trench samples were converted into mol. %. To consider the oxidation state of iron the measured Fe^{3+}/Fe_{total} ratios by MB were used [*Morris et al.,* this issue]. We assumed that all SO_3 occurred as $MgSO_4$ and all Cl as $MgCl_2$ in the soil surface. The leftover MgO, which was not bound to S and Cl, resided in silicates. The higher contents of S in the floor and wall targets diluted the amount of silicates. Based on these diluted SiO_2 contents, the corresponding amounts of MgO were taken for the silicates. The excess MgO content was attributed to $MgSO_4$, which only accounted for 70 % of the measured SO_3 content. For the remaining 30 % SO_3, we assumed ferric sulfates as a suitable compound, based on MB data of the (np-Ox) component that is associated with Fe^{3+} sulfates [*Morris et al.,* this issue]. Three to 4 mol. % of $Fe_2(SO_4)_3$ could be

estimated for the wall and floor targets of The Boroughs trench. Figure 24 shows the good correlation of the calculated amounts of MgO with SO_3 in the three trench samples.

The three trenches could trigger the notion that starting with the Laguna Hollow trench near the landing site the amount of subsurface S content was increasing while approaching the Columbia Hills. However, since the number of trenches was very small, no definitive conclusion on the spatial distribution of subsurface material can be drawn: the increase of S content could be simply coincidental.

Rock Undisturbed Surface

APXS measurements of rocks were usually first done on the undisturbed, natural surface (also called 'as is'). Based on the ubiquitous airborne dust, the natural surfaces of rocks are more or less covered with this fine material. Whenever possible, vertical surfaces were selected for IDD measurements, but adhering air-borne dust cannot be excluded. The relative concentrations of undisturbed soils normalized to rock 'Humphrey RAT2' show an M shaped pattern for the elements from Si to Ca (Figure 15). A similar pattern can be seen for natural rocks (Figure 25) suggesting that rock surfaces are 'coated' with soil. However, rocks in the Columbia Hills reveal a skewed M shaped pattern, which indicates that either their soil coverage is less or their composition is much different than Humphrey (Figure 26 to 31). The abundance of Br seems to be randomly distributed in rocks and soils. However, the highest Br contents were observed on natural and brushed surface of some rocks (up to sol 470). It has been speculated that the very soluble Br precipitates as salts at some rock surfaces under current local weather conditions in Gusev crater [*Yen et al.,* 2005].

Brushed Rocks

Brushing of the rock surfaces by the RAT removes some of the adhering soil and exposes an underlying layer, which may be different from both the natural surface and the subsurface abraded by a RAT grind operation. Gusev plains rocks exhibited the familiar M-shaped enrichment pattern of elements from Si to Ca as described above; this enrichment pattern suggests that some soil is adhering to the brushed surface. The brushed surface of the rock dubbed 'Mazatzal' has an enrichment of Ni, Zn, and Br, a hint for Br salts on rock surfaces. Mazatzal's brushed surface looks black in Pancam color images, while the underlying abraded basalt layer is grayish and the top natural surface is bright pink-reddish [*Bell et al.,* this issue]. Here we encountered a complex weathering history at the rocks' surface, possibly creating multiple layers of either adhering materials and/or weathering rinds [*Gellert et al.,* 2004, Haskin et al., 2005].

Brushed rocks in the Columbia Hills show a different enrichment pattern compared to the plains basalts (Figure 27). In West Spur, a group of rocks (Clovis, Ebenezer, Uchben, and Lutefisk) are enriched in S, Cl, K, Ti, Ni, and Br.

Driving further up into the hills, P on most brushed surfaces is enriched by up to a factor of 5. Exceptions to this typical P enrichment is a peculiar rock called Ben's Clod', which is enriched up to 9 times in P and the outcrops called 'Peace' and 'Alligator' that had much lower P with no enrichments compared to Humphrey basalt.

For some rocks, only brushed surface analyses are available, such as 'Lutefisk', 'Alligator', and 'Methuselah'. Lutefisk belongs to the very high-Cl West Spur Clovis class (the rock classification mainly results from the abraded rock chemistry, see below). 'Alligator' has a high-S and high-Ni brushed surface. 'Methuselah', which is part of the outcrop on the

Cumberland Ridge, belongs to high-P, high-K, high-Ti rocks; and has low Ni and nearly no Cr in the brushed surface measurement. Interestingly, the brushed outcrop 'Watchtower' has a very similar enrichment pattern as brushed Methuselah (Figure 28), suggesting that both are part of an extended outcrop of similar material; however, they are located at opposite ends of the outcrop on Cumberland Ridge.

Abraded Rocks

The RAT is a valuable tool, which can remove several millimeters of thick layers depending on the hardness of the rock and hence, provide a surface that may best represent the composition of its interior. Inside the borehole either the fresh rock or a weathered layer is exposed. Combining elemental compositions of the natural, brushed, and abraded rock surface can provide information on possible materials adhering to the surface, the presence of an alteration or weathering rind, and the interior composition.

Rocks analyzed at different places can be grouped based on their chemistry. There are two major regions the rover Spirit passed through: Plains and Columbia Hills.

The three rocks, 'Adirondack', 'Humphrey', and 'Mazatzal', that were located in the area around the Columbia Memorial Station and at the rim of crater 'Bonneville' were classified as primitive basalts [*Gellert et al.,* 2004; *McSween et al.,* 2004].

The Columbia Hill rocks can be subdivided into West Spur and Cumberland Ridge [*Arvidson et al.,* this issue]. In the hills, the abraded rocks differ markedly in composition from the primitive basalts. Most of the hill rocks show enrichments in P, S, Cl, K, Ti, Ni, and Br compared to 'Humphrey RAT2', while Cr is always depleted, except for 'Peace'.

In West Spur, the foot hill of the Columbia Hills where rover Spirit started its climb, a substantial change in rock types was encountered compared to the plains basalts. Rocks had a heavily weathered appearance, such as 'Pot of Gold', which was covered with small tentacle-like protrusions, or the rock 'Breadbox' (Figure 26), where only walls were remaining or, which appeared to have weathered by cavernous weathering. Two rock types were recognized in the West Spur: West Spur Wooly Patch subclass including 'Pot of Gold' (Figure 29) and West Spur Clovis Class including 'Ebenezer' and 'Uchben' (Figure 30). The abraded rock compositions, normalized to 'Humphrey RAT2', revealed enrichments of P, S, Cl, Ti, Ni, and Br, while Ca and Cr were depleted. The highest Br content (675 ppm) of all abraded rocks in Gusev crater was found in rock Uchben, while the lowest Ca content of 2.5 wt.-% was obtained from Wooly Patch. The mean S content of all abraded Columbia Hill rocks, except for rock 'Peace', of 1.52 ± 0.86 wt.-% was lower compared to undisturbed or brushed rock surfaces. The Fe/Mn ratio was highest (up to 160) for some rock samples and was mainly due to very low Mn contents, while Fe was varying between 11 and 15 wt.-% [see *Ming et al.,* this issue]. The discovery of high S, Cl, Br, and often Ni contents even in abraded surfaces suggests that these materials were altered in an aqueous environment.

The Cumberland Ridge Wishstone class includes the rocks 'Wishstone' and 'Champagne'. Comparing Wishstone with the rock Watchtower there are similarities in concentration for most elements above Si, but, differences for Na to Al when normalized to Humphrey RAT2 (Figure 31). That leads to a new class, the Cumberland Ridge Watchtower class. Watchtower and Wishstone class, both contain the elements P, K, and Ti that are highly enriched (up to 2.3 wt.-% P, 0.5 wt.-% K, and 1.8 wt.-% Ti), while no Cr is detected. Wishstone and Champagne show highest concentrations in Na, Al, and Ca (up to 3.7 wt.-% Na, 8 wt.-% Al,

and 6.4 wt.-% Ca) of all abraded rocks in Gusev crater (except for Peace) with the lowest concentrations in Mg, Fe, and Ni (down to 2.1 wt.-% Mg, 9 wt.-% Fe, and 50 ppm Ni).

The x-ray spectrum of rock Wishstone revealed a signal (Figure 32) that was identified unambiguously as Pb by its Lα and Lβ lines taking a small instrument background into account; this is the first time Pb has been detected on Mars. A preliminary lead calibration resulted in 100 ± 50 ppm and 75 ± 50 ppm Pb for the abraded and brushed surfaces of Wishstone, respectively. Since the As Kα peak may partially interfere with the Pb Lα peak, a rather large concentration error had to be attributed to the Pb content in Wishstone.

The Cumberland Ridge Peace class is distinct from any other targets found in the Columbia Hills (Figure 33). The abraded surface of 'Peace' has the highest Mg and S contents (up to 12 wt.-% Mg and 5.2 wt.-% S) and the lowest Al and Si contents (down to 1.5 wt.-% Al and 17.5 wt.-% Si) of all rocks found in Gusev crater so far. A modal calculation based on MB and APXS data [*Ming at al.,* this issue] was carried out for Peace. In addition to high Mg and Ca sulfates, low feldspar, olivine, Mg-rich pyroxenes, magnetite, and SiO_2 polymorphs were modeled. This unusual occurrence of olivine and SiO_2 polymorphs could be explained by partial weathering of olivine.

At least five different rock classes (up to sol 470) can be classified based on chemistry: Adirondack class, Clovis class, Peace class, Wishstone class, and Watchtower class [*Arvidson et al.,* this issue, *Squyres et al,* this issue]. Most rocks have high P, S, Cl, and Br concentrations when compared to the Adirondack class basalts. With the exception of the Wishstone class rocks, the Columbia Hill rocks show high concentrations of Ni. The ratio of Cl to Br is always lower compared to the CI carbonaceous chondrite ratio of 270 (Figure 34), which means that Br is

enriched compared to Cl. Since Br salts are more soluble than Cl salts, aqueous or moist environments could explain the ubiquitous enrichment of Br [*Yen et al*., 2005].

Phosphate-rich Rocks

Along the rover traverse, high P concentrations of 1 to 2 wt.-% were detected by APXS measurements of brushed and abraded rocks. However, the highest P content of 2.45 wt.-% was found in a bright disturbed soil named 'Paso Robles'. The bright color could result from the dominance of Fe^{3+} sulfates as detected by the MB [*Morris et al.,* this issue]. Using the APXS concentration data, a Fe^{3+}-sulfate content of 49 wt.-% could be derived. If we assume apatite as a major carrier of P, the contents of 2.45 wt.-% P and 4.8 wt.-% Ca in 'Paso Robles' would correspond to 14 wt.-% apatite, i.e. phosphate would be here the main host mineral for Ca. Assuming brushite as main phosphate mineral, than only 3.2 wt.-% Ca could satisfy P in the soil [*Ming et al.,* this issue].

The P contents in the soils and rocks of Gusev plains are more than a factor of 5 lower compared to 'Paso Robles'. Nevertheless, compared to Earth, the martian mantle and crust is enriched in P by a factor of 10 [*Dreibus and Wänke,* 1987]. Compared to the plains basalts, the rocks along the Columbia Hills traverse have a higher Fe^{3+}/total Fe ratio [*Morris et al.,* this issue] and all except the Peace-class are enriched in P and Ti.

The discoveries of goethite and hematite in the hill rocks by MB measurements [*Klingelhöfer et al.,* this issue] indicate that aqueous processes altered the rocks and outcrops in the Columbia Hills. The chemical compositions of brushed and abraded surfaces of the three P-rich rocks, Champagne, Wishstone, and Watchtower, illustrate that the brushed samples compared to the abraded samples exhibit a loss of Ca phosphates and no loss of feldspars as

shown in the following. The chemical composition in mol % of these samples together with that of Methuselah, a brushed only rock, is provided in Table 3. Champagne and Wishstone are chemically very similar, while Watchtower with a high ferric ion oxide and a Fe^{3+}/total Fe ratio of 0.83 [*Morris et al.,* this issue] has a lower feldspar component but similar amounts of phosphates. Only significant concentration differences in Ca and P were observed between all three brushed and abraded surfaces; whereas, the concentrations of the feldspathic elements Na, K, and Al are mostly unchanged (Figure 35). The P contents in the brushed samples are approximately a factor of2 lower than the abraded surfaces. When calculating mol concentrations of P and Ca as apatite and the remaining Ca and all Na and K as feldspar, a loss of apatite but no loss of feldspar was found for the brushed surfaces (Table 3). This could be explained by an acidic environment: in martian meteorites phosphates dissolve readily in dilute acids, whereas plagioclase is stable [*Dreibus et al.,* 1996]. Sulfate- and chloride-rich acidic water could easily leach the phosphates from the rock surfaces, yet not weather the feldspar component.

Indicator for a Meteoritic Component

Since the concentration of Ni is much higher in most meteorites than in planetary surficial material, it may be utilized to identify potential meteoritic components on the martian surface. The mean Ni concentration in Gusev soils of 500 ± 150 ppm is three times higher than that in mean primitive Gusev basalts (Figure 15 and 16). Nickel together with the mobile elements S, Cl, and Zn shows the largest deviations between the Gusev soils and Gusev basalts, while otherwise their compositions are quite similar. Hence, the Mg/Ni ratio can be used to distinguish between intrinsic and meteoritic Ni in the soil.

The most common host mineral for Ni in basalts is olivine. In the Earth's mantle the Ni abundances, normalized to CI and Si, are only slightly lower than for Fe, which is incompatible to all models requiring a chemical equilibrium of the Earth's mantle with a pure FeNi metal phase. In terrestrial samples the Mg/Ni ratio varies from 100 to 350 due to fractionation of olivine. It is 105 in lherzolites, 120 to 200 in komatiites and alkali-olivine basalts, and up to 350 in MORB [*Wänke and Dreibus,* 1986]. A similar fractionation trend is found for the martian meteorites [*Wänke and Dreibus,* 1988], however, with a distinctly higher Mg/Ni ratio. Compared to Earth, Ni and all other chalcophile elements are depleted in the martian mantle because of their postulated extraction into the Fe-FeS core at equilibrium conditions [*Wänke and Dreibus,* 1988]. The Mg/Ni ratio in SNC meteorites varies between 400 in Chassigny, 460 in olivine-phyric and lherzolitic shergottites, and up to 700 in the basaltic shergottites.

The abraded primitive basaltic rocks 'Adirondack', 'Humphrey', and 'Mazatzal', with about 35 wt.-% olivine as determined by MB [*Morris et al.,* this issue], have a mean Mg/Ni ratio of 408 similar to the dunite Chassigny. The measured low mean Ni content in the primitive Gusev basalts of 150 ± 20 ppm confirms the predicted depletion of chalcophile elements in the martian mantle [*Dreibus and Wänke,* 1987].

The chemical compositions of soils measured by the APXS at Gusev is similar to those at other landing sites; i.e. a basaltic soil with high abundance of S and Cl [*Gellert et al.,* 2004, *Foley et al*., 2003b and *Brückner et al*., 2003]. The Ni contents in undisturbed soils (measured with long integrations times) vary between 318 up to 641 ppm, which results in a mean value of 475 ± 130 ppm. This value is distinctly higher compared to the abraded basaltic rocks. This high Ni content in soils could be attributed to a meteoritic component [Gellert et al., 2004; Yen et al., 2005]. To obtain the amount of meteoritic Ni we have to estimate the intrinsic Ni content of the

soil. From the mean Mg content in the soil of 5.10 ± 0.12 wt.-% and the Mg/Ni ratio of 408 in the basaltic rocks we calculate an indigenous Ni of 125 ± 26 ppm. Accordingly 350 ± 130 ppm Ni could be of meteoritic origin. This Ni content corresponds to an admixture of 3.2 wt.-% carbonaceous chondrite type 1 (CI) [*Palme and Beer,* 1993] as an upper limit. Considering only iron meteorites with Fe/Ni ratios of ~ 11 [*Mason,* 1971], the contribution of the meteoritic component could be as low as 0.4 wt.-%. Even in this case, only up to 0.38 wt.-% meteoritic Fe would have been added to the soil. In fact, an iron meteorite was discovered at the Meridiani landing site.

Conclusions

During the first 470 sols on Mars, the APXS measured x-ray spectra of about 100 samples of soils and rocks at Gusev Crater. The instrument performance at low temperatures (below -30 ºC) was comparable to measurements in the laboratory. There were no signs of energy resolution degradation or detector window contamination during the mission. Effects encountered on Mars such as diurnal temperature variation, radiation background, and uncertainties in sample-detector distance were investigated, and compensated or corrected.

An extensive calibration of the two flight units and a bread board instrument was carried out. Based on this data, an advanced analysis and evaluation routine was developed and the specific characteristics of each instrument were compensated. The refined calibration took into account an unintentional swap of the two flight units that led to minor adjustments of the lowest Z elements compared to earlier published results.

The rocks of the Columbia Hills, which were reached by the rover Spirit after a long drive, are chemically very distinct from the primitive basalts in the plains. The chemical data

reveal alteration of these rocks in an aqueous and acidic environment. Even after abrasion of outcrops and rocks in the Columbia Hills to a depth of 9 mm there is a high abundance of salts as indicated by the elevated levels of S, Cl, and Br.

Although a variety of different rock types was found, the chemical composition of the undisturbed soil surfaces remained remarkably constant along the rover's traverse. In a trench, excavated by the rover wheels in the plains, significant differences were found relative to the topmost surface soil composition.

Oxide concentrations of all measured samples during the first 470 sols of the mission are reported. Most of the undisturbed soils show similar elemental compositions with almost constant Mg/Si, Fe/Mn, and Cl/S ratios. In these soils, the element P has the smallest compositional variation of all elements in the soils.

Disturbed soils can be similar to undisturbed ones or completely different, such as the soil Paso Robles in Husband Hill. Enriched in elements like P, S, and Br, Paso Robles points to an ancient aqueous environment.

Trenches either showed typical Gusev soil compositions or, such as in The Boroughs, subsurface enrichments of S and Br in a thin layer of several centimeters suggesting that water interacted with these soils.

Brushed rocks have only small amounts of airborne dust adhering to their surfaces; hence, brushed surfaces reveal either dust coatings, weathering rinds, or rock interior compositions. Their relative concentration patterns can be used to group the rock into classes.

The abraded rocks are the best measure of the intrinsic rock compositions, provided the subsurface material is not weathered and the adhering dust is removed during the grinding process. Five major rock classes have been encountered throughout Gusev crater from the

landing site up to Cumberland Ridge on Husband Hill. These rock classes are Adirondack, Clovis, Peace, Wishstone, and Watchtower.

The different P contents in brushed and abraded surfaces of P-rich rocks on Husband Hill are an indicator for weathering in an acidic environment. Acidified water can easily leach phosphates out of the rock surface, but, does not dissolve feldpars, as observed in brushed samples.

The meteoritic component in the soil was estimated based on Ni concentrations. The upper limit for meteoritic debris is estimated to be about 3 wt.-% assuming carbonaceous chondrite type 1 material, while iron meteorites would yield only 0.4 wt.-%.

Acknowledgements

We acknowledge the reviewers C. N. Foley and J. Greenwood, who greatly improved the manuscript. The APXS was mainly funded by the Max-Planck-Society and, in part, by the German Space Agency (DLR) [grant [No. 50QM0014]. G.K. and R.G. also acknowledge DLR grant 50QM0005. Part of the work was supported under INTAS contract no. 001-348. Funding for Athena science team members was provided by NASA contracts through Cornell and JPL. A portion of this work was conducted at the Jet Propulsion Laboratory, California Institute of Technology, under a contract with the National Aeronautics and Space Administration. We acknowledge the unwavering support of JPL engineering and MER operations staff.

References

Arvidson, R. E., S. W. Squyres, R. C. Anderson, J. F. Bell III, J. Brückner, N. A. Cabrol, W. M. Calvin, M. H. Carr, P. R. Christensen, B. C. Clark, L. Crumpler, D. J. Des Marais, C. d'Uston, T. Economou, J. Farmer, W. H. Farrand, W. Folkner, M. Golombek, S. Gorevan, J. A. Grant, R. Greeley, J. Grotzinger, E. Guinness, B. C. Hahn, L. Haskin, K. E. Herkenhoff, J. A. Hurowitz, S. Hviid, J. R. Johnson, G. Klingelhöfer, A. H. Knoll, G. Landis, C. Leff, M. Lemmon, R. Li, M. B. Madsen, M. C. Malin, S. M. McLennan, H. Y. McSween, D. W. Ming, J. Moersch, R. V. Morris, T. Parker, J. W. Rice Jr., L. Richter, R. Rieder, D. S. Rodionov, C. Schröder, M. Sims, M. Smith, P. Smith, L. A. Soderblom, R. Sullivan, S. D. Thompson, N. J. Tosca, A. Wang, H. Wänke, J. Ward, T. Wdowiak, M. Wolff, A. Yen (2005), Overview of the Spirit Mars Exploration Rover Mission to Gusev Crater: Landing Site to the Methuselah Outcrop in the Columbia Hills, *J. Geophys. Res.*– Planets, this issue

Bell et al., this issue

Brückner J., G. Dreibus, R. Rieder, and H. Wänke (2003), Refined data of APXS analyses of soils and rocks at the Mars Pathfinder site: Implications for surface chemistry, *J. Geophys. Res., 108(E12)*, 8094, doi:10.1029/2003JE002060, 2003.

Dreibus, G. and H. Wänke (1987), Volatiles on Earth and Mars: a comparison. *Icarus, 71*, 225-240.

Dreibus G. and R. Haubold (2004), Phosphorus sorption by terrestrial basalt and granite and implications for the martian mantle, Icarus, 167, 166-169.

Dreibus, G., E. Jagoutz, B. Spettel, and H. Wänke (1996), Lunar and Planetary Science XXVII, Lunar and Planetary Institute, Houston, pp. 323-324, abstract.

Foley, C. N., T. E. Economou, R. N. Clayton, and W. Dietrich (2003a), Calibration of the Mars Pathfinder alpha proton X-ray spectrometer, J. Geophys. Res., 108(E12), 8095, doi:10.1029/2002JE002018.

Foley, C. N., T. Economou, and R. N. Clayton (2003b), Final chemical results from the Mars Pathfinder alpha proton X-ray spectrometer, J. Geophys. Res., 108(E12), 8096, doi:10.1029/2002JE002019.

Gellert, R., R. Rieder, R. C. Anderson, J. Brückner, B. C. Clark, G. Dreibus, T. Economou, G. Klingelhöfer, G. W. Lugmair, D. W. Ming, S. W. Squyres, C. d'Uston, H. Wänke, A. Yen, J. Zipfel (2004), Chemistry of rocks and soils in Gusev crater from the alpha particle x-ray spectrometer, *Science, 305*, 829-832.

Golombek, M. P., J. A. Grant, T. J. Parker, D. M. Kass, J. A. Crisp, S. W. Squyres, A. F. C. Haldemann, M. Adler, W. J. Lee, N. T. Bridges, R. E. Arvidson, M. H. Carr, R. L. Kirk, P. C. Knocke, R. B. Roncoli, C. M. Weitz, J. T. Schofield, R. W. Zurek, P. R. Christensen, R. L. Fergason, F. S. Anderson, and J. W. Rice Jr. (2003), Selection of the Mars Exploration Rover landing sites, *J. Geophys. Res., 108 (E12),* 8072, doi:10.1029/2003JE002074.

Haskin, L. A., A. Wang, B. L. Jolliff, H. Y. McSween, B. C. Clark, D. J. Des Marais, S. M. McLennan, N. J. Tosca, J. A. Hurowitz, J. D. Farmer, A. Yen, S. W. Squyres, R. E. Arvidson, G. Klingelhöfer, C. Schröder, P. A. de Souza Jr, D. W. Ming, R. Gellert, J. Zipfel, J. Brückner, J. F. Bell III, K. Herkenhoff, P. R. Christensen, S. Ruff, D. Blaney, S. Gorevan, N. A. Cabrol, L. Crumpler, J. G. L. Soderblom (2005), Water alteration of rocks and soils on Mars at the Spirit rover site in Gusev crater, *Nature, 436*, 66-69, doi:10.1038/nature03640.

Herkenhoff et al., this issue,

Hurowitz et al., this issue

James, F., and M. Roos (1989), MINUIT, Function Minimization and Error Analysis, CERN D506.

Klingelhöfer et al., this issue

Mason, B. (1971), *Handbook of elemental abundances in meteorites*, Gordon and Breach Science Publishers, New York.

McSween, H. Y., R. E. Arvidson, J. F. Bell III, D. Blaney, N. A. Cabrol, P. R. Christensen, B. C. Clark, J. A. Crisp, L. S. Crumpler, D. J. Des Marais, J. D. Farmer, R. Gellert, A. Ghosh, S. Gorevan, T. Graff, J. Grant, L. A. Haskin, K. E. Herkenhoff, J. R. Johnson, B. L. Jolliff, G. Klingelhöfer, A. T. Knudson, S. McLennan, K. A. Milam, J. E. Moersch, R. V. Morris, R. Rieder, S. W. Ruff, P. A. de Souza Jr., S. W. Squyres, H. Wänke, A. Wang, M. B. Wyatt, A. Yen, J. Zipfel (2004), Basaltic Rocks Analyzed by the Spirit Rover in Gusev Crater, *Science, 305*, 842-845.

Ming et al., this issue

Morris et al., this issue

Omand, M., J. L. Campbell, J. A. Maxwell (2005), Simulation of the relationship between element concentrations and X-ray yields in the Mars Exploration Rover's X-ray spectrometer, *Nucl. Instr. and Meth. B 229,* 123-136.

Palme H. and H. Beer (1993), Abundances of the elements in the solar system, in *Landolt-Börnstein, Group VI: Astronomy and Astrophysics*, New Series VI/3a, Springer Verlag, Berlin, pp. 196-221.

Rieder, R., H. Wänke, T. Economou, and A. Turkevich (1997), Determination of the chemical composition of Martian soil and rocks: The alpha proton X ray spectrometer, *J. Geophys. Res., 102(E2),* 4027– 4044.

Rieder R., R. Gellert, J. Brückner, G. Klingelhöfer, G. Dreibus, A. Yen, and S. W. Squyres (2003), The new Athena alpha particle X-ray spectrometer for the Mars Exploration Rovers, *J. Geophys. Res., 108(E12),* 8066, doi:10.1029/2003JE002150.

Rieder, R., R. Gellert, R. C. Anderson, J. Brückner, B. C. Clark, G. Dreibus, T. Economou, G. Klingelhöfer, G. W. Lugmair, D. W. Ming, S. W. Squyres, C. d'Uston, H. Wänke, A. Yen, J. Zipfel (2004), Chemistry of rocks and soils at Meridiani Planum from the alpha particle x-ray spectrometer, *Science, 306*, 1746-1749.

Squyres, S. W., E. Arvidson, E. T. Baumgartner, J. F. Bell III, P. R. Christensen, S. Gorevan, K. E. Herkenhoff, G. Klingelhöfer, M. B. Madsen, R. V. Morris, R. Rieder, and R. A. Romero (2003), The Athena Mars Rover science investigation, *J. Geophys. Res., 108 (E12),* 8062, doi:10.1029/2003JE002121

Thompson, A., et al. (2001), *X-Ray Data Booklet*, eds. A. C. Thompson and D. Vaugham, Lawrence Berkeley National Laboratory, LBNL/PUB-490, Rev 2.

Van Gysel, M., P. Lemberge and P. Van Espen (2003), Description of Compton peaks in energy-dispersive x-ray fluorescence spectra, *X-Ray Spectrometry, 32,* 139-147.

Wang et al, this issue

Wänke H. and G. Dreibus (1988), Chemical composition and accretion history of terrestrial planets. *Phil. Trans. R. Soc. Lond. A 325,* 545-557.

Wänke, H. and G. Dreibus (1986). Geochemical Evidence for the Formation of the Moon by Impact-Induced Fission of the Proto-Earth. In: *Origin of the Moon*, (Eds. W. K. Hartmann et al.), Lunar Planet. Inst., Houston, pp. 649-672.

Yen, A. S., R. Gellert, C. Schröder, R. V. Morris, J. F. Bell III, A. T. Knudson, B. C. Clark, D. W. Ming, J. A. Crisp, R. E. Arvidson, D. Blaney, J. Brückner, P. R. Christensen, D. J. DesMarais, P. A. de Souza Jr, T. E. Economou, A. Ghosh, B. C. Hahn, K. E. Herkenhoff, L. A. Haskin, J. A. Hurowitz, B. L. Joliff, J. R. Johnson, G. Klingelhöfer, M. Bo Madsen, S. M. McLennan, H. Y. McSween, L. Richter, R. Rieder, D. Rodionov, L. Soderblom, S. W. Squyres, N. J. Tosca, A. Wang, M. Wyatt, and J. Zipfel (2005), An integrated view of the chemistry and mineralogy of martian soils, *Nature, 436,* 49-54, doi:10.1038/nature03637.

Figure Captions

Figure 1 Schematic drawing of the APXS sensor head.

Figure 2 PANCAM picture of the IDD with the in situ instruments. The APXS, top right, is pointing to the right with closed dust protective door.

Figure 3 X-ray spectrum obtained on Mars together with the deconvolution model components. The main elemental characteristic peaks (Kα lines) are labeled, while Kβ are unlabeled. Signals from elastic scattering (E) and inelastic scattering (I) are labeled. The background, labeled (0, 1, 2) is fit with a step function, as shown. All these spectral features are discussed in the Peak Fit Analysis section.

Figure 4 Response results of the APXS calibration. The biggest changes compared to the previous calibration concern chlorine and bromine. For both elements only a limited set of good geological certified samples was available. In future, a recalibration using better geological standards or model calculations might help to reduce the error. The lower Z peaks are almost exclusively produced by alpha particles. This PIXE type of excitation decreases with increasing Z. The minimum excitation occurs at titanium, where the XRF type of excitation with plutonium x-ray radiation takes over.

Figure 5 Scheme of the various hardware configurations of APXS sensor heads and sources used for calibration measurements. The nomenclature defined by the letters ‘A’ to ‘G’ of the different configurations is used in the following graphs to shed light on the influences of sensor heads and sources. Sensor heads were named FM1, FM2 for the flight modules and BB10 for the bread board. The names of the instruments are the actual ones, not those (erroneously) assumed.

Configuration A: The bread board sensor head BB10 with a laboratory source named S10. Using Configuration A measurements were made after the launch of MER to refine the method and to extend the calibration to previously not available elements. Also, investigations of environmental parameters like source to sample distance and atmospheric pressure were performed. Reference materials like the martian meteorite EETA79001 or the Iron-Nickel meteorite Mundrabilla were measured, because they are similar to 'Bounce Rock' and 'Heatshield Rock', respectively, both found at the Opportunity landing site.

Configuration B and C: The bread board sensor including its x-ray detector was used to test the various alpha detectors that were later integrated into the flight sensors. The flight source S1 was used to provide cross calibration of the sources S1 and S10.

Configuration D and F: Both flight modules were calibrated using 11 reference standards and several chemical compounds. These sensors were equipped with their original sources.

Configuration E: Prior to delivery, the flight sensor head 2 that finally was attached to the Opportunity Rover was equipped with the source S1. From this moment on, both flight modules remained separated as the other flight module was already delivered to NASA/JPL. The last measurement clearly showed that compared to D the sensor heads were swapped and remained in this configuration on Mars as well. Here, only one measurement using the reference sample SSK1 in vacuum was performed. To compare this measurement with those carried out in 10 mbar CO_2, their peak areas were corrected for the attenuation in gas.

Configuration G: Thin alpha detectors were integrated into the flight modules and mechanically and thermally qualified. Afterwards, measurements were taken with flight module 1 and the attached source S2 assuming that this sensor head would be FM2. The comparison with configuration F clearly shows that both flight modules were swapped. However, these measurements allow cross calibration of the sources S1 and S2 as both were measured with FM1.

Figure 6 The ratio of measurement F to G and E to D is shown. The energy dependence clearly reveals that measurements G and E were taken with unintentionally swapped instruments. In case of no swapping, all data points should scatter around unity. FM2 has a thicker beryllium window attenuating the lines as a function of energy. Measurement E consisted of only one vacuum measurement that was corrected to 10 mbar CO_2. The distance between source and sample seems to have been slightly increased resulting in a ~ 6 % lower value for E/D compared to F/G, which included more measurements.

Figure 7 The cross calibration of measurements D to G and E to F are shown. Both ratios represent the ratios of measurements taken with the same instrument but different sources. The energy dependence is much smaller than the ratios in figure 5 that showed the influence of the instruments. Measurement E again seems to be ~ 5 % lower in intensity. The ratio D to G shows a constant ratio from zinc to ~ silicon. Below silicon, a decrease up to 10 % occurs, which is not observed for E to F. The ratio of the lab source S10 to S1 doesn't show a significant influence (Figure 8). Therefore, the influence of the source can be estimated to be at most 10 % for Na and 5 % for Mg. Otherwise it is constant.

Figure 8 Ratios of elemental signals from three samples (Allende, Murchison and SSK) were measured with BB10-S1 and the BB10-S10. The measurements were performed in vacuum as well as in 10 mbar CO_2. Red symbols are the ratios of single measurements. The black squares show the average fit for all measurements. The peak area ratios show that the main difference between the sources is only the absolute intensity. There might be a slightly higher intensity for S1 at lower Z elements but this effect is below 3 percent relative.

Figure 9 Cross calibration of the flight modules with the bread board. Peak area ratios of measurements taken with FM1, FM2, and BB10 are shown. 11 certified geological samples were used for these ratios. The symbols show the actual evaluated ratios while the line connects those data points that were selected for the cross calibration. Obviously, some element data points are outliers. Elements like chlorine and zinc have low counting statistics but manganese seems to have a 5 % higher response on both flight instruments. The reason for this may be a differently compensated exponential tailing of the Fe peak for different main electronics.

Figure 10 Comparison of the elemental concentrations of the rock 'Temples Dwarf' determined at different APXS standoff distances. Plotted is the ratio of three different distances to the closest distance of 3.1 mm. The ratios of all elements agree within their error bars. Indicated by black arrows are the elements affected by background: P, K, and Ti. The deviations for K and Ti are below 10 %.

Figure 11 Geometry calibration performed in the laboratory. The sample SSK was measured in 10 mbar CO_2 at different standoff distances. The peak areas for Na, Al, Si and Ca were normalized to the area at nominal distance of 2 mm. These element ratios show

that the additional attenuation can be neglected for all elements higher than Al. For Na the deviation is below approximately 15 % at standoffs higher than 20 mm. The black line indicates the geometric norm given by the analysis routine. Black triangles show that the measurements on 'Temples Dwarf' on Mars with defined standoffs can be well reproduced.

Figure 12 Spectra from the instrument FM1 in the laboratory and on Mars. The data are not scaled. The energy resolution on Mars for the usual night measurement is comparable to the laboratory. The additional background on Mars clearly visible at 8 keV stems mainly from the MB source. The zirconium K peak is within the energy range on Mars as the gain is decreased by approximately 5 % compared to the laboratory by the high IDD cable capacitance.

Figure 13 APXS spectra taken while looking into the martian atmosphere. Several peaks can be identified. Argon Kα line (at 2.96 keV) is a component of the martian atmosphere. The zirconium collimator (in front of the x-ray detector) produces Kα and Lα lines at 15.8 keV and 2.05 keV, respectively. A copper Kα line resulting from the copper doors and the detector body is found at 8.05 keV. Very small background peaks of nickel, gold and lead can be attributed to structural elements of the sensor. The linear backgrounds as well as the Zr peaks decreased with time and indicate that an important part of their excitation results from the Mössbauer source, which decays with 271 days half life. The L lines of Zr overlap with the phosphorus Kα line (at 2.01 keV) and their contributions are taken into account. The height of the Zr Lα line is coupled by a fixed ratio to the Zr Kα line. This ratio was determined using these

atmospheric spectra. The peak area of the Zr L peak is about 0.07 cps. This would correspond to a P concentration of about 400 ppm and was corrected.

Figure 14 Zirconium peak areas versus sol. The Zr peaks increase when a measurement was taken in a trench. No significant variations in the samples imply a zirconium signal below approx. 0.05, which corresponds to a concentration below 250 ppm.

Figure 15 Concentrations normalized to rock 'Humphrey RAT2' of undisturbed Gusev soils (SU): 'Gusev Soil' (sol 14), 'Grandflats', 'Sugar', and 'Gobi'; in logarithmic display.

Figure 16 Concentrations relative to rock Humphrey RAT2 of undisturbed Gusev soils (SU): 'Gusev Soil' (sol 14), 'Bighole', 'Crumble', and 'Liberty Bell'; in logarithmic display. Note that Crumble exhibits many lithic fragments.

Figure 17 Chlorine versus sulfur concentrations for disturbed soils, undisturbed soils, and trenches.

Figure 18 Phosphorus concentrations for disturbed soils, undisturbed soils, and trenches.

Figure 19 Concentrations normalized to Gusev Soil target (sol 14) of disturbed Gusev soils (SD): 'Track', 'Serpent', 'Disturbance Soil', 'Coffee', and 'Tofurkey'.

Figure 20 Concentrations normalized to Gusev Soil target (sol 14) of disturbed Gusev soils (SD): 'Penny', 'Paso Robles', 'Paso Light', 'Paso Dark', and 'Paso Dark Light'.

Figure 21 Iron versus sulfur concentrations for disturbed soils, undisturbed soils, and trenches.

Figure 22 Concentrations normalized to Gusev Soil target (sol 14) of two Gusev trenches (ST): 'Road Cut' (surface, floor, and wall) and 'Big Hole' (surface and 2 floors).

Figure 23 Concentrations normalized to Gusev Soil target (sol 14) of the Gusev trench (ST) 'The Boroughs' (surface, floor, and wall).

Figure 24 Concentrations in mol. % of Mg and Fe compounds versus SO_3 based on mineralogical compositions: total MgO, Mg sulfate, total Fe as FeO plus Fe_2O_3, and Fe^{3+} sulfate as derived from MB.

Figure 25 Concentrations normalized to Humphrey RAT2 of Gusev rocks as is (RA): 'Adirondack', 'Mimi', and 'Mazatzal' (different targets).

Figure 26 Concentrations normalized to Humphrey RAT2 of West Spur rocks as is (RA): 'Goldklumpen', 'Fool's Gold', 'Breadbox', 'String of Pearls', and 'Wooly Patch'.

Figure 27 Concentrations normalized to rock Humphrey RAT2 of West Spur Clovis class brushed rocks (RB): 'Clovis', 'Ebenezer', 'Uchben', and 'Lutefisk' (two targets).

Figure 28 Concentrations normalized to rock Humphrey RAT2 of Cumberland Ridge Watchtower class brushed rocks (RB): 'Watchtower', and 'Methuselah' (two targets).

Figure 29 Concentrations normalized to rock Humphrey RAT2 of West Spur Wooly Patch type abraded rocks (RR): 'Wooly Patch' (two targets), and 'Pot of Gold'.

Figure 30 Concentrations normalized to rock Humphrey RAT2 of Cumberland Ridge Clovis class abraded rocks (RR): 'Clovis', 'Ebenezer' (two targets), and 'Uchben'.

Figure 31 Concentrations normalized to rock Humphrey RAT2 of Cumberland Ridge Wishstone class abraded rocks (RR): 'Wishstone', 'Champagne', and Cumberland Ridge Watchtower class rock 'Watchtower'. Note the difference in concentration between the elements Na to Al.

Figure 32 Spectra of the rock Wishstone compared to Humphrey. The main elemental lines that differ remarkably are labeled. For the first time the trace element lead was identified in this rock. The Lα and Lβ lines of lead are marked.

Figure 33 Concentrations normalized to rock Humphrey RAT2 of Cumberland Ridge Peace class abraded outcrop (two targets).

Figure 34 Chlorine concentrations versus bromine including the CI carbonaceous chondrite Cl/Br ratio. Note: RB = rocks brushed, RR = rocks ratted (abraded), SD = soils disturbed, ST = soils trenched, SU = soils undisturbed.

Figure 35 Concentrations normalized to rock Humphrey RAT2 of Cumberland Ridge Wishstone class rocks and Cumberland Ridge Watchtower rock, each brushed and abraded.

Tables

Table 1 APXS method calibration performed with the bread board BB10. The fit results for the parameters of equation (1) are given for the reported elements. For description of the listed parameters, see comments for formula (2). Key: * = larger uncertainty because of inhomogeneous matrix

Z	El	Offset	Resp	Const	μmean	Deviation in percent	No. of samples	Lowest concentration
11	Na	-0.18	0.70	0.42	3510	11	33	0.5
12	Mg	-0.5	1.49	0.68	2286	14	29	0.5
13	Al	0.18	2.07	0.49	1514	7	40	0.5
14	Si	-2.8	2.11	0.498	1242	3	38	5
15	P	0	1.95	0.927	1474	15	28	0.03
16	S	0	1.23	0.477	1047	15	17	0.03
17	Cl	0	1.15	0.468	755	30*	11	0.03
19	K	0.1	0.86	0.941	410	15	35	0.05
20	Ca	-0.04	0.79	0.833	325	7	31	0.5
22	Ti	0.094	0.52	0.533	228	20	31	0.05
24	Cr	0	0.57	0.094	150	19	11	0.02
25	Mn	0	0.74	0.254	121	8	33	0.02
26	Fe	-0.35	1.02	0.342	99	7	33	1
28	Ni	0	1.44	0	97	16	17	0.005
30	Zn	0	2.35	0.149	69	16	31	0.005
35	Br	0	6.39	0	36	20*	3	0.001

Table 3 Concentrations in mol. % for different Columbia Hill rocks, brushed or abraded (RAT). Based on the measured bulk composition some oxides were attributed to apatite and feldspar. Notes: 1) Measured APXS concentrations [mol. %]; 2) Calculated [mol. %]: Assuming all P in apatite, remaining Ca and all Na and K in feldspar; 3) Deviation between measured and calculated; a) Al in the feldspar component is calculated according to 2); b) Sum of elements [mol. %], not all elements are listed, Fe^{3+}/Fe_{total} taken from MB [*Morris et al.,* this issue].

Sample	Assemblage	Na_2O	Al_2O_3 [a)]	P_2O_5	K_2O	CaO	Sum [b)]
Champagne brushed	Bulk [1)]	5.80	10.5	1.26	0.37	7.95	100.0
	Apatite + Feldspar [2)]	5.80	9.96	1.26	0.37	7.95	25.3
	Dev. % [3)]		5				
Champagne RAT2	Bulk [1)]	5.54	9.94	2.43	0.38	10.7	100.0
	Apatite + Feldspar [2)]	5.54	8.56	2.43	0.38	10.7	27.6
	Dev. % [3)]		14				
Wishstone chisel brushed	Bulk [1)]	5.54	10.3	1.24	0.38	8.19	100.0
	Apatite + Feldspar [2)]	5.42	10.0	1.21	0.38	8.19	25.2
	Dev. % [3)]		2				
Wishstone chisel RAT	Bulk [1)]	5.47	10.0	2.49	0.41	10.77	100.0
	Apatite+ Feldspar [2)]	5.35	8.45	2.43	0.40	10.77	27.4
	Dev. % [3)]		16				
Watchtower Joker brushed	Bulk [1)]	2.97	7.93	1.27	0.53	7.14	100.0
	Apatite + Feldspar [2)]	2.97	6.46	1.27	0.53	7.14	18.4
	Dev. % [3)]		19				
Watchtower Joker RAT	Bulk [1)]	2.88	8.09	2.12	0.53	8.87	100.0
	Apatite + Feldspar [2)]	2.88	5.28	2.12	0.53	8.87	19.7
	Dev. % [3)]		35				
Methuselah Pittsburg brushed	Bulk [1)]	3.49	7.95	1.45	0.31	8.57	100.0
	Apatite + Feldspar [2)]	3.49	7.58	1.45	0.31	8.57	21.4
	Dev. % [3)]		5				

Table 2 Compositions of all Gusev samples from sol 14 to 470, concentration in weight % of oxides or parts per million by weight. Absolute statistical error (SE) is a 2σ error for the precision of this value. The accuracy error values derived for during the calibration are given in Table 1. The geometric norm is the sum of oxides and is a relative indicator for the distance between detector and the sample surface.
Keys: 1) Geometric norm, 2) Total integration time [hours], 3) Standard error (2 sigma).
Types: RB = Rock brushed, RR = Rock 'ratted' (abraded), RU = Rock undisturbed (as is), RF = RAT fines, SD = Soil disturbed, ST = Soil trench, SU = Soil undisturbed.

Sol	Type	Sample	N[1)]	T[2)]	Na_2O	SE[3)]	MgO	SE	Al_2O_3	SE
14	SU	Gusev_Soil	45	13.5	2.8	0.3	8.34	0.12	9.89	0.14
18	RU	Adirondack_asis	126	0.1	2.3	1.6	9.09	0.50	10.93	0.46
33	RB	Adirondack_brush	129	11.2	2.8	0.2	9.51	0.10	11.35	0.11
34	RR	Adirondack_RAT	123	5.5	2.4	0.2	10.83	0.12	10.87	0.12
41	SU	Crest_morning	76	0.7	2.8	0.9	8.67	0.27	10.02	0.29
42	RU	Mimi	95	4.5	2.9	0.2	8.39	0.12	10.04	0.13
43	SD	Track	72	2.4	2.9	0.3	8.45	0.15	10.30	0.17
44	SF	Rampflats	68	0.3	2.5	1.3	8.69	0.37	10.23	0.38
45	SU	Angelflats	59	0.5	3.1	1.8	8.59	0.47	9.96	0.36
47	SU	Grandeflats	70	4.5	3.1	0.2	8.41	0.11	10.05	0.11
49	ST	Road Cut_Floor3_	57	6.5	2.4	0.3	8.90	0.13	9.83	0.14
50	ST	Road Cut_WallMIonl	62	7.6	2.7	0.3	8.77	0.13	9.96	0.16
52	SU	Sugar_T1	74	0.5	3.2	1.0	8.47	0.28	9.67	0.29
55	RU	Humphrey_Ashley_asis	131	0.3	3.0	0.9	8.76	0.23	10.66	0.23
57	RU	Humphrey_Heyworth_asis	129	0.6	2.9	1.2	8.69	0.33	11.13	0.27
58	RB	Humphrey_brush	134	3.4	3.0	0.2	8.82	0.12	11.20	0.14
59	RR	Humphrey_RAT1	128	5.0	2.8	0.2	9.49	0.12	10.78	0.15
60	RR	Humphrey_RAT2	125	5.0	2.5	0.3	10.41	0.14	10.68	0.13
63	RU	Plank_Asis	113	0.4	3.0	0.8	8.27	0.24	9.72	0.26
65	SU	SugarLoafFlats_soi	70	0.5	3.2	1.0	8.57	0.30	9.86	0.28
71	SU	Gobi1_soil	58	2.9	2.9	0.3	8.25	0.15	9.56	0.16
74	SD	Serpent_Scuffed	71	4.0	2.9	0.3	8.86	0.14	10.12	0.15
81	RB	Mazatzal_NewYork_Brush	110	1.8	2.5	0.3	7.70	0.14	8.50	0.16
81b	RU	Mazatzal_Texas_asisRAT1	114	2.5	3.1	0.2	8.23	0.13	9.15	0.13
82	RU	Mazatzal_NewYork_RAT1 Oregon_Asis	107	4.6	2.7	0.2	9.02	0.12	9.92	0.13
83	RU	Mazatzal_Oregon_Asis	101	2.7	2.8	0.2	8.09	0.13	8.94	0.13
86	RR	Mazatzal_Brooklyn_RAT2	107	6.4	2.8	0.2	9.72	0.11	10.70	0.12
100	RB	Route66_brushed	132	6.0	2.9	0.2	8.67	0.11	10.78	0.14
105	SU	Bitterrootflats_flats1	48	0.6	3.0	1.2	8.43	0.34	9.68	0.31
113	SU	Bighole_Mayfly_surface	69	0.6	3.1	1.2	8.39	0.33	9.92	0.26
114	ST	Bighole_RS2	84	9.9	2.5	0.2	9.19	0.11	9.06	0.13
115	ST	Bighole_Trico	67	4.0	2.5	0.3	9.04	0.14	9.08	0.14
122	SD	Owens_soil_Track	83	0.5	3.1	1.0	8.41	0.29	10.65	0.27
126	SU	Accelerator_Soil	47	0.6	3.1	1.7	8.15	0.46	10.02	0.40
135	SD	Santa_Anita_trench_surface	91	0.6	3.0	1.7	8.73	0.46	10.71	0.37
140	ST	Boroughs_Mills_bottom	76	8.3	2.4	0.2	9.82	0.13	8.47	0.13
141	ST	Boroughs_Hellskitchen_side	83	4.0	2.5	0.2	10.48	0.14	7.85	0.12
150a	RU	Mojave_Joshua_Asis	127	0.4	3.1	1.0	9.38	0.29	10.36	0.29
158	SD	Shredded_dark4_soil	89	0.5	3.3	0.9	8.73	0.26	11.29	0.26
164	RU	Goldklumpen_Asis	94	4.5	3.1	0.2	8.89	0.12	10.32	0.13
167	SU	Goldfinger_Jaws_soil	92	0.5	3.3	1.2	9.84	0.36	10.08	0.41
170	RU	Fools_gold_Asis	92	3.0	2.6	0.3	9.37	0.16	10.86	0.15
172	RR	Pot_of_Gold_RAT	89	5.0	3.0	0.2	9.91	0.13	10.32	0.13

Sol	Type	Sample	N[1]	T[2]	Na_2O	SE	MgO	SE	Al_2O_3	SE
176	RU	Breadbox_Sourdough	56	4.0	3.0	0.3	8.56	0.12	10.17	0.12
178	RU	String_of_pearls_Perlx	70	4.0	2.9	0.2	8.95	0.14	9.89	0.14
195	RU	WoolyPatch_Sabre_asis	100	5.8	3.4	0.2	8.54	0.11	9.68	0.12
197	RR	WoolyPatch_Sabre_RAT	86	5.7	3.3	0.2	10.92	0.14	12.60	0.17
199	RR	Woolypatch_Mastodon_ RAT	99	5.6	2.9	0.2	11.62	0.13	10.34	0.12
214	RU	Clovis_Plano_asis	105	5.3	3.5	0.21	8.80	0.11	9.66	0.12
216	RB	Clovis_Plano_Brush	90	4.7	3.6	0.23	10.79	0.14	9.34	0.13
218	RR	Clovis_Plano_RAT	72	4.7	3.6	0.23	11.52	0.13	8.95	0.10
225	RB	Clovis_BrushMosaic	90	0.8	3.0	1.1	11.46	0.30	8.85	0.27
227	SU	Kilmary_soil	74	0.7	2.8	0.9	8.42	0.26	9.59	0.26
228	RU	Ebenezer_TinyTim	123	0.5	2.9	0.8	11.16	0.25	10.71	0.24
229	RU	Ebenezer_Cratchit_asis	120	5.3	3.2	0.2	10.89	0.13	10.40	0.12
231	RB	Ebenezer_brushed	95	6.0	2.6	0.2	13.57	0.15	9.93	0.12
232	RR	Ebenezer_RAT	72	6.0	2.3	0.2	14.82	0.17	9.28	0.13
235	RF	Ebenezer_Fritz_RATgrind.	103	0.6	3.0	0.8	13.49	0.28	10.18	0.24
240	SU	Greeneyes_soilTG	78	0.7	2.9	0.9	8.39	0.25	9.85	0.23
259	SD	Disturbance_soil	84	4.7	3.2	0.2	8.42	0.12	10.13	0.14
266	RU	Temples_dwarf_asis	99	7.7	3.3	0.2	9.06	0.11	9.47	0.11
274	RU	Tetl_clumb_asis	70	6.3	3.3	0.2	9.49	0.11	10.10	0.11
280	SD	Coffee_disturbed_soil	73	6.5	3.2	0.2	8.94	0.12	9.80	0.12
284	RU	Uchban_Koolik_asis	76	6.1	3.2	0.2	9.14	0.12	9.74	0.12
287	RR	Uchben_Koolik_RAT	90	8.3	2.4	0.2	14.28	0.13	9.52	0.10
291	RB	Uchben_Chiikbes_brush	86	6.5	2.8	0.2	12.14	0.14	9.96	0.12
300	RB	Lutefisk_flatfish_Brushed	95	7.3	2.6	0.2	14.34	0.15	10.29	0.12
304	RB	Lutefisk_RATRoe_brushed	88	5.5	2.5	0.2	15.12	0.17	10.17	0.13
315	SD	Tofurkey_disturbedsoil	100	2.7	3.4	0.3	8.68	0.16	10.31	0.16
334	RB	Wishstone_chisel_brush	102	2.7	5.1	0.3	4.94	0.14	15.64	0.24
335	RR	Wishstone_chisel_RAT	97	3.3	5.0	0.3	4.50	0.10	15.03	0.17
342	SD	Penny_dist_soil	101	3.3	3.5	0.2	9.42	0.13	10.63	0.14
349	RU	dreaming_asis	76	2.5	4.5	0.3	5.64	0.13	14.68	0.21
353	RU	champagne_asis	73	3.3	4.2	0.2	6.15	0.10	13.48	0.15
355	RB	champagne_brush	129	9.0	5.3	0.2	4.56	0.07	15.75	0.15
356	RR1	champagne_RAT1	53	9.0	5.0	0.3	3.94	0.09	14.86	0.17
357	RR2	champagne_RAT2	53	9.0	5.0	0.2	3.98	0.08	14.83	0.14
374	RB	Peace_brushed	81	4.7	2.3	0.2	14.20	0.14	6.29	0.08
377	RR1	Peace_RAT1	90	4.7	0.4	0.4	19.75	0.23	2.80	0.10
380	RR2	Peace_RAT2	43	4.7	0.0	0.4	21.53	0.27	2.24	0.06
380b	RU	Alligator_APXSspot_TG	86	0.4	3.3	0.9	11.24	0.28	7.78	0.25
381	RU	Alligator_APXSspot_long	86	4.7	3.0	0.2	10.90	0.14	7.81	0.11
385b	RB	Alligator_scale_brushed	77	0.2	1.6	1.5	16.27	0.41	5.49	0.33
401	SD	PasoRobles_disturbed soil	88	2.7	1.6	0.2	5.53	0.09	4.13	0.07
416	RB	Watchtower_Joker_Brush	78	2.7	2.8	0.3	10.10	0.16	12.22	0.19
417	RR	Watchtower_Joker_RAT	85	5.3	2.7	0.2	10.00	0.13	12.33	0.15
427	SD	Paso_light	85	6.5	1.4	0.2	5.19	0.08	6.27	0.08
428	SD	Paso_dark	88	6.1	3.2	0.2	8.74	0.11	10.44	0.13
429b	RB	BensClod_brushed	73	8.2	3.3	0.2	5.11	0.09	15.12	0.15
430	SD	Paso_DarkLight	84	9.3	3.0	0.3	8.64	0.12	9.72	0.11
457	SU	Crumble	78	10	3.4	0.2	8.73	0.09	11.83	0.11
469	RU	Methuselah_Keystone	72	5.8	3.3	0.2	8.38	0.11	12.44	0.13
470	RB	Methuselah_Haunch	76	8.9	3.4	0.2	8.48	0.09	13.61	0.12

Sol	SiO_2	SE	P_2O_5	SE	SO_3	SE	Cl	SE	K_2O	SE	CaO	SE	TiO_2	SE
14	46.3	0.5	0.87	0.08	6.61	0.08	0.78	0.02	0.48	0.06	6.36	0.05	0.86	0.07
18	45.6	1.0	0.72	0.37	3.47	0.27	0.43	0.06	0.14	0.15	7.52	0.23	0.71	0.23
33	45.7	0.4	0.57	0.06	2.16	0.03	0.36	0.01	0.12	0.05	7.84	0.05	0.49	0.06
34	45.7	0.4	0.52	0.07	1.23	0.03	0.20	0.01	0.07	0.05	7.75	0.05	0.48	0.06
41	46.0	0.7	0.80	0.26	5.26	0.17	0.69	0.04	0.43	0.15	6.98	0.12	0.72	0.20
42	45.0	0.4	0.85	0.08	5.50	0.08	0.74	0.02	0.49	0.06	7.07	0.06	0.68	0.07
43	46.8	0.5	0.81	0.09	5.00	0.10	0.60	0.02	0.45	0.06	6.52	0.07	0.91	0.08
44	46.3	0.9	0.87	0.32	6.06	0.26	0.71	0.06	0.43	0.17	6.58	0.16	0.77	0.23
45	45.5	0.6	0.78	0.28	6.19	0.21	0.78	0.05	0.48	0.16	6.69	0.14	0.68	0.15
47	46.0	0.4	0.86	0.08	6.33	0.09	0.73	0.02	0.44	0.06	6.32	0.05	0.89	0.07
49	46.2	0.5	0.68	0.08	6.11	0.09	0.69	0.02	0.38	0.06	6.14	0.06	1.00	0.08
50	46.1	0.5	0.73	0.08	5.69	0.08	0.77	0.02	0.37	0.06	6.24	0.05	1.02	0.07
52	45.6	0.8	0.83	0.26	6.10	0.21	0.80	0.05	0.41	0.15	6.60	0.13	0.81	0.18
55	45.9	0.6	0.65	0.22	3.53	0.13	0.58	0.04	0.19	0.13	7.53	0.12	0.48	0.12
57	45.7	0.6	0.63	0.21	3.24	0.11	0.54	0.03	0.19	0.12	7.54	0.11	0.53	0.11
58	45.9	0.4	0.62	0.07	2.63	0.05	0.49	0.01	0.18	0.06	7.76	0.06	0.54	0.06
59	46.3	0.4	0.57	0.07	1.09	0.03	0.32	0.01	0.13	0.05	8.19	0.06	0.58	0.06
60	45.9	0.4	0.56	0.07	1.28	0.03	0.26	0.01	0.10	0.05	7.84	0.05	0.55	0.06
63	44.0	0.7	0.75	0.23	5.85	0.18	0.72	0.04	0.33	0.14	6.81	0.12	0.57	0.13
65	45.9	0.8	0.81	0.26	6.76	0.23	0.84	0.05	0.47	0.16	6.04	0.13	0.83	0.16
71	45.0	0.5	0.91	0.09	7.61	0.13	0.88	0.03	0.49	0.07	6.17	0.07	0.89	0.08
74	46.7	0.5	0.66	0.08	4.39	0.08	0.54	0.02	0.40	0.06	6.57	0.06	0.94	0.07
81	44.5	0.5	1.19	0.09	7.62	0.12	1.28	0.03	0.54	0.06	6.63	0.07	0.84	0.08
81b	43.7	0.5	0.97	0.08	7.62	0.11	0.99	0.02	0.45	0.06	6.23	0.06	0.81	0.07
82	45.7	0.4	0.82	0.07	3.33	0.05	0.54	0.01	0.29	0.06	7.57	0.06	0.69	0.07
83	44.5	0.5	1.03	0.08	7.77	0.11	1.11	0.02	0.51	0.06	6.35	0.06	0.77	0.07
86	45.8	0.4	0.65	0.07	1.48	0.03	0.23	0.01	0.16	0.05	8.02	0.06	0.59	0.06
100	44.8	0.4	0.74	0.07	4.20	0.05	0.55	0.01	0.23	0.05	7.83	0.05	0.59	0.06
105	46.3	0.8	0.79	0.29	6.67	0.25	0.72	0.05	0.44	0.17	6.45	0.15	0.89	0.18
113	46.1	0.6	0.88	0.24	6.37	0.18	0.79	0.04	0.47	0.15	6.07	0.11	1.00	0.16
114	43.7	0.4	0.80	0.08	9.13	0.10	1.00	0.02	0.35	0.06	5.74	0.04	0.87	0.07
115	44.2	0.5	0.74	0.08	8.37	0.12	1.00	0.02	0.34	0.06	5.86	0.06	0.89	0.07
122	47.0	0.7	0.95	0.26	5.45	0.19	0.63	0.04	0.47	0.15	6.38	0.12	0.88	0.16
126	46.3	0.8	0.83	0.30	6.40	0.24	0.77	0.05	0.45	0.17	6.50	0.14	0.96	0.19
135	47.0	0.7	0.77	0.27	4.67	0.16	0.54	0.03	0.42	0.15	6.27	0.11	0.89	0.20
140	41.4	0.4	0.71	0.08	11.2	0.12	0.68	0.01	0.35	0.06	5.77	0.05	0.90	0.07
141	39.2	0.4	0.80	0.08	14.1	0.16	0.73	0.02	0.36	0.06	5.76	0.05	0.85	0.08
150a	44.8	0.7	0.53	0.25	3.47	0.14	0.57	0.04	0.20	0.13	7.39	0.12	0.57	0.12
158	47.8	0.7	0.75	0.23	4.10	0.15	0.52	0.03	0.45	0.15	6.31	0.12	0.67	0.16
164	45.0	0.4	1.12	0.08	8.36	0.10	0.83	0.02	0.31	0.06	5.26	0.05	0.72	0.07
167	46.3	0.8	0.80	0.26	5.26	0.18	0.62	0.04	0.41	0.15	5.90	0.12	0.73	0.14
170	44.2	0.5	1.14	0.08	9.71	0.13	0.68	0.02	0.18	0.06	5.13	0.05	0.60	0.07
172	42.9	0.4	1.08	0.08	7.96	0.10	0.57	0.01	0.20	0.06	5.86	0.05	0.77	0.07

Sol	SiO_2	SE	P_2O_5	SE	SO_3	SE	Cl	SE	K_2O	SE	CaO	SE	TiO_2	SE
176	46.0	0.4	1.06	0.08	7.12	0.10	0.76	0.02	0.40	0.06	6.04	0.06	0.85	0.07
178	43.4	0.5	1.09	0.08	8.34	0.12	0.67	0.02	0.34	0.06	6.37	0.06	0.76	0.07
195	44.8	0.4	0.96	0.07	7.33	0.09	1.08	0.02	0.40	0.06	5.62	0.04	0.89	0.07
197	46.8	0.4	1.24	0.08	2.87	0.05	0.78	0.02	0.07	0.05	3.64	0.04	0.94	0.07
199	46.4	0.4	1.20	0.08	2.41	0.04	1.03	0.02	0.04	0.05	3.44	0.03	0.91	0.07
214	44.9	0.4	1.02	0.08	7.77	0.09	1.23	0.02	0.42	0.06	6.15	0.05	0.85	0.07
216	43.4	0.4	1.13	0.08	7.98	0.10	1.88	0.03	0.35	0.06	5.86	0.05	0.75	0.07
218	42.2	0.4	1.05	0.08	7.53	0.10	1.63	0.03	0.35	0.06	6.04	0.05	0.84	0.07
225	42.6	0.5	0.81	0.36	9.29	0.25	1.74	0.06	0.45	0.15	5.39	0.09	0.84	0.14
227	45.7	0.7	0.87	0.25	7.50	0.20	0.94	0.04	0.49	0.15	5.88	0.10	0.84	0.14
228	47.4	0.7	0.94	0.21	4.67	0.14	1.33	0.05	0.36	0.14	4.24	0.08	0.79	0.13
229	46.8	0.4	1.00	0.07	5.18	0.07	1.32	0.02	0.35	0.06	4.31	0.04	0.78	0.06
231	47.5	0.4	0.97	0.07	3.81	0.06	1.54	0.02	0.32	0.06	3.63	0.03	0.76	0.06
232	47.4	0.5	0.97	0.08	3.20	0.06	1.46	0.02	0.33	0.06	3.44	0.04	0.79	0.07
235	45.3	0.6	0.94	0.22	3.01	0.12	1.38	0.05	0.30	0.13	3.93	0.08	0.90	0.14
240	45.8	0.6	0.95	0.24	7.44	0.19	0.85	0.04	0.44	0.15	6.17	0.11	0.82	0.14
259	46.4	0.5	0.90	0.08	6.65	0.09	0.76	0.02	0.46	0.06	6.22	0.05	0.84	0.07
266	45.3	0.4	0.98	0.07	7.37	0.08	1.33	0.02	0.41	0.06	5.75	0.04	0.85	0.06
274	46.4	0.4	0.91	0.08	6.52	0.08	1.42	0.02	0.43	0.06	5.18	0.04	0.86	0.07
280	45.0	0.4	1.02	0.08	6.48	0.08	0.87	0.02	0.42	0.06	6.36	0.05	0.88	0.07
284	45.1	0.4	0.98	0.08	7.38	0.09	1.32	0.02	0.43	0.06	5.90	0.05	0.86	0.07
287	45.6	0.4	0.94	0.07	5.26	0.06	1.85	0.02	0.35	0.06	4.48	0.03	0.80	0.06
291	45.4	0.4	1.04	0.08	5.92	0.08	2.62	0.03	0.40	0.06	4.39	0.04	0.80	0.07
300	46.0	0.4	0.95	0.07	3.44	0.05	2.02	0.02	0.29	0.06	4.59	0.04	0.80	0.06
304	45.5	0.4	1.04	0.08	3.05	0.05	2.47	0.03	0.24	0.06	4.62	0.04	0.78	0.07
315	46.9	0.5	0.88	0.08	5.82	0.09	0.68	0.02	0.43	0.06	6.24	0.06	0.84	0.07
334	46.3	0.5	2.63	0.11	3.47	0.07	0.59	0.02	0.54	0.06	6.86	0.07	2.16	0.09
335	43.8	0.4	5.19	0.13	2.20	0.05	0.35	0.01	0.57	0.06	8.89	0.07	2.59	0.10
342	46.7	0.5	0.84	0.08	4.80	0.08	0.57	0.01	0.40	0.06	6.20	0.06	0.70	0.07
349	47.0	0.5	1.74	0.10	4.10	0.09	0.71	0.02	0.56	0.06	6.62	0.07	1.86	0.10
353	46.4	0.4	1.79	0.09	4.40	0.08	0.72	0.02	0.53	0.06	6.67	0.06	1.97	0.09
355	45.8	0.4	2.64	0.08	2.50	0.04	0.62	0.01	0.51	0.06	6.59	0.04	2.84	0.08
356	43.4	0.4	5.07	0.12	1.94	0.04	0.60	0.01	0.53	0.06	8.78	0.07	2.99	0.10
357	43.5	0.4	5.05	0.11	1.96	0.04	0.60	0.01	0.53	0.06	8.75	0.06	2.96	0.09
374	41.6	0.4	0.99	0.08	7.86	0.09	0.92	0.02	0.16	0.05	4.85	0.04	0.71	0.07
377	37.1	0.4	0.59	0.08	12.9	0.15	0.89	0.02	0.01	0.05	5.44	0.05	0.41	0.06
380	37.3	0.4	0.49	0.08	10.6	0.15	0.72	0.02	0.00	0.05	4.90	0.06	0.45	0.07
380b	42.7	0.5	0.75	0.27	7.81	0.21	1.33	0.06	0.27	0.14	4.83	0.10	0.57	0.13
381	42.5	0.4	0.86	0.08	7.71	0.10	1.37	0.02	0.27	0.06	4.98	0.05	0.68	0.07
385b	41.8	0.6	0.29	0.83	8.48	0.52	1.26	0.08	0.19	0.15	4.72	0.13	0.53	0.16
401	21.8	0.3	5.61	0.14	31.7	0.30	0.55	0.02	0.19	0.06	6.84	0.06	0.62	0.07
416	44.1	0.5	2.72	0.11	4.70	0.08	1.14	0.03	0.76	0.07	6.06	0.06	1.89	0.09
417	42.4	0.4	4.50	0.11	3.43	0.06	0.80	0.02	0.74	0.06	7.44	0.06	2.21	0.08
427	24.9	0.3	4.69	0.11	31.6	0.25	0.73	0.02	0.40	0.06	6.94	0.05	0.88	0.07
428	46.1	0.4	0.96	0.07	5.68	0.07	0.55	0.01	0.39	0.06	6.25	0.05	0.89	0.07
429b	49.8	0.4	4.66	0.11	5.02	0.06	0.85	0.02	0.65	0.06	7.62	0.05	1.40	0.07
430	43.2	0.4	1.38	0.08	7.73	0.08	0.58	0.01	0.38	0.06	6.39	0.05	0.99	0.07
457	47.1	0.4	1.39	0.07	4.02	0.05	0.60	0.01	0.41	0.06	6.53	0.04	1.02	0.07
469	47.0	0.4	1.23	0.08	4.95	0.07	0.92	0.02	0.51	0.06	5.75	0.05	2.21	0.08
470	46.9	0.4	2.41	0.09	4.15	0.05	1.23	0.02	0.56	0.06	6.36	0.04	1.96	0.07

Sol	Cr_2O_3	SE	MnO	SE	FeO	SE	Ni	SE	Zn	SE	Br	SE
14	0.31	0.03	0.33	0.01	16.0	0.11	556	51	293	18	31	17
18	0.69	0.11	0.40	0.14	18.0	0.39	241	171	242	100	6	44
33	0.63	0.03	0.39	0.01	18.0	0.10	149	33	80	8	16	14
34	0.61	0.03	0.41	0.01	18.8	0.12	165	39	81	11	14	15
41	0.49	0.06	0.36	0.06	16.6	0.21	341	100	329	51	112	30
42	0.55	0.04	0.40	0.01	17.3	0.12	249	45	182	16	53	17
43	0.41	0.04	0.36	0.02	16.5	0.15	364	65	257	27	56	21
44	0.26	0.07	0.29	0.09	16.2	0.29	287	138	246	74	38	39
45	0.38	0.07	0.30	0.07	16.5	0.18	551	135	211	63	69	37
47	0.33	0.03	0.34	0.01	16.1	0.08	318	51	288	20	19	17
49	0.43	0.04	0.34	0.01	16.8	0.12	443	61	318	26	61	21
50	0.40	0.04	0.35	0.01	16.8	0.12	592	56	255	20	65	18
52	0.37	0.06	0.34	0.07	16.7	0.24	429	112	229	53	63	34
55	0.57	0.06	0.40	0.06	17.7	0.19	151	85	159	42	49	26
57	0.61	0.06	0.39	0.05	17.9	0.20	105	70	72	30	39	26
58	0.60	0.04	0.39	0.01	17.9	0.12	158	41	95	13	37	16
59	0.68	0.03	0.41	0.01	18.6	0.12	202	39	117	11	49	16
60	0.60	0.03	0.41	0.01	18.8	0.12	164	39	112	11	52	16
63	0.57	0.06	0.42	0.07	18.9	0.24	27	81	134	43	42	31
65	0.31	0.06	0.31	0.07	15.9	0.24	620	131	435	67	0	10
71	0.31	0.04	0.31	0.02	16.5	0.15	641	73	409	32	30	22
74	0.46	0.04	0.36	0.01	17.0	0.13	475	60	210	22	53	19
81	0.26	0.04	0.32	0.02	17.9	0.15	553	63	457	28	100	21
81b	0.35	0.04	0.33	0.01	18.0	0.14	471	54	391	23	37	18
82	0.45	0.03	0.40	0.01	18.4	0.12	342	46	222	16	144	18
83	0.21	0.03	0.33	0.01	17.4	0.13	607	58	579	26	64	20
86	0.54	0.03	0.42	0.01	18.9	0.12	132	39	75	11	161	17
100	0.53	0.03	0.39	0.01	17.7	0.11	181	37	125	10	46	15
105	0.32	0.07	0.34	0.08	15.8	0.25	237	129	308	74	11	35
113	0.37	0.06	0.31	0.06	16.1	0.19	467	108	192	50	32	31
114	0.36	0.03	0.34	0.01	16.8	0.10	466	45	460	17	64	16
115	0.43	0.04	0.34	0.02	17.1	0.14	466	64	382	28	47	21
122	0.33	0.06	0.28	0.07	15.4	0.21	391	100	239	48	31	31
126	0.29	0.07	0.32	0.08	15.9	0.25	641	141	402	73	0	10
135	0.42	0.06	0.34	0.06	16.1	0.20	483	95	291	45	19	26
140	0.39	0.03	0.36	0.01	17.5	0.11	507	49	285	17	162	19
141	0.39	0.04	0.34	0.01	16.5	0.12	438	54	253	20	205	21
150a	0.53	0.06	0.37	0.07	18.7	0.22	97	80	159	39	89	28
158	0.36	0.06	0.33	0.06	15.3	0.21	536	102	200	45	36	29
164	0.21	0.03	0.20	0.01	15.6	0.11	737	51	97	13	73	18
167	0.27	0.06	0.32	0.06	16.0	0.21	854	118	110	42	36	27
170	0.19	0.03	0.17	0.01	15.1	0.12	777	57	80	15	73	18
172	0.27	0.03	0.24	0.01	16.7	0.12	894	52	112	13	77	17

Sol	Cr_2O_3	SE	MnO	SE	FeO	SE	Ni	SE	Zn	SE	Br	SE
176	0.31	0.04	0.28	0.01	15.3	0.09	704	63	150	21	34	18
178	0.23	0.03	0.29	0.01	16.6	0.13	533	56	201	19	69	18
195	0.24	0.03	0.20	0.01	16.7	0.11	516	44	193	13	185	17
197	0.27	0.03	0.10	0.01	16.3	0.11	607	47	89	12	318	20
199	0.18	0.03	0.13	0.01	19.2	0.12	553	46	54	11	493	21
214	0.19	0.03	0.27	0.01	15.0	0.10	562	44	175	12	908	24
216	0.18	0.03	0.27	0.01	14.3	0.10	538	47	107	13	901	26
218	0.17	0.03	0.30	0.01	15.6	0.08	735	55	118	16	239	20
225	0.18	0.05	0.23	0.06	14.9	0.15	670	94	99	33	993	45
227	0.28	0.05	0.31	0.06	16.3	0.20	533	100	264	44	263	37
228	0.14	0.04	0.21	0.04	15.1	0.18	453	80	146	32	193	29
229	0.17	0.03	0.17	0.01	15.3	0.10	478	41	92	9	267	17
231	0.16	0.03	0.15	0.01	15.0	0.10	497	43	72	10	293	18
232	0.16	0.03	0.16	0.01	15.6	0.11	523	47	99	13	222	19
235	0.18	0.05	0.18	0.04	17.1	0.20	731	93	56	29	352	36
240	0.21	0.05	0.29	0.05	15.8	0.19	548	95	285	42	9	27
259	0.29	0.03	0.30	0.01	15.3	0.11	467	48	293	17	24	16
266	0.19	0.03	0.35	0.01	15.4	0.10	568	42	175	11	1543	28
274	0.20	0.03	0.28	0.01	14.7	0.08	558	48	204	15	694	23
280	0.34	0.03	0.34	0.01	16.2	0.11	469	47	252	15	101	17
284	0.19	0.03	0.30	0.01	15.2	0.11	564	47	206	14	735	24
287	0.15	0.03	0.25	0.01	13.9	0.06	593	41	118	9	674	20
291	0.16	0.03	0.23	0.01	13.9	0.10	547	44	158	12	903	24
300	0.16	0.03	0.17	0.01	14.2	0.09	629	42	103	10	581	20
304	0.16	0.03	0.18	0.01	14.1	0.10	605	46	112	12	339	19
315	0.31	0.04	0.32	0.01	15.1	0.12	412	51	237	18	13	17
334	0.01	0.03	0.22	0.01	11.5	0.10	99	41	96	14	14	17
335	0.00	0.02	0.22	0.01	11.6	0.10	67	40	64	13	22	16
342	0.33	0.03	0.31	0.01	15.5	0.12	679	52	162	15	37	17
349	0.03	0.03	0.25	0.01	12.2	0.11	57	48	122	19	58	19
353	0.04	0.03	0.25	0.01	13.3	0.08	86	44	105	15	54	18
355	0.00	0.02	0.22	0.01	12.6	0.08	41	30	71	7	38	13
356	0.00	0.02	0.24	0.01	12.5	0.09	24	40	81	13	72	18
357	0.00	0.02	0.25	0.01	12.5	0.08	45	41	58	13	68	16
374	0.57	0.04	0.41	0.01	19.1	0.09	603	52	138	15	160	18
377	0.59	0.04	0.42	0.01	18.7	0.13	540	49	94	13	181	19
380	0.75	0.05	0.47	0.02	20.4	0.16	774	72	64	22	71	22
380b	0.54	0.06	0.40	0.08	18.4	0.18	498	113	287	55	237	37
381	0.57	0.04	0.40	0.01	18.8	0.13	565	49	225	15	244	19
385b	0.63	0.09	0.33	0.10	18.3	0.23	506	171	205	78	217	47
401	0.04	0.03	0.25	0.01	21.0	0.12	109	49	98	18	494	26
416	0.00	0.03	0.22	0.01	13.3	0.11	58	45	132	17	262	21
417	0.00	0.02	0.22	0.01	13.2	0.10	67	37	140	12	251	19
427	0.35	0.03	0.30	0.01	16.1	0.09	561	46	116	12	478	20
428	0.38	0.03	0.33	0.01	15.9	0.11	414	43	209	13	52	15
429b	0.47	0.03	0.16	0.01	5.6	0.04	592	40	58	8	65	14
430	0.37	0.03	0.34	0.01	17.2	0.11	395	40	235	12	69	15
457	0.23	0.03	0.30	0.01	14.4	0.06	424	39	123	9	52	14
469	0.11	0.03	0.31	0.01	12.8	0.07	155	40	117	13	232	18
470	0.05	0.03	0.27	0.01	10.5	0.05	92	34	81	9	204	16

APXS Sensor Head

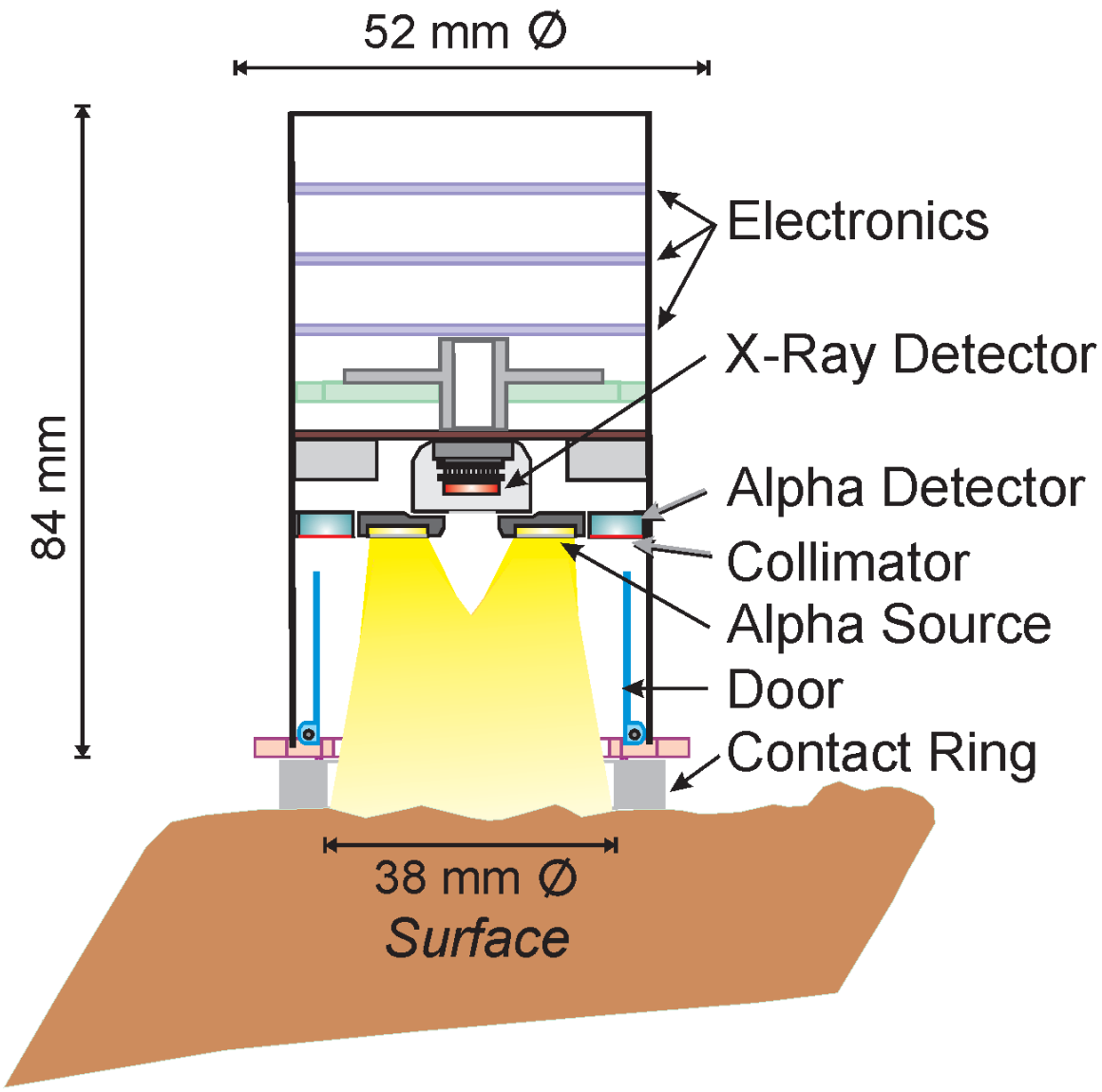

APXS Front View

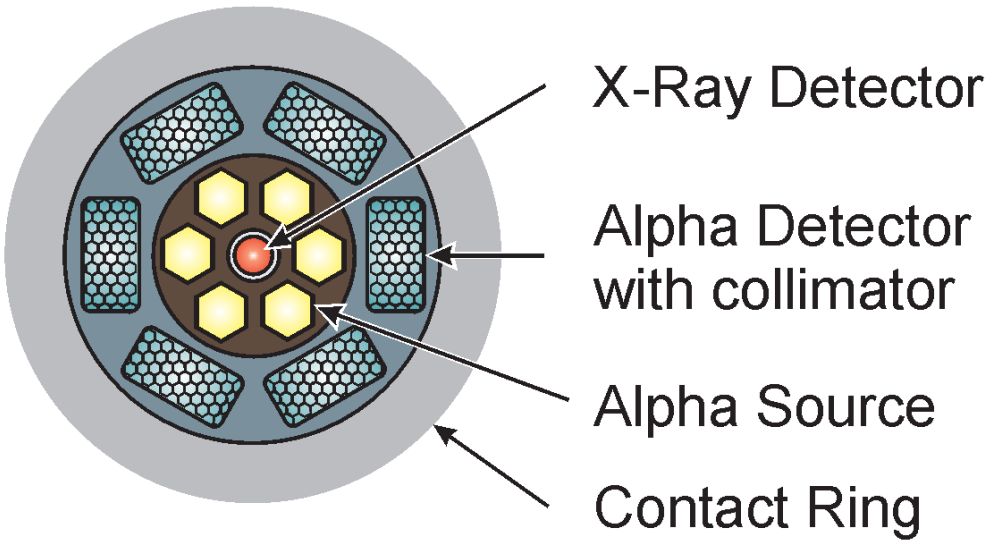

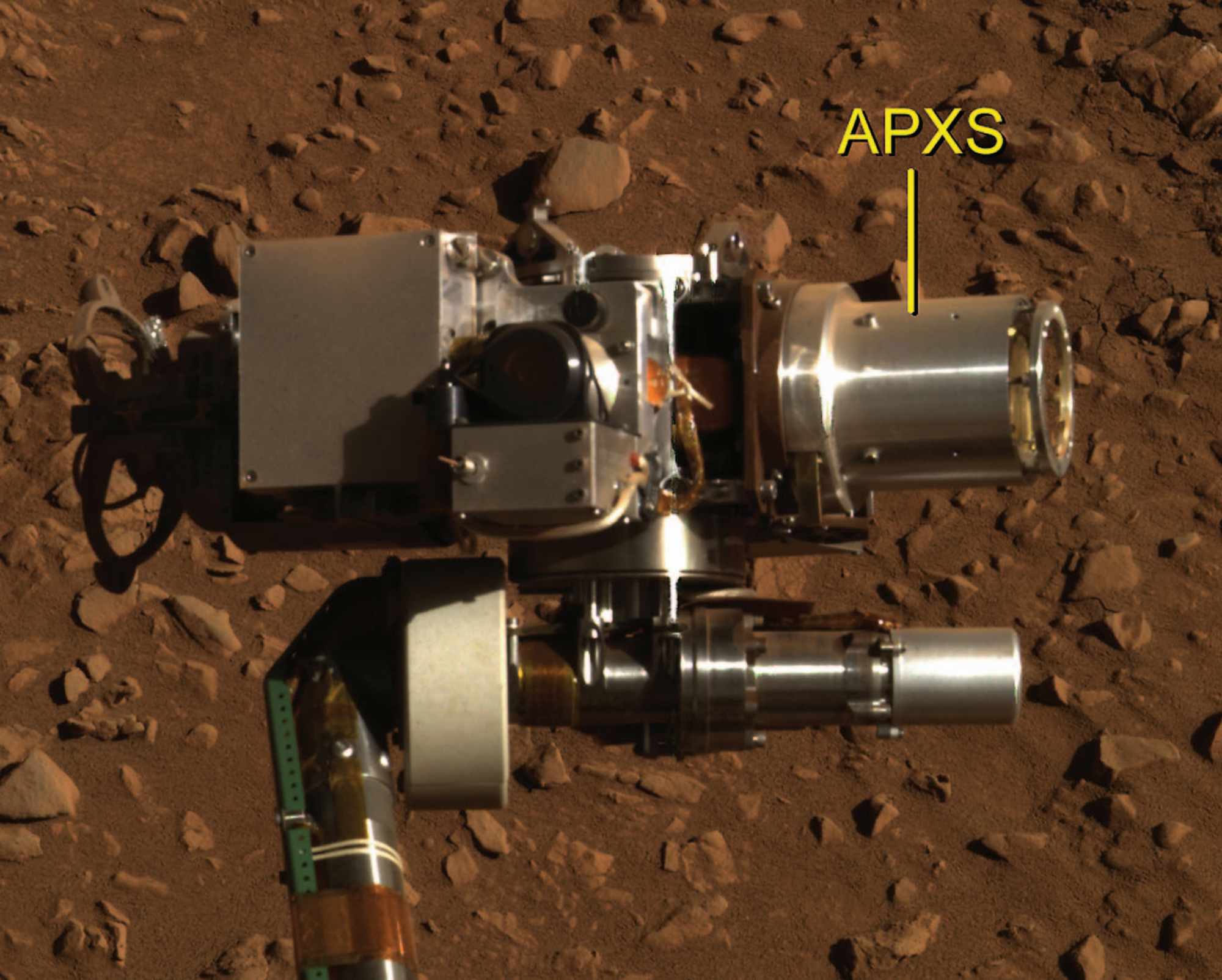
APXS

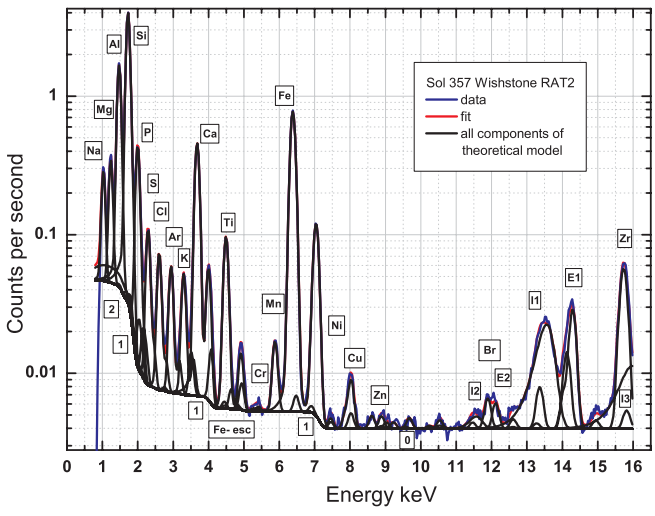
Sol 357 Wishstone RAT2
data
fit
all components of theoretical model
Counts per second
Energy keV
Al
Si
Mg
Na
P
S
Cl
Ar
K
Ca
Ti
Fe
Mn
Cr
Ni
Cu
Zn
Br
E1
I1
E2
I2
I3
Zr
Fe- esc
1
2
0
0.01
0.1
1
0 1 2 3 4 5 6 7 8 9 10 11 12 13 14 15 16

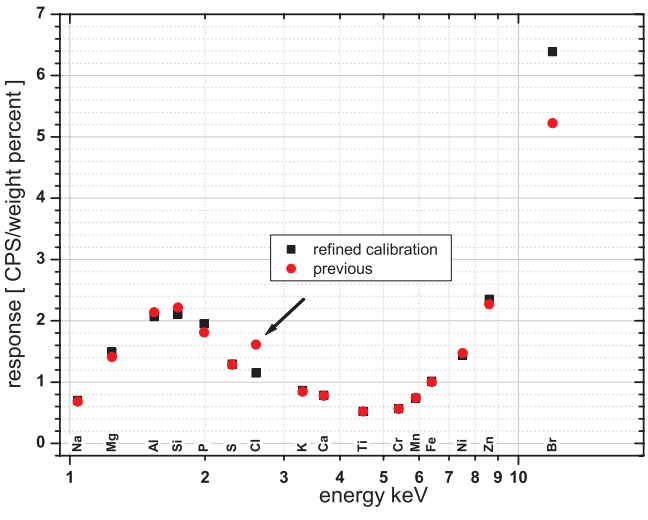
response [CPS/weight percent]
energy keV
refined calibration
previous
Na
Mg
Al
Si
P
S
Cl
K
Ca
Ti
Cr
Mn
Fe
Ni
Zn
Br

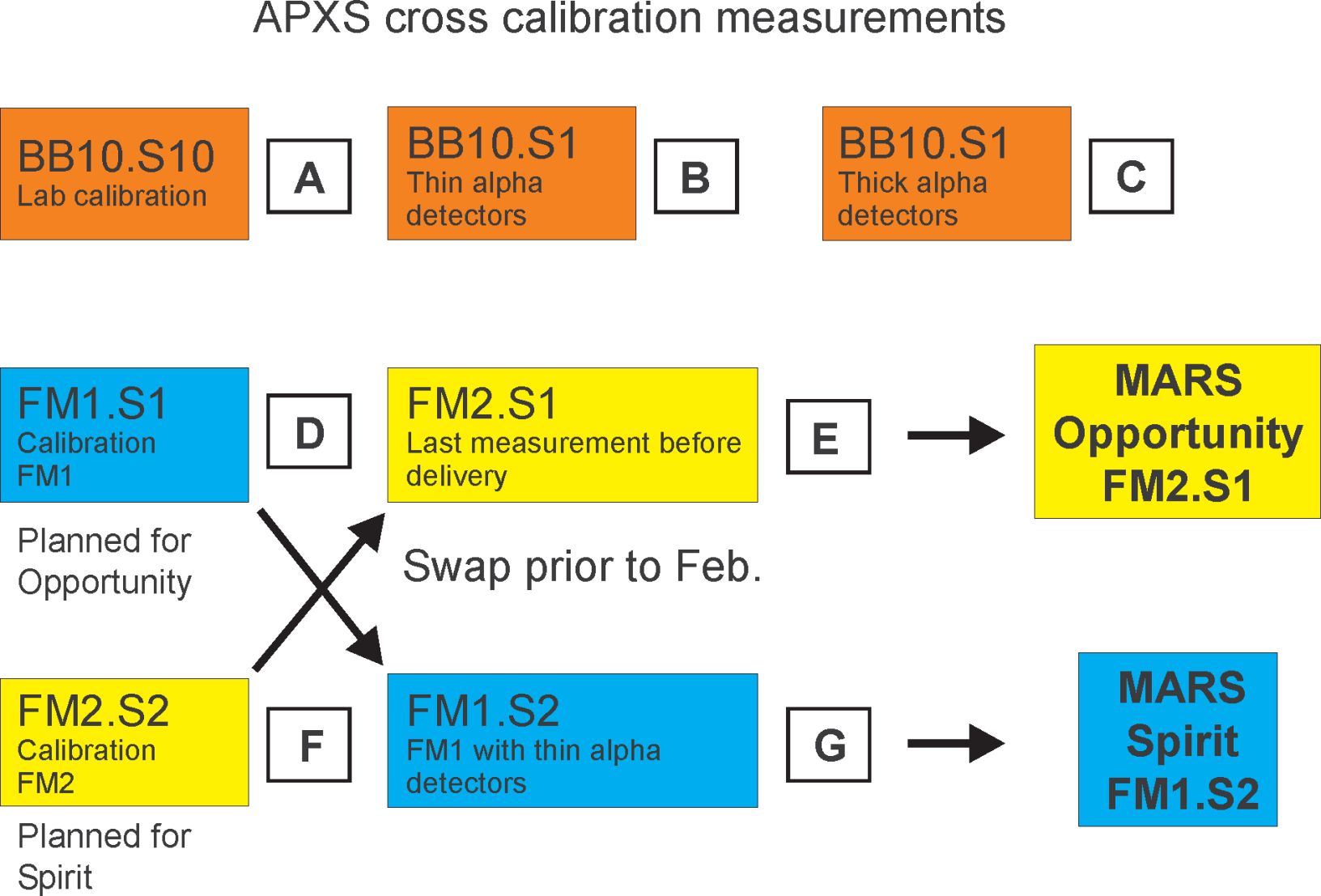
APXS cross calibration measurements
BB10.S10
Lab calibration
A
BB10.S1
Thin alpha
detectors
B
BB10.S1
Thick alpha
detectors
C
FM1.S1
Calibration
FM1
D
FM2.S1
Last measurement before
delivery
E
MARS
Opportunity
FM2.S1
Planned for
Opportunity
Swap prior to Feb.
FM2.S2
Calibration
FM2
F
FM1.S2
FM1 with thin alpha
detectors
G
MARS
Spirit
FM1.S2
Planned for
Spirit

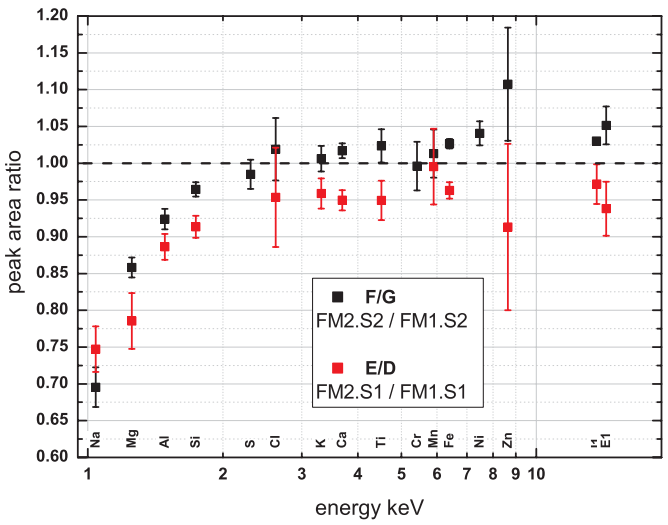
peak area ratio
energy keV
F/G
FM2.S2 / FM1.S2
E/D
FM2.S1 / FM1.S1
Na
Mg
Al
Si
S
Cl
K
Ca
Ti
Cr
Mn
Fe
Ni
Zn

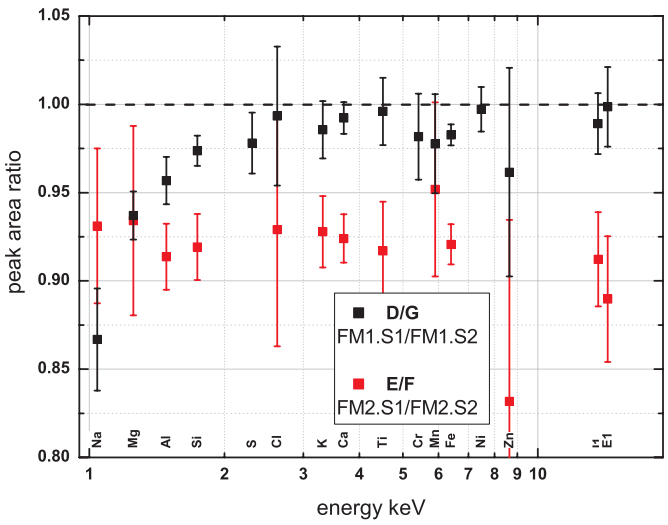
peak area ratio
energy keV
D/G
FM1.S1/FM1.S2
E/F
FM2.S1/FM2.S2
Na
Mg
Al
Si
S
Cl
K
Ca
Ti
Cr
Mn
Fe
Ni
Zn
E1

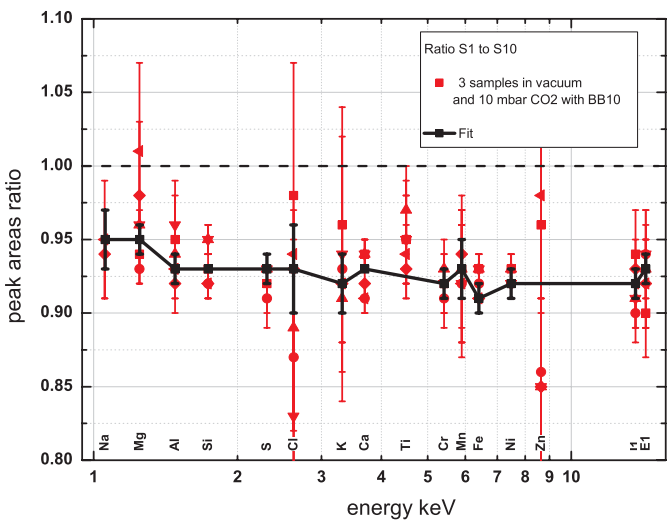
Ratio S1 to S10
3 samples in vacuum
and 10 mbar CO2 with BB10
Fit
peak areas ratio
energy keV
1.10
1.05
1.00
0.95
0.90
0.85
0.80
1
2
3
4
5
6
7
8
9
10
Na
Mg
Al
Si
S
Cl
K
Ca
Ti
Cr
Mn
Fe
Ni
Zn
E1
E1

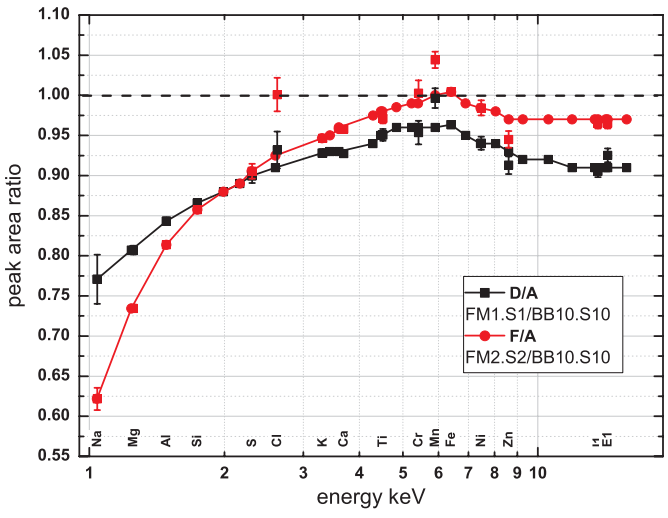
peak area ratio
energy keV
D/A
FM1.S1/BB10.S10
F/A
FM2.S2/BB10.S10
Na
Mg
Al
Si
S
Cl
K
Ca
Ti
Cr
Mn
Fe
Ni
Zn

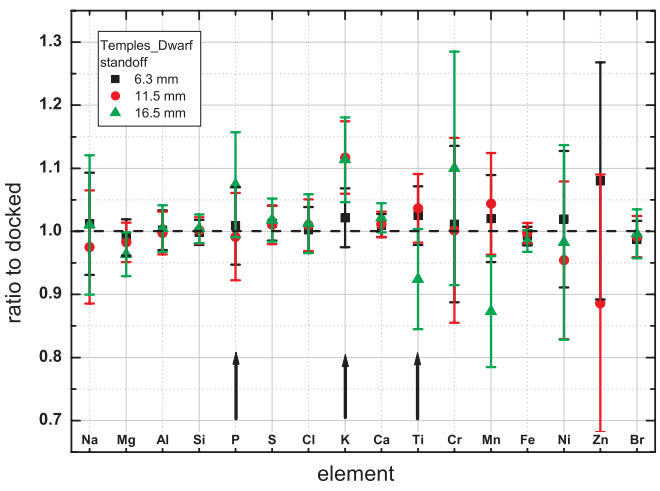
Temples_Dwarf
standoff
6.3 mm
11.5 mm
16.5 mm
ratio to docked
element
1.3
1.2
1.1
1.0
0.9
0.8
0.7
Na
Mg
Al
Si
P
S
Cl
K
Ca
Ti
Cr
Mn
Fe
Ni
Zn
Br

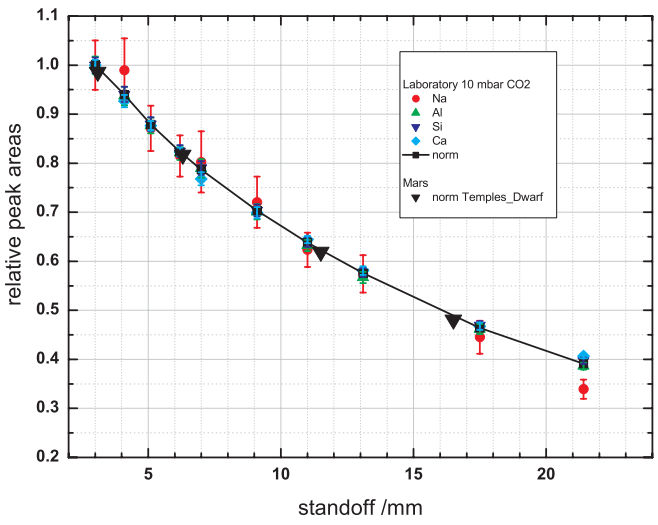
relative peak areas
standoff /mm
1.1
1.0
0.9
0.8
0.7
0.6
0.5
0.4
0.3
0.2
5
10
15
20
Laboratory 10 mbar CO2
Na
Al
Si
Ca
norm
Mars
norm Temples_Dwarf

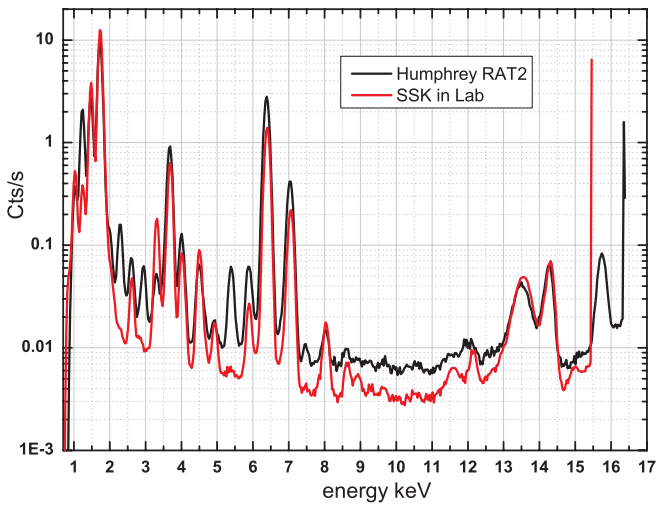
Humphrey RAT2
SSK in Lab
Cts/s
10
1
0.1
0.01
1E-3
1
2
3
4
5
6
7
8
9
10
11
12
13
14
15
16
17
energy keV

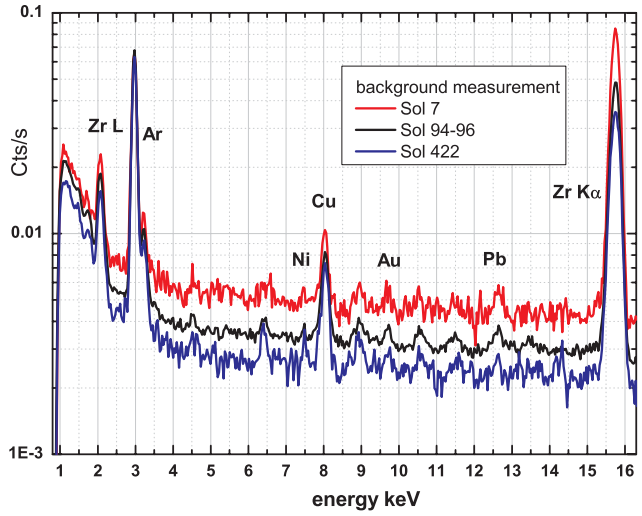
0.1
0.01
1E-3
Cts/s
1
2
3
4
5
6
7
8
9
10
11
12
13
14
15
16
energy keV
background measurement
Sol 7
Sol 94-96
Sol 422
Zr L
Ar
Cu
Ni
Au
Pb
Zr Kα

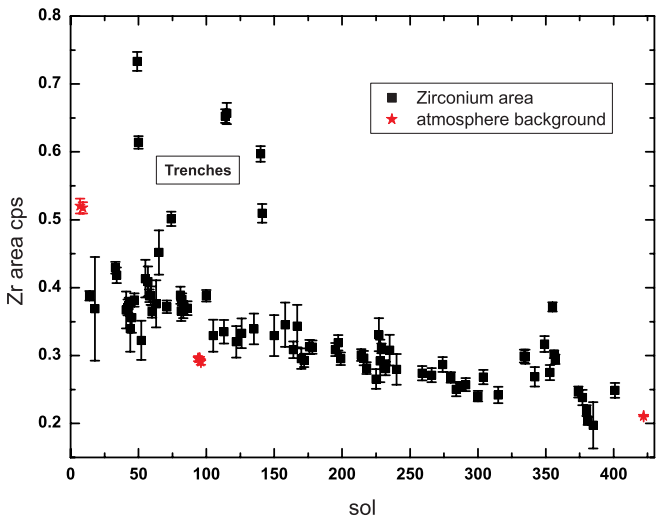
Zirconium area
atmosphere background
Trenches
Zr area cps
sol
0.8
0.7
0.6
0.5
0.4
0.3
0.2
0
50
100
150
200
250
300
350
400

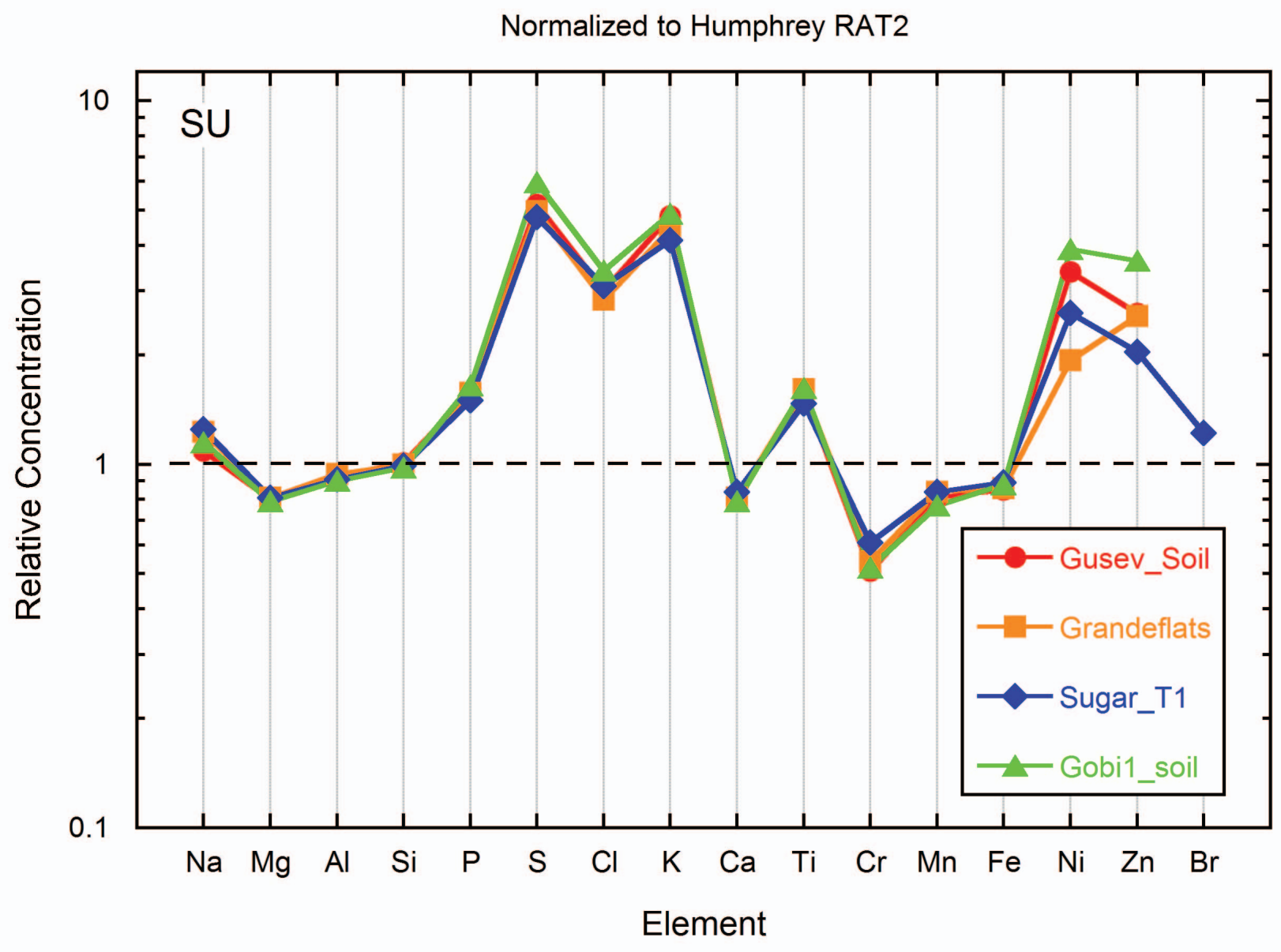
Normalized to Humphrey RAT2
SU
10
1
0.1
Relative Concentration
Na
Mg
Al
Si
P
S
Cl
K
Ca
Ti
Cr
Mn
Fe
Ni
Zn
Br
Element
Gusev_Soil
Grandeflats
Sugar_T1
Gobi1_soil

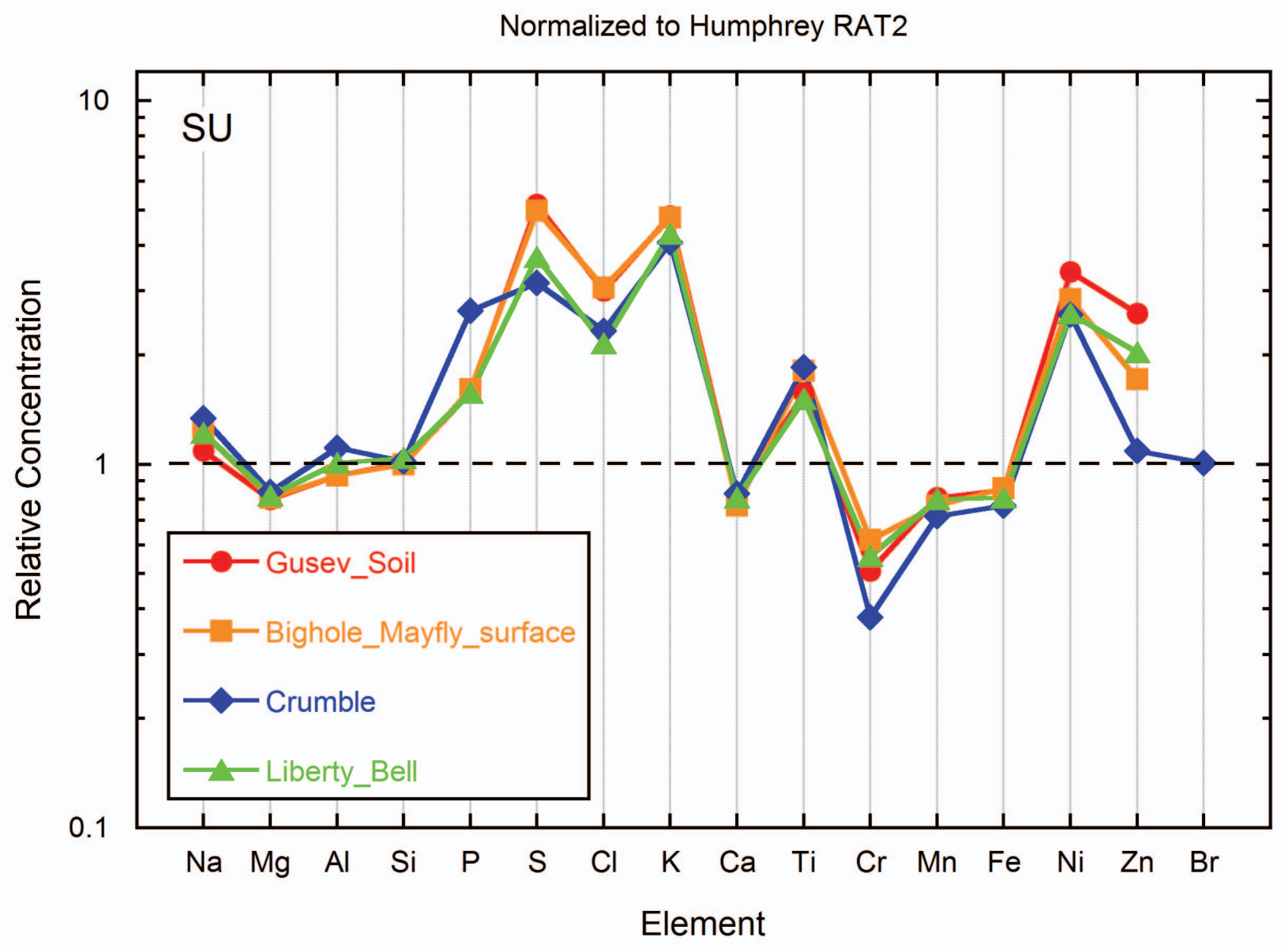
Normalized to Humphrey RAT2
SU
10
1
0.1
Relative Concentration
Gusev_Soil
Bighole_Mayfly_surface
Crumble
Liberty_Bell
Na
Mg
Al
Si
P
S
Cl
K
Ca
Ti
Cr
Mn
Fe
Ni
Zn
Br
Element

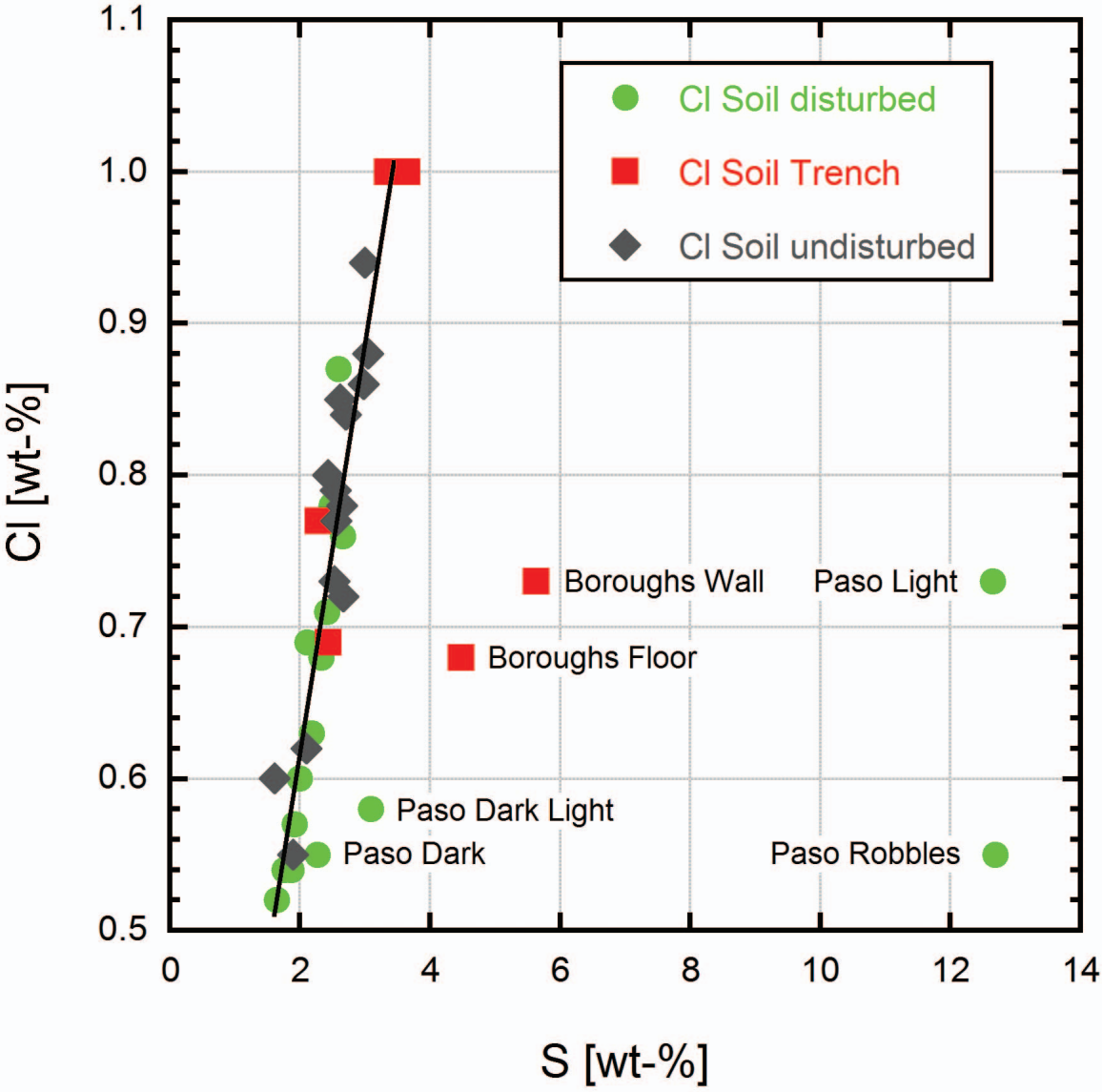
Cl Soil disturbed
Cl Soil Trench
Cl Soil undisturbed
Boroughs Wall
Paso Light
Boroughs Floor
Paso Dark Light
Paso Dark
Paso Robbles
Cl [wt-%]
S [wt-%]
1.1
1.0
0.9
0.8
0.7
0.6
0.5
0
2
4
6
8
10
12
14

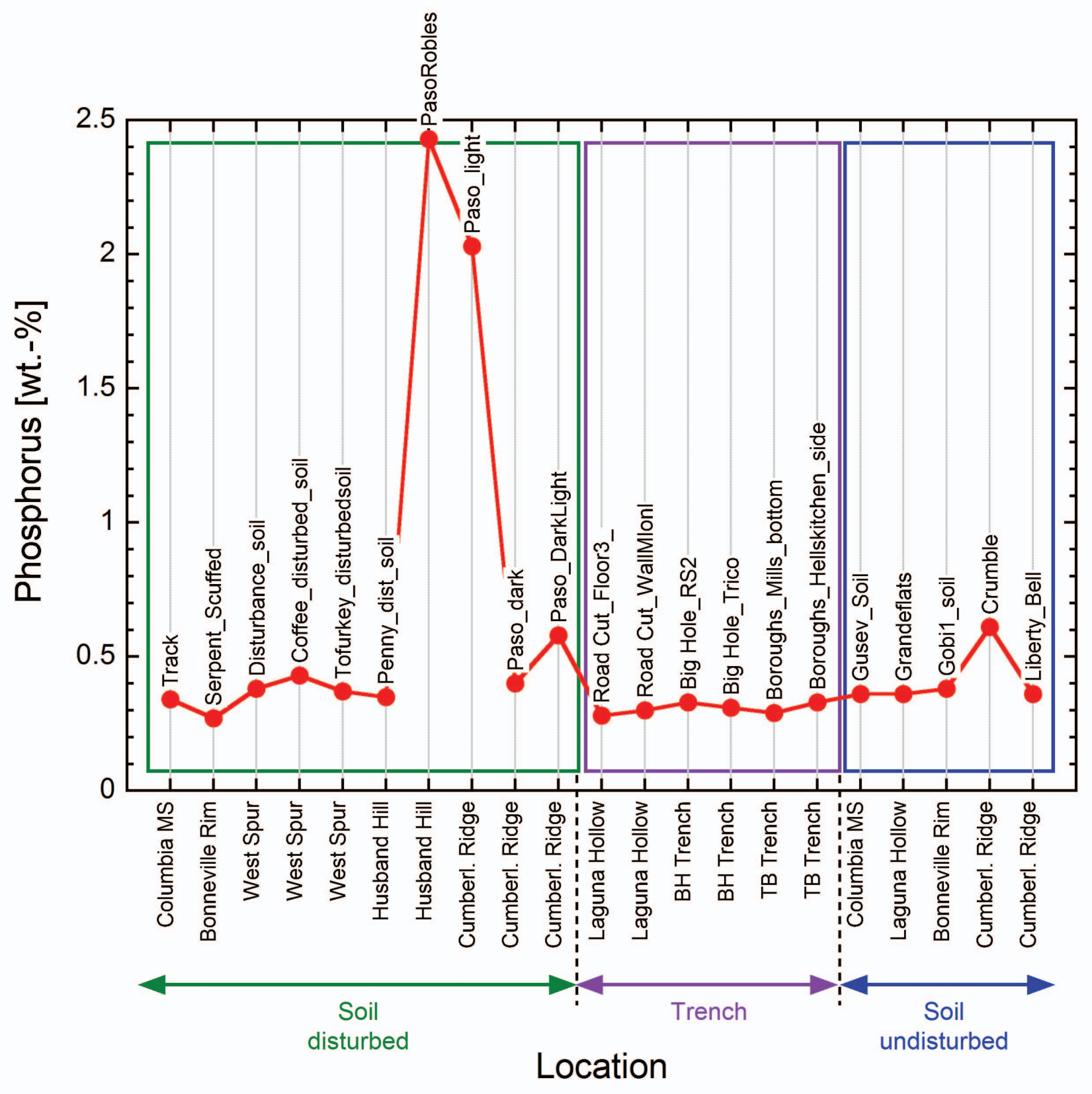
Phosphorus [wt.-%]
2.5
2
1.5
1
0.5
0
PasoRobles
Paso_light
Track
Serpent_Scuffed
Disturbance_soil
Coffee_disturbed_soil
Tofurkey_disturbedsoil
Penny_dist_soil
Paso_dark
Paso_DarkLight
Road Cut_Floor3_
Road Cut_WallMIonl
Big Hole_RS2
Big Hole_Trico
Boroughs_Mills_bottom
Boroughs_Hellskitchen_side
Gusev_Soil
Grandeflats
Gobi1_soil
Crumble
Liberty_Bell
Columbia MS
Bonneville Rim
West Spur
West Spur
West Spur
Husband Hill
Husband Hill
Cumberl. Ridge
Cumberl. Ridge
Cumberl. Ridge
Laguna Hollow
Laguna Hollow
BH Trench
BH Trench
TB Trench
TB Trench
Columbia MS
Laguna Hollow
Bonneville Rim
Cumberl. Ridge
Cumberl. Ridge
Soil
disturbed
Trench
Soil
undisturbed
Location

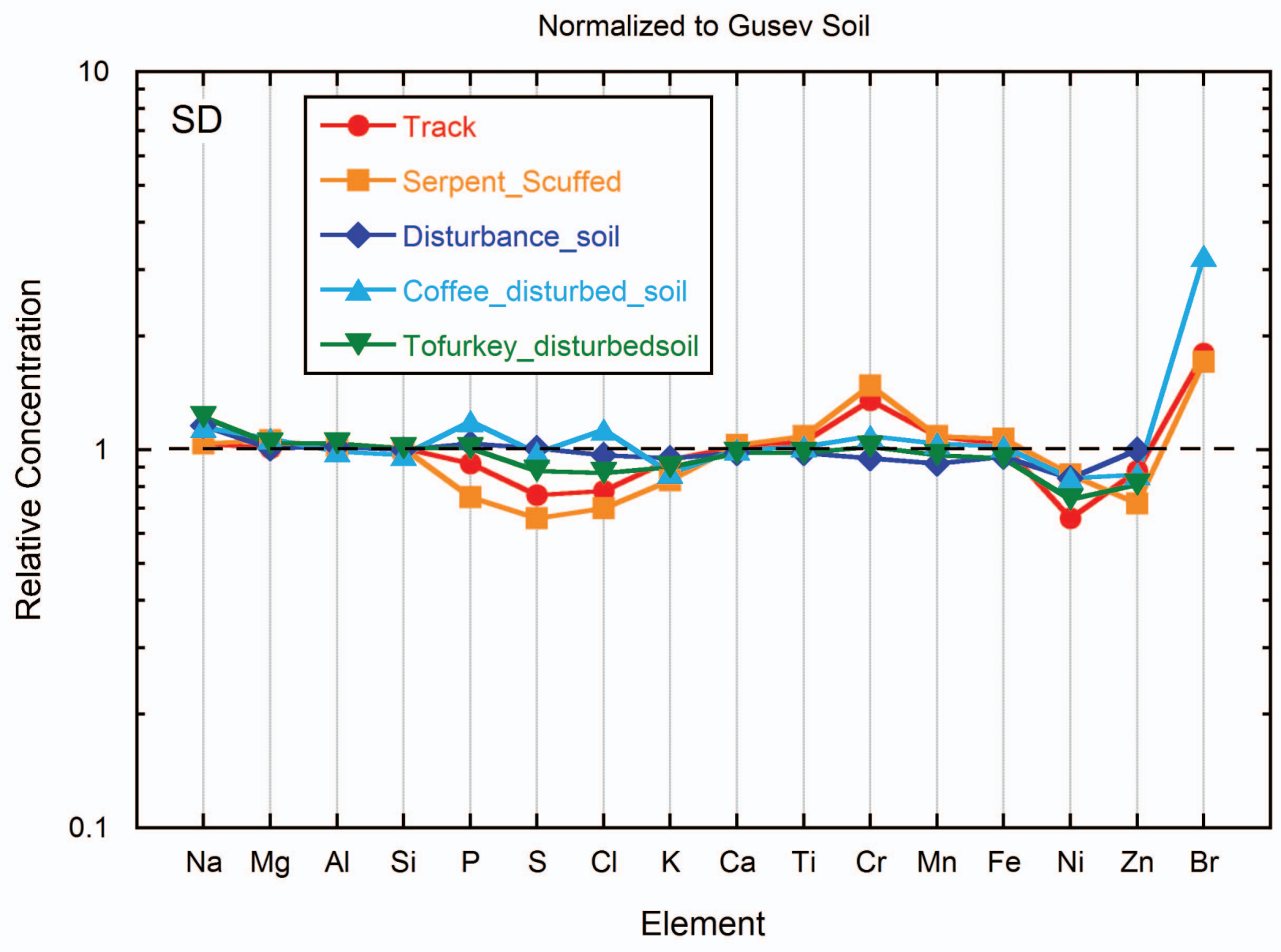
Normalized to Gusev Soil
SD
Track
Serpent_Scuffed
Disturbance_soil
Coffee_disturbed_soil
Tofurkey_disturbedsoil
Relative Concentration
10
1
0.1
Na
Mg
Al
Si
P
S
Cl
K
Ca
Ti
Cr
Mn
Fe
Ni
Zn
Br
Element

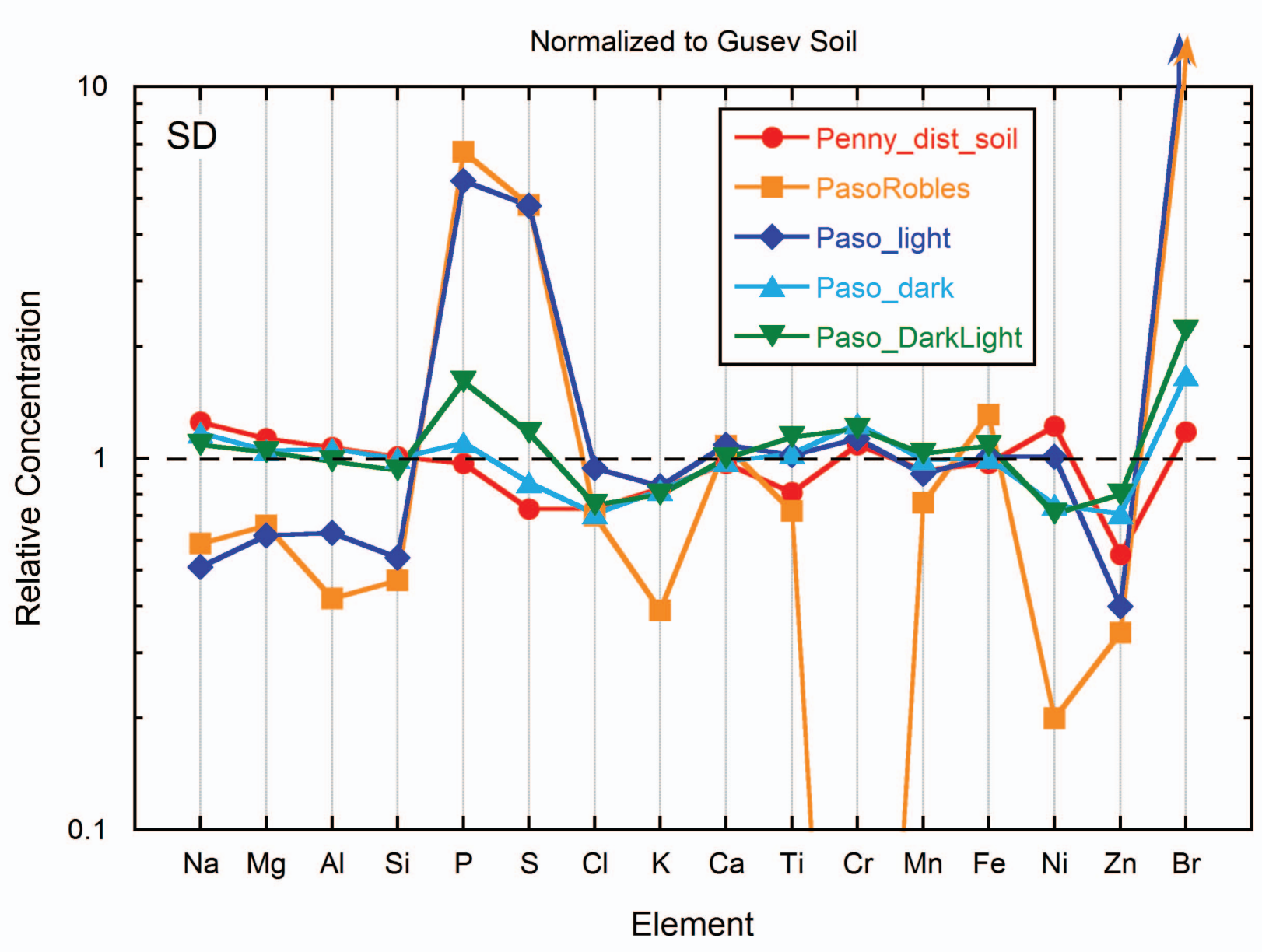
Normalized to Gusev Soil
SD
Penny_dist_soil
PasoRobles
Paso_light
Paso_dark
Paso_DarkLight
10
1
0.1
Relative Concentration
Na
Mg
Al
Si
P
S
Cl
K
Ca
Ti
Cr
Mn
Fe
Ni
Zn
Br
Element

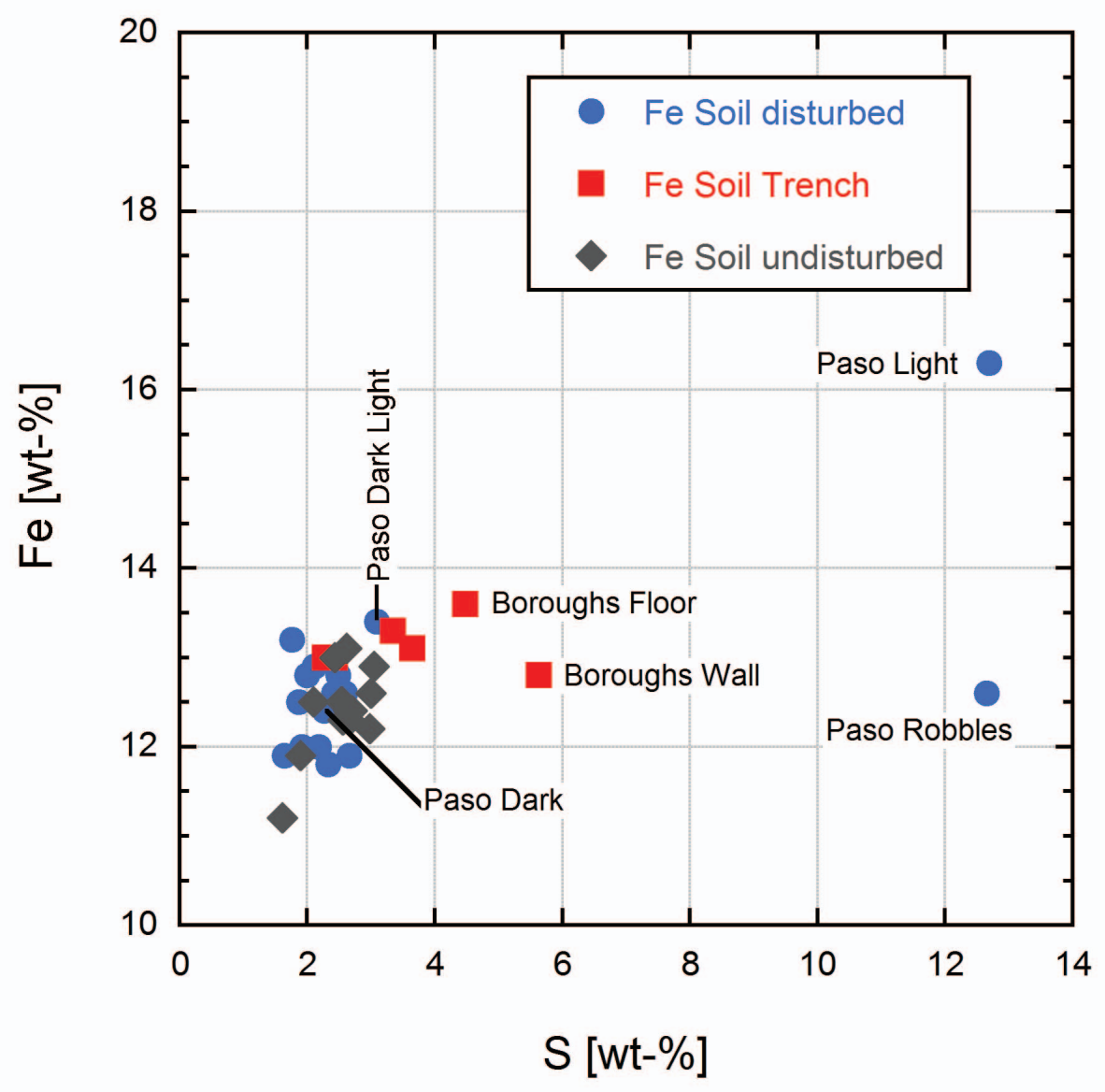
Fe Soil disturbed
Fe Soil Trench
Fe Soil undisturbed
Paso Light
Paso Dark Light
Boroughs Floor
Boroughs Wall
Paso Robbles
Paso Dark
Fe [wt-%]
S [wt-%]
20
18
16
14
12
10
0
2
4
6
8
10
12
14

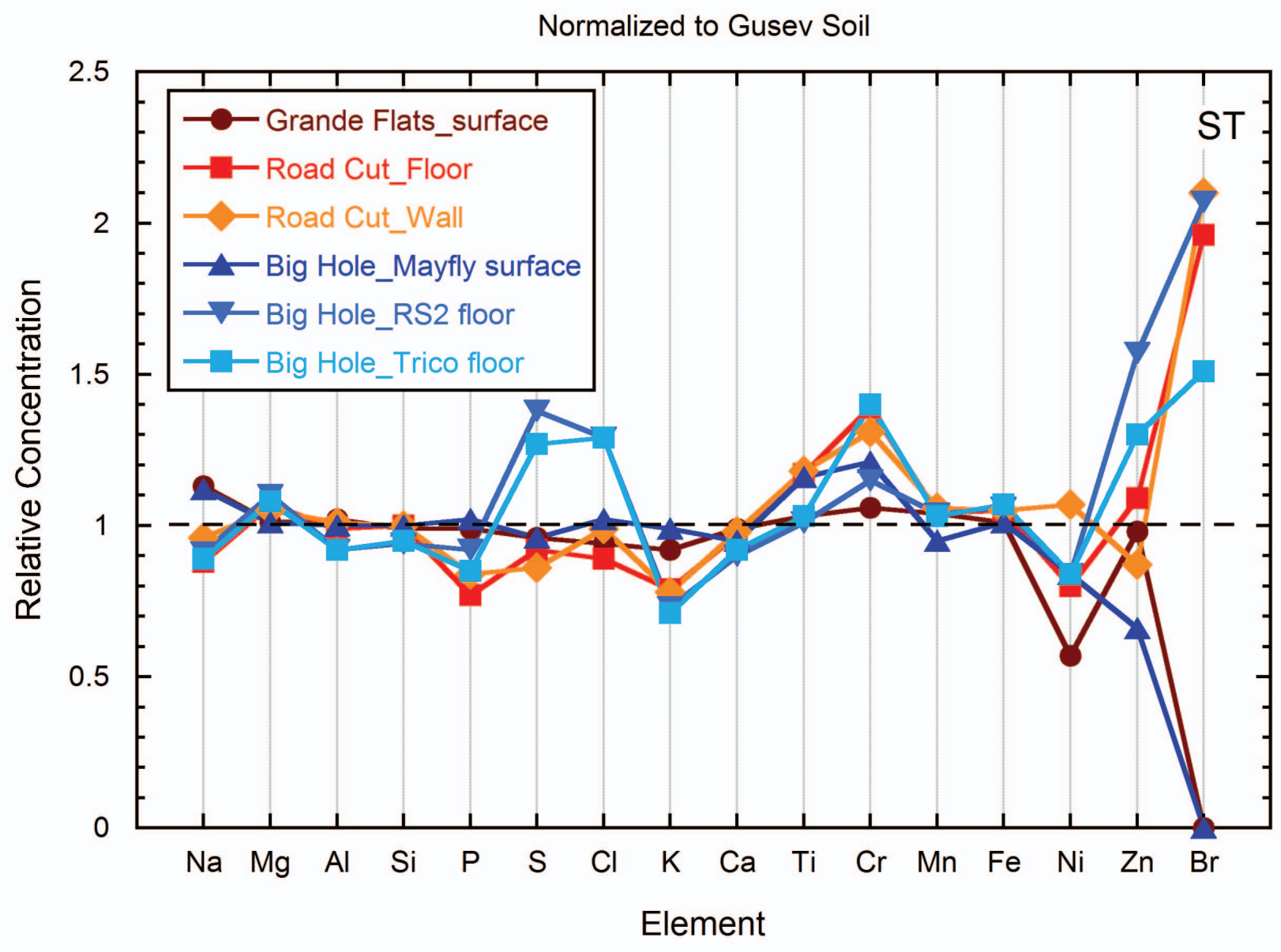
Normalized to Gusev Soil
Grande Flats_surface
Road Cut_Floor
Road Cut_Wall
Big Hole_Mayfly surface
Big Hole_RS2 floor
Big Hole_Trico floor
ST
Relative Concentration
2.5
2
1.5
1
0.5
0
Na
Mg
Al
Si
P
S
Cl
K
Ca
Ti
Cr
Mn
Fe
Ni
Zn
Br
Element

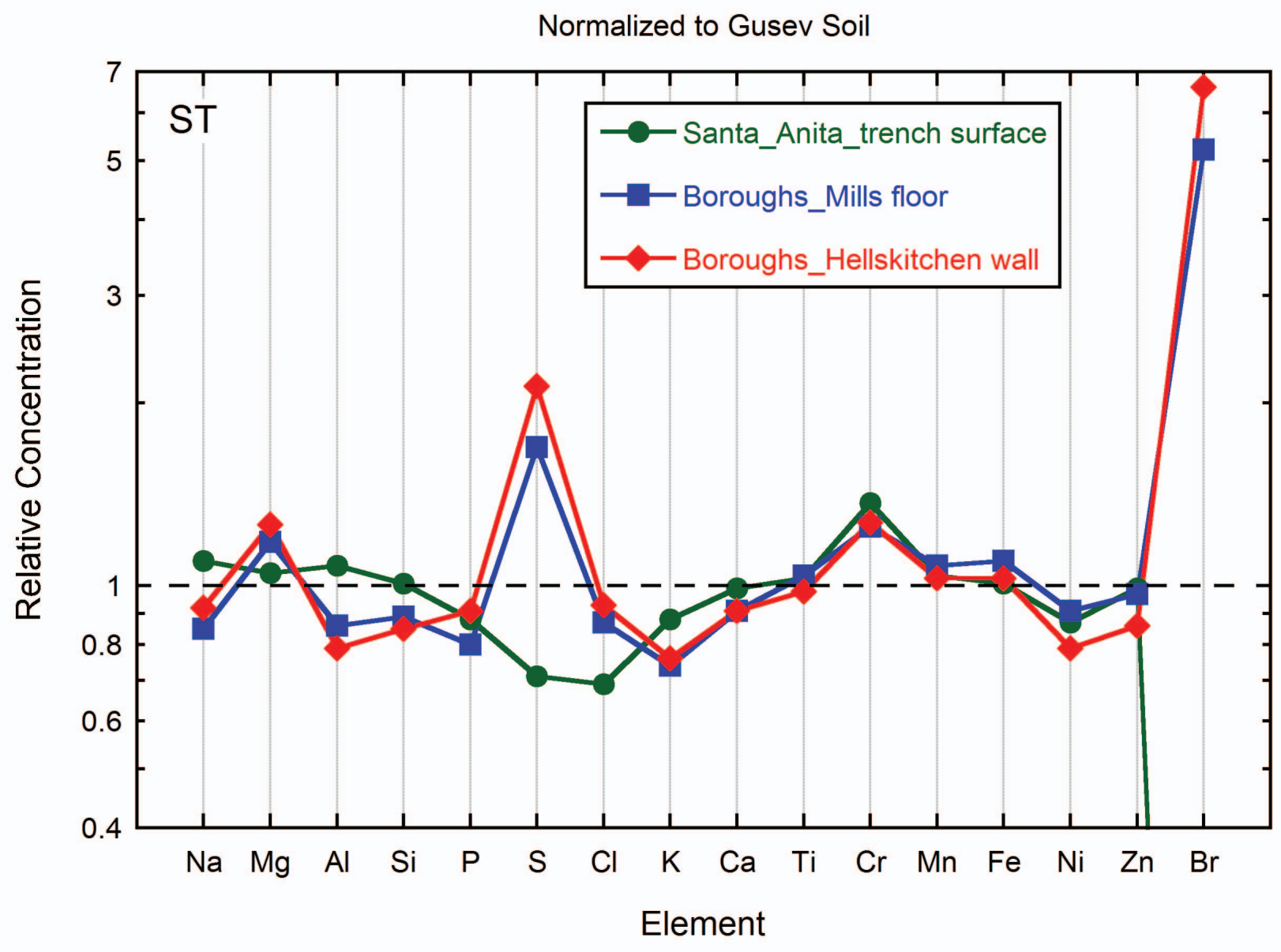
Normalized to Gusev Soil
ST
Santa_Anita_trench surface
Boroughs_Mills floor
Boroughs_Hellskitchen wall
Relative Concentration
7
5
3
1
0.8
0.6
0.4
Na
Mg
Al
Si
P
S
Cl
K
Ca
Ti
Cr
Mn
Fe
Ni
Zn
Br
Element

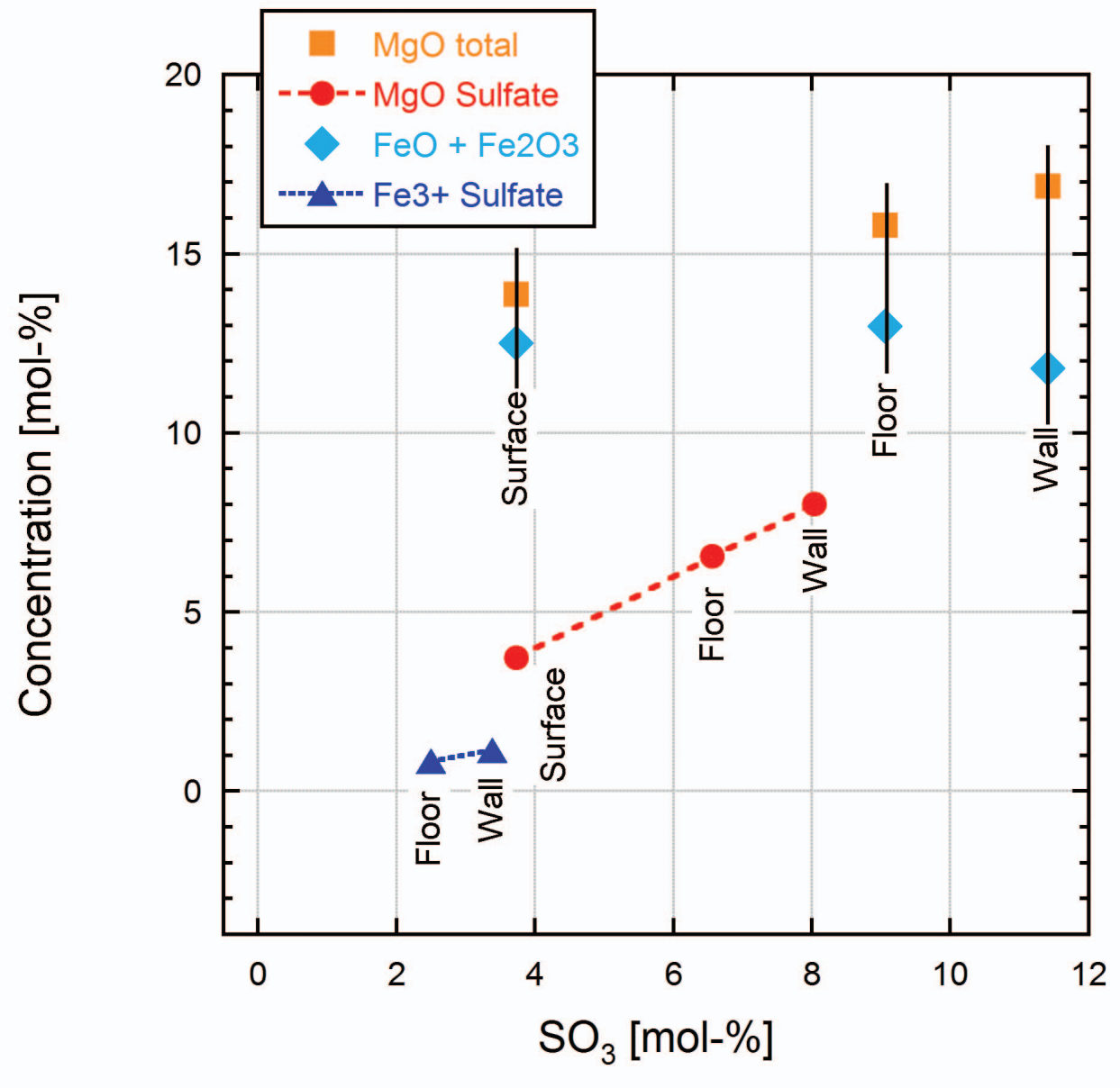
MgO total
MgO Sulfate
FeO + Fe2O3
Fe3+ Sulfate
Concentration [mol-%]
SO3 [mol-%]
0
5
10
15
20
0
2
4
6
8
10
12
Surface
Floor
Wall
Surface
Floor
Wall
Floor
Wall

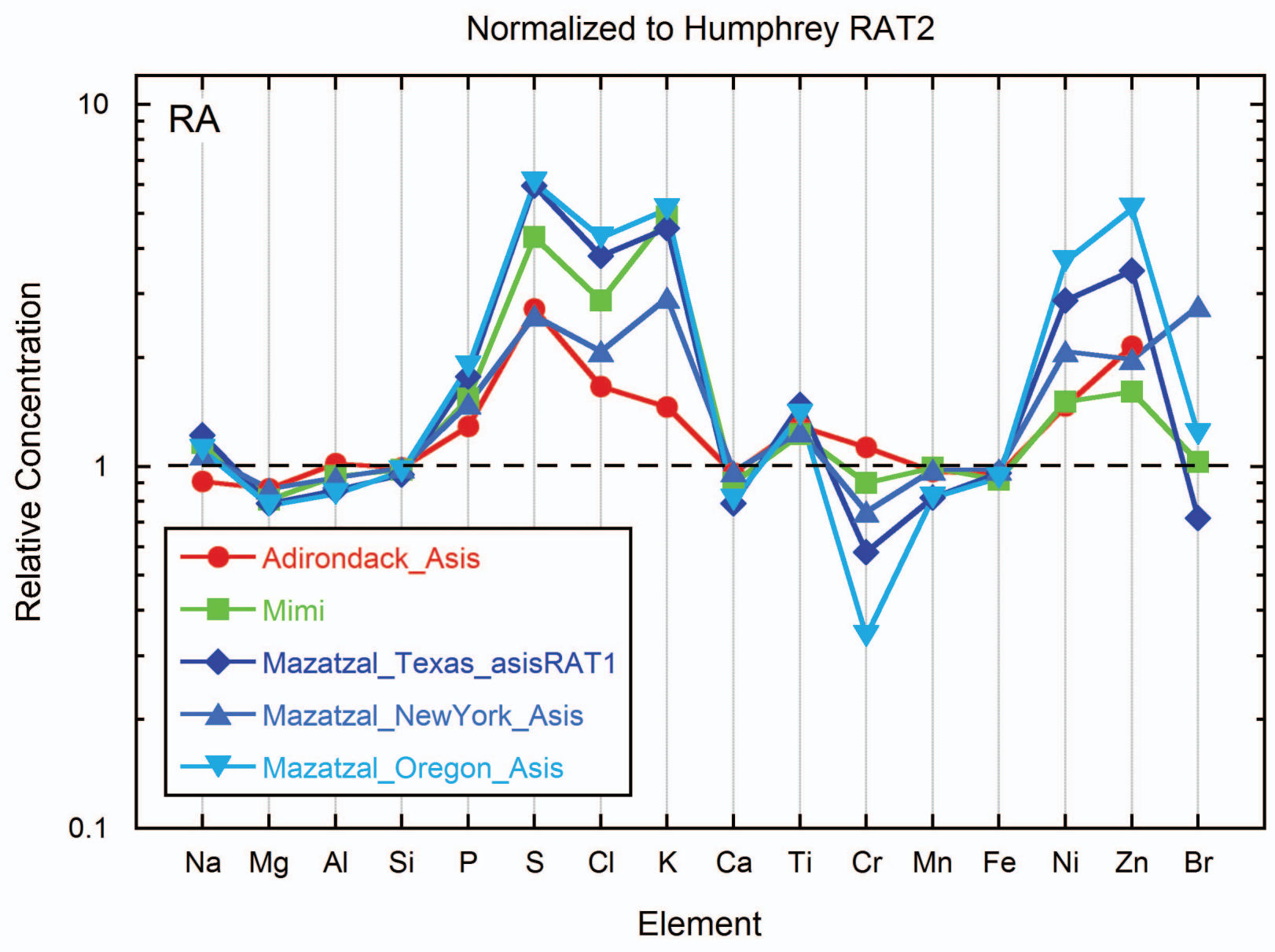
Normalized to Humphrey RAT2
RA
10
1
0.1
Relative Concentration
Adirondack_Asis
Mimi
Mazatzal_Texas_asisRAT1
Mazatzal_NewYork_Asis
Mazatzal_Oregon_Asis
Na
Mg
Al
Si
P
S
Cl
K
Ca
Ti
Cr
Mn
Fe
Ni
Zn
Br
Element

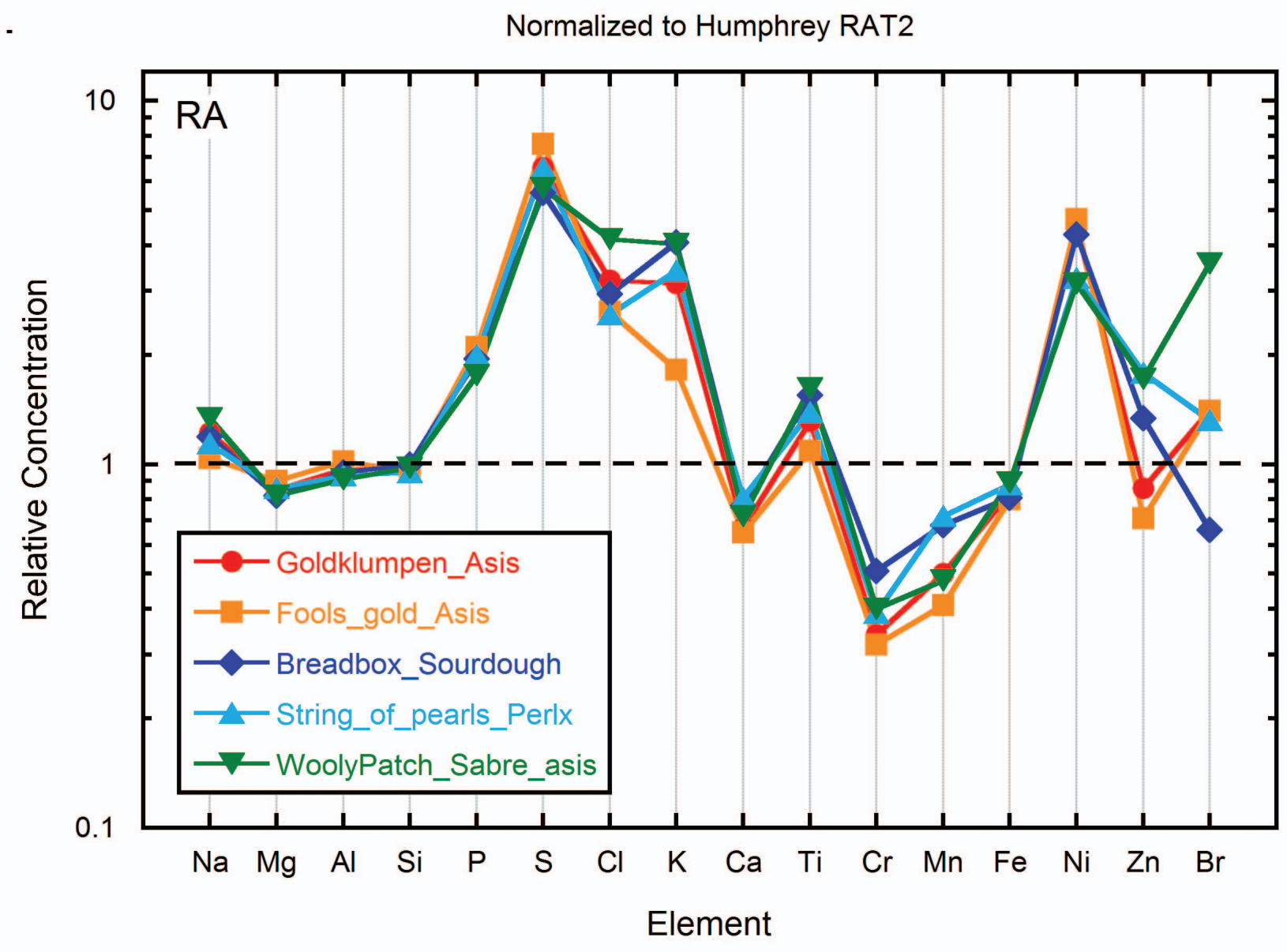
Normalized to Humphrey RAT2
RA
10
1
0.1
Relative Concentration
Goldklumpen_Asis
Fools_gold_Asis
Breadbox_Sourdough
String_of_pearls_Perlx
WoolyPatch_Sabre_asis
Na
Mg
Al
Si
P
S
Cl
K
Ca
Ti
Cr
Mn
Fe
Ni
Zn
Br
Element

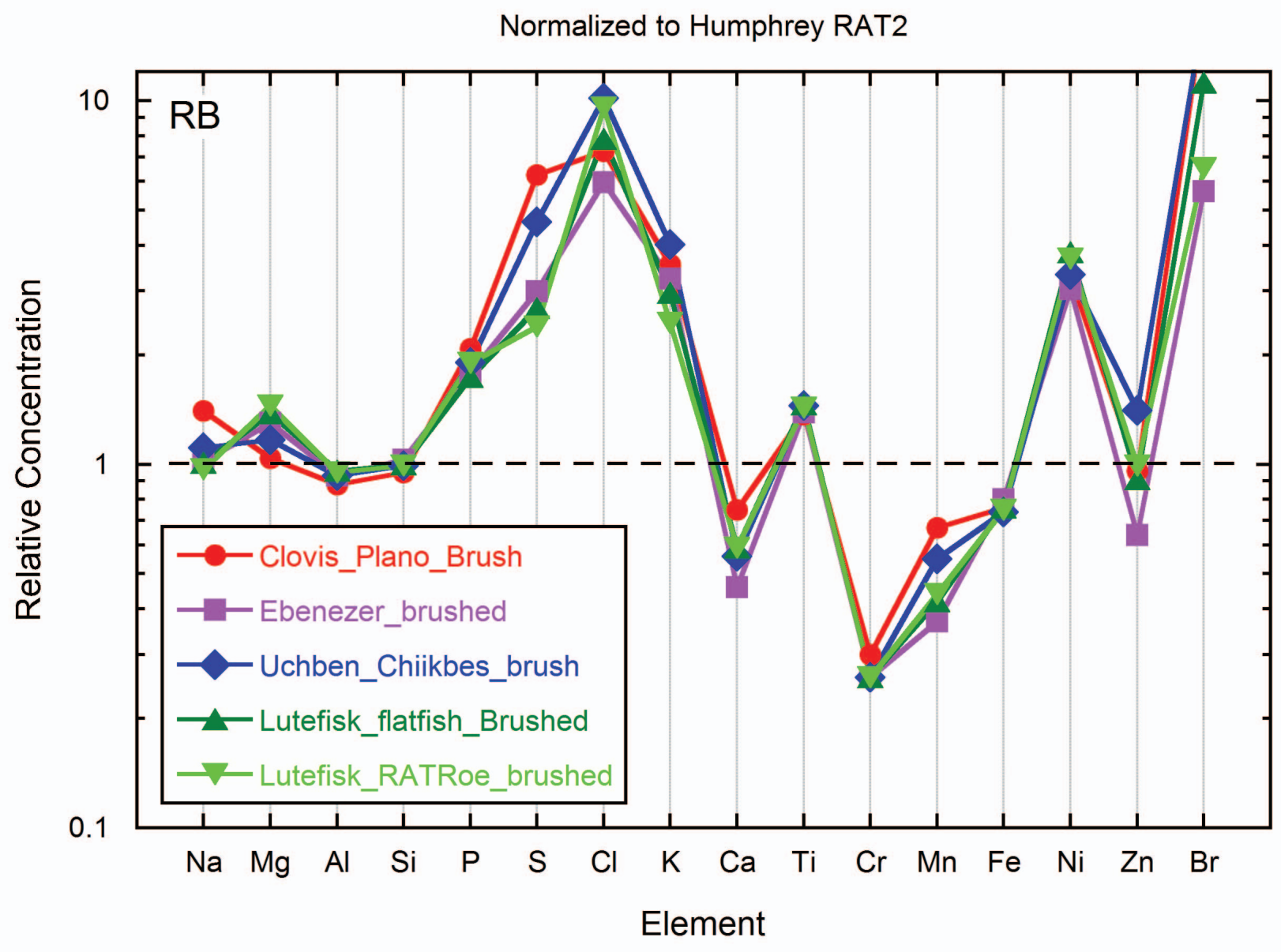
Normalized to Humphrey RAT2
RB
10
1
0.1
Relative Concentration
Clovis_Plano_Brush
Ebenezer_brushed
Uchben_Chiikbes_brush
Lutefisk_flatfish_Brushed
Lutefisk_RATRoe_brushed
Na
Mg
Al
Si
P
S
Cl
K
Ca
Ti
Cr
Mn
Fe
Ni
Zn
Br
Element

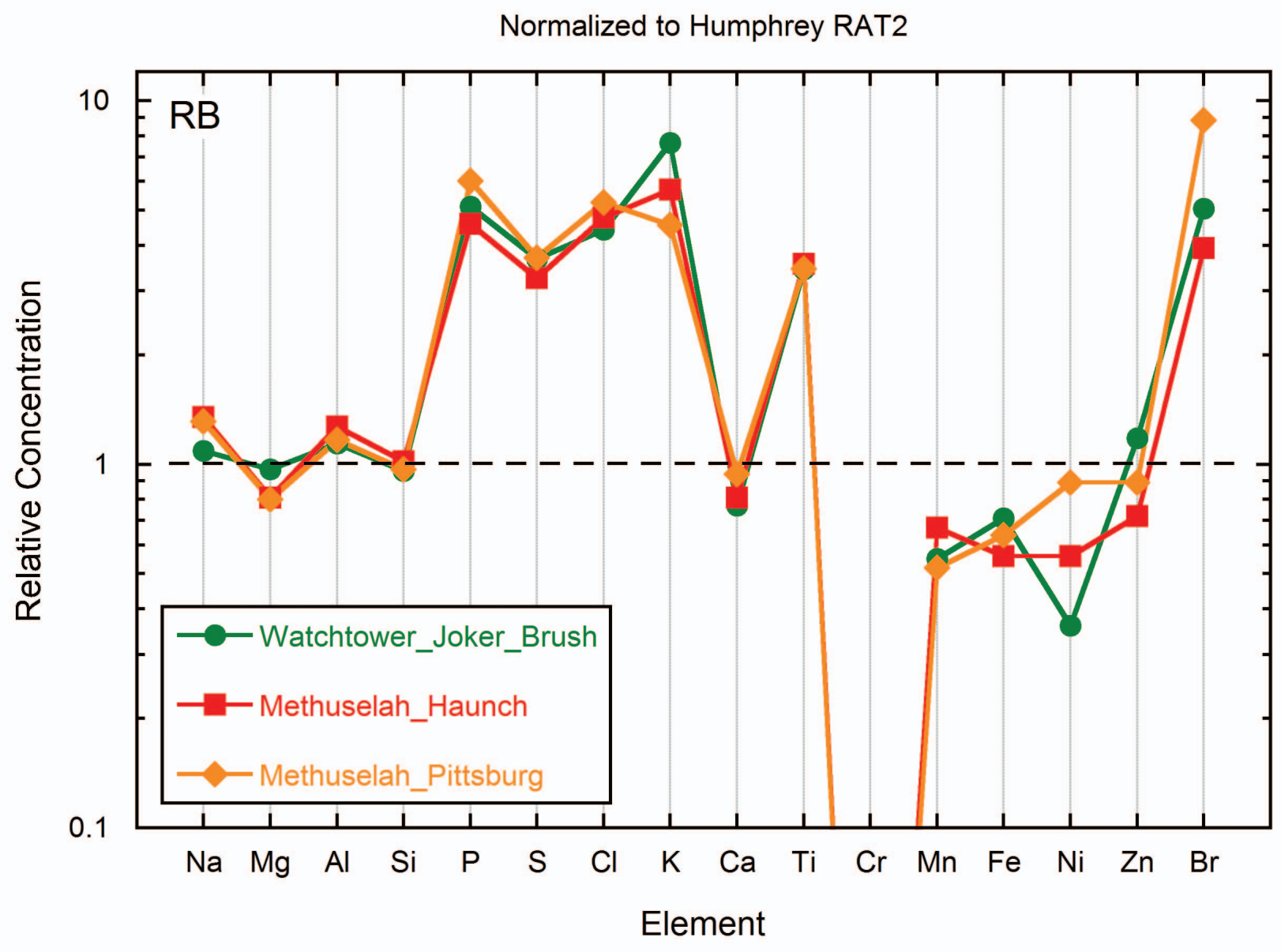
Normalized to Humphrey RAT2
RB
10
1
0.1
Relative Concentration
Watchtower_Joker_Brush
Methuselah_Haunch
Methuselah_Pittsburg
Na
Mg
Al
Si
P
S
Cl
K
Ca
Ti
Cr
Mn
Fe
Ni
Zn
Br
Element

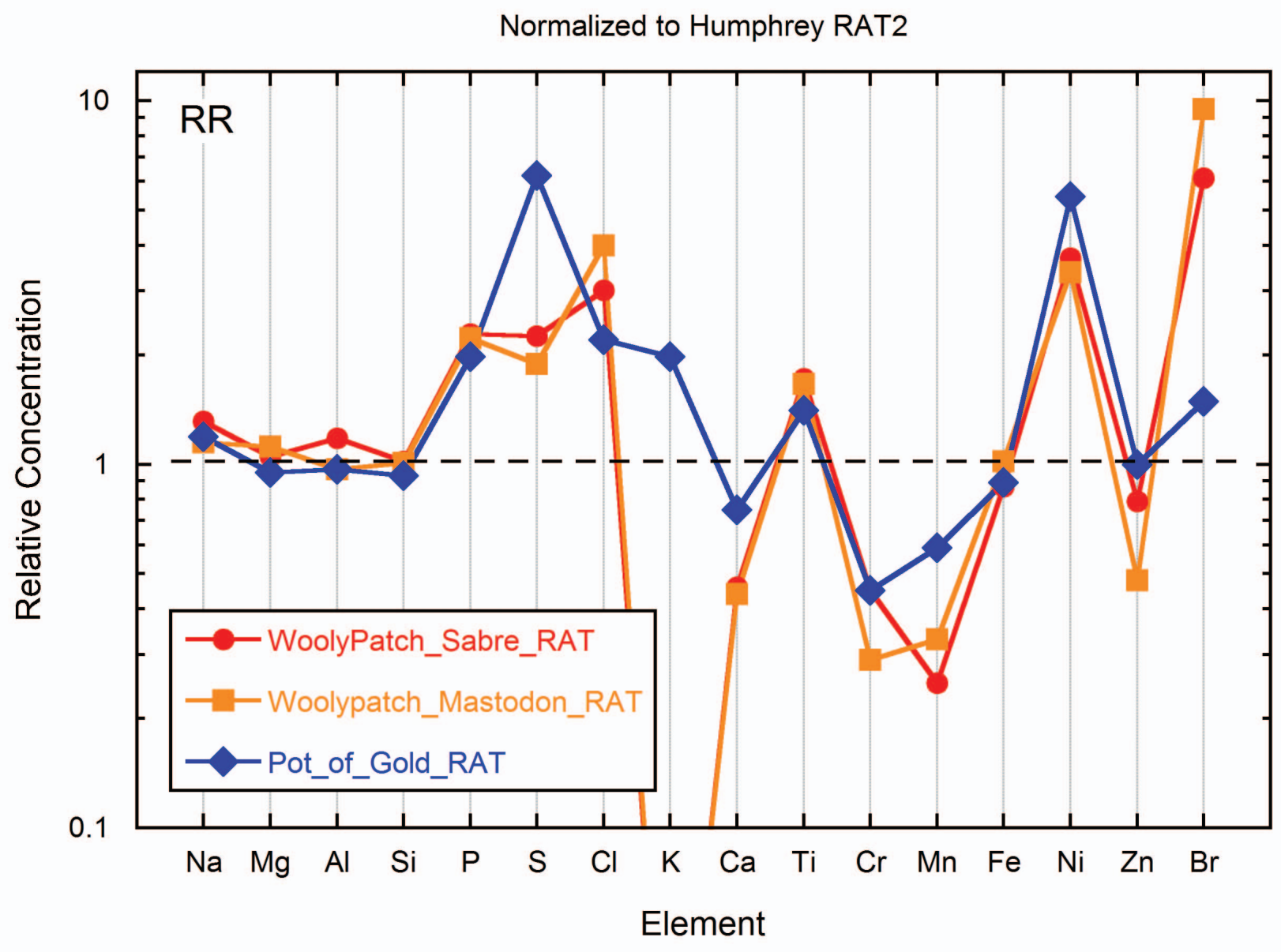
Normalized to Humphrey RAT2
RR
10
1
0.1
Relative Concentration
WoolyPatch_Sabre_RAT
Woolypatch_Mastodon_RAT
Pot_of_Gold_RAT
Na
Mg
Al
Si
P
S
Cl
K
Ca
Ti
Cr
Mn
Fe
Ni
Zn
Br
Element

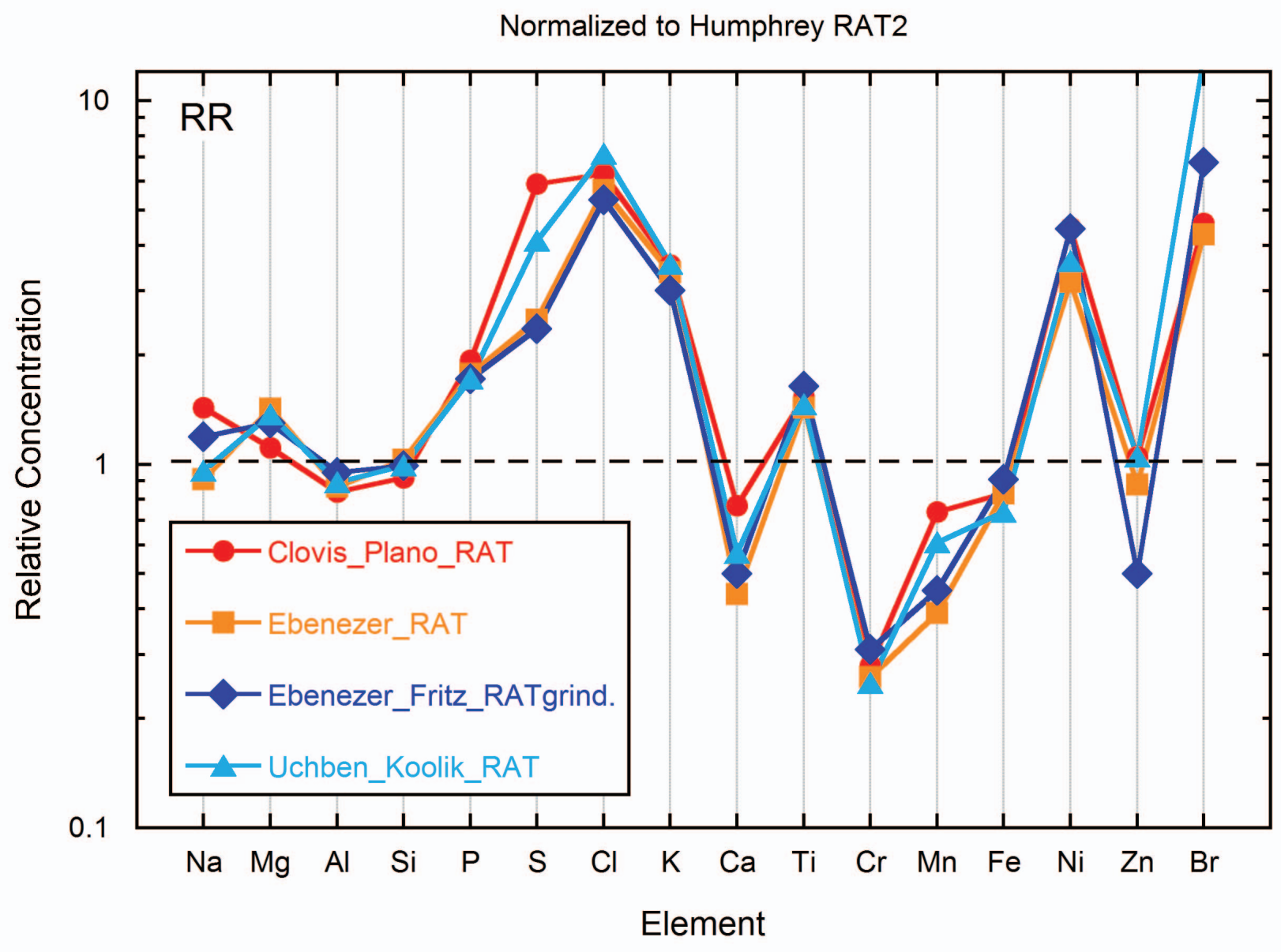
Normalized to Humphrey RAT2
RR
10
1
0.1
Relative Concentration
Clovis_Plano_RAT
Ebenezer_RAT
Ebenezer_Fritz_RATgrind.
Uchben_Koolik_RAT
Na
Mg
Al
Si
P
S
Cl
K
Ca
Ti
Cr
Mn
Fe
Ni
Zn
Br
Element

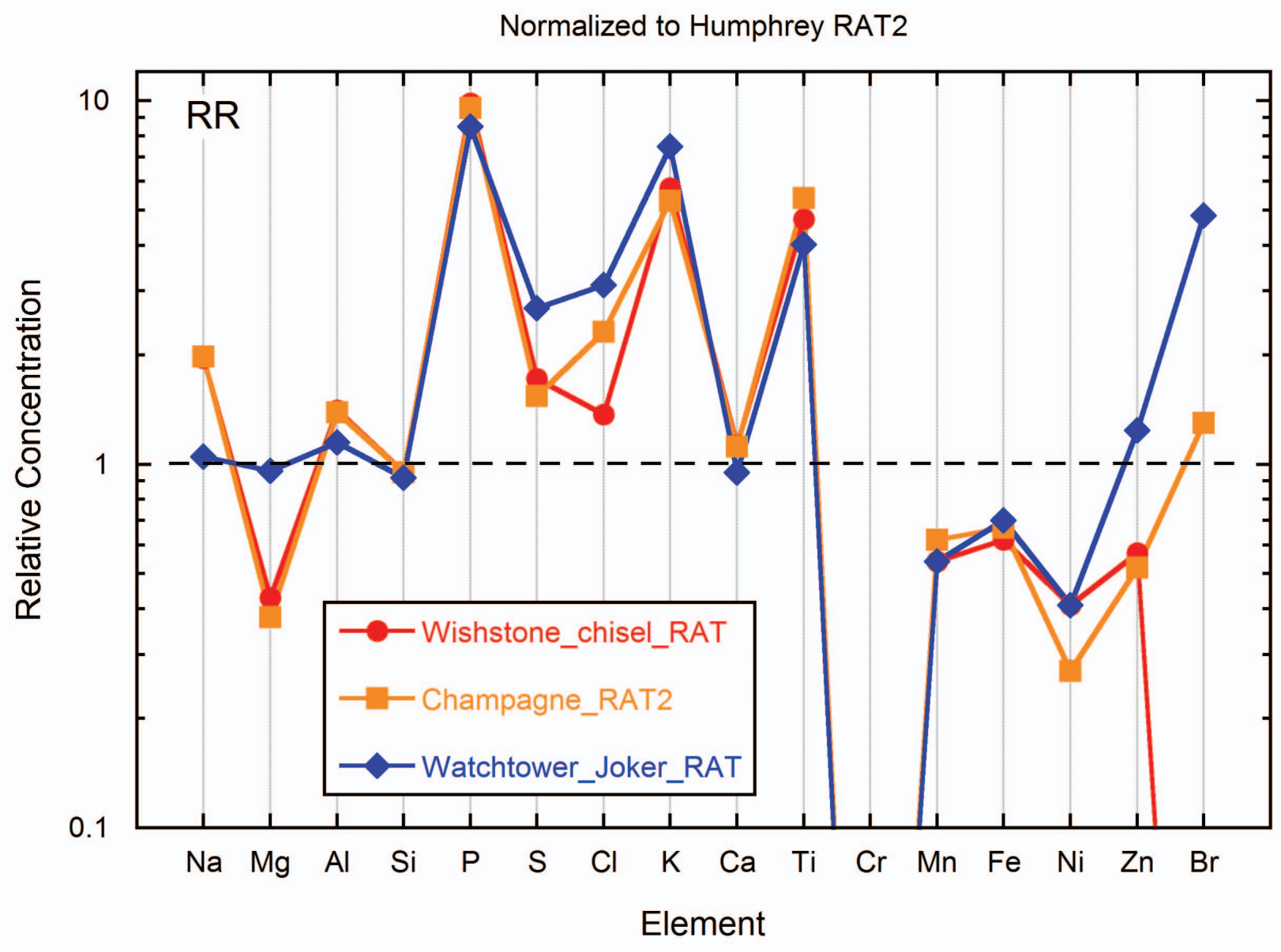
Normalized to Humphrey RAT2
RR
10
1
0.1
Relative Concentration
Wishstone_chisel_RAT
Champagne_RAT2
Watchtower_Joker_RAT
Na
Mg
Al
Si
P
S
Cl
K
Ca
Ti
Cr
Mn
Fe
Ni
Zn
Br
Element

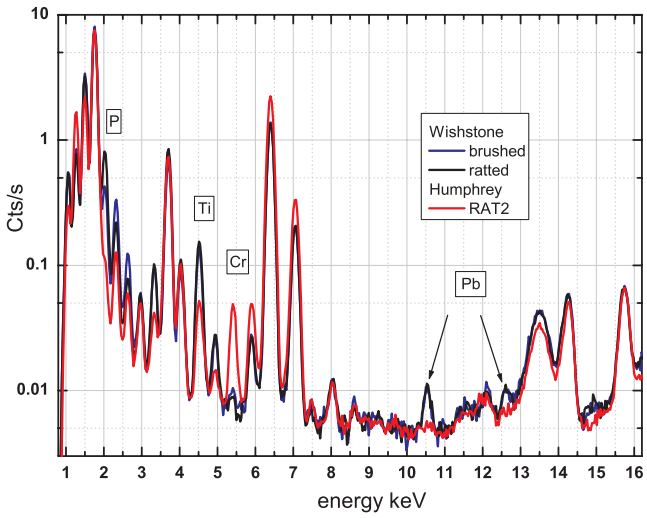
10
1
0.1
0.01
Cts/s
P
Ti
Cr
Pb
Wishstone
brushed
ratted
Humphrey
RAT2
1
2
3
4
5
6
7
8
9
10
11
12
13
14
15
16
energy keV

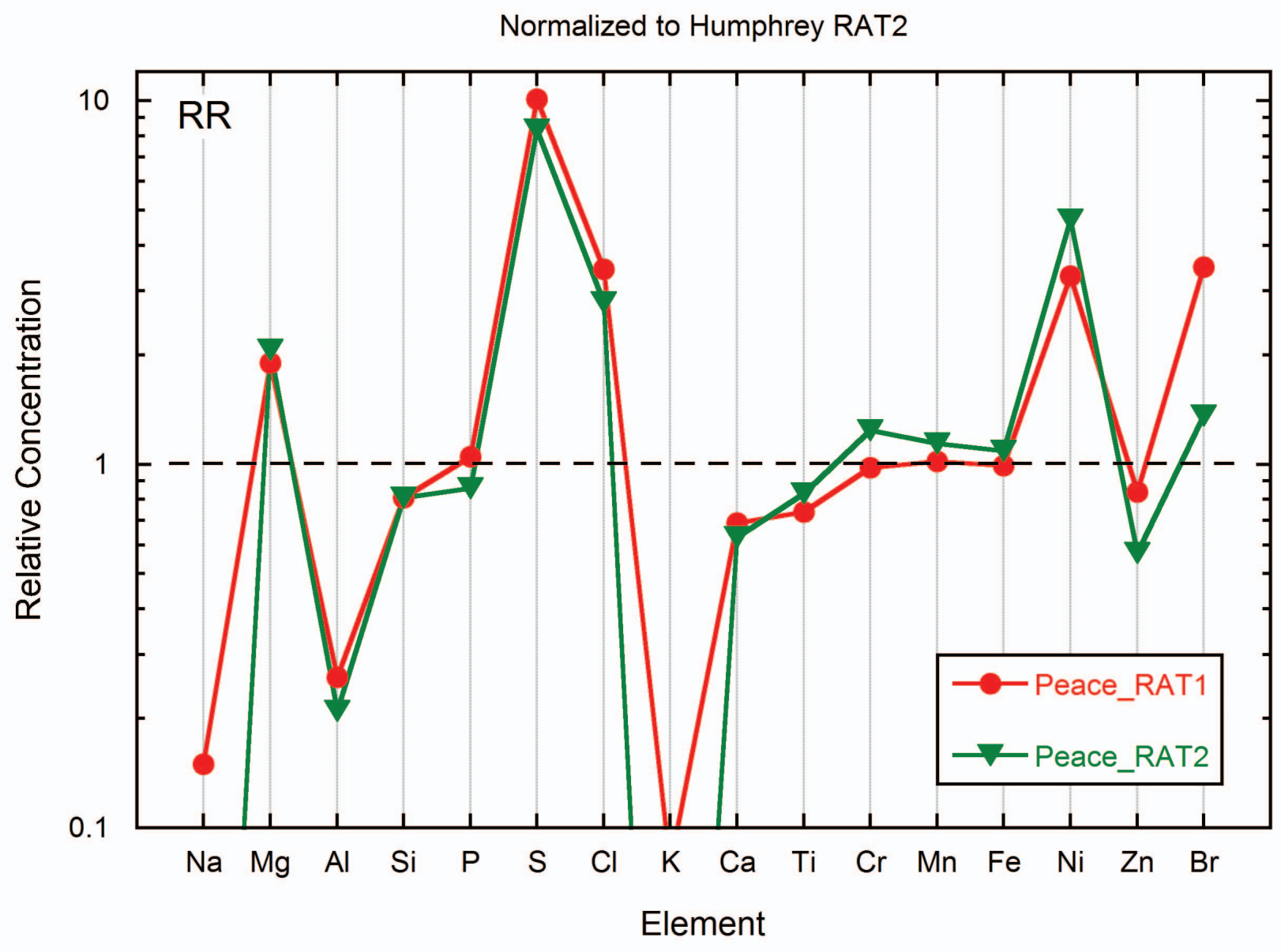
Normalized to Humphrey RAT2
RR
10
1
0.1
Relative Concentration
Na
Mg
Al
Si
P
S
Cl
K
Ca
Ti
Cr
Mn
Fe
Ni
Zn
Br
Element
Peace_RAT1
Peace_RAT2

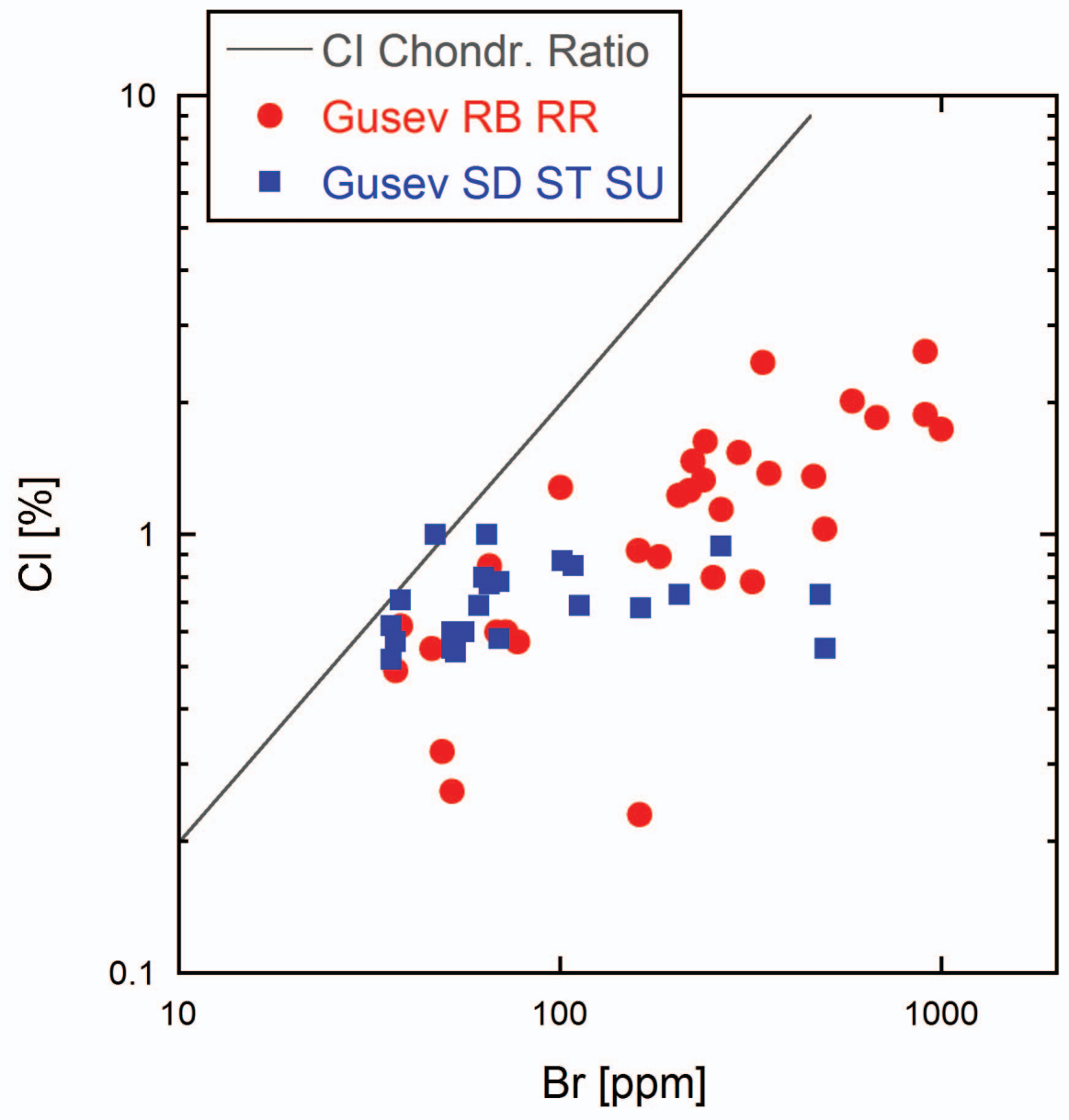
CI Chondr. Ratio
Gusev RB RR
Gusev SD ST SU
10
1
0.1
CI [%]
10
100
1000
Br [ppm]

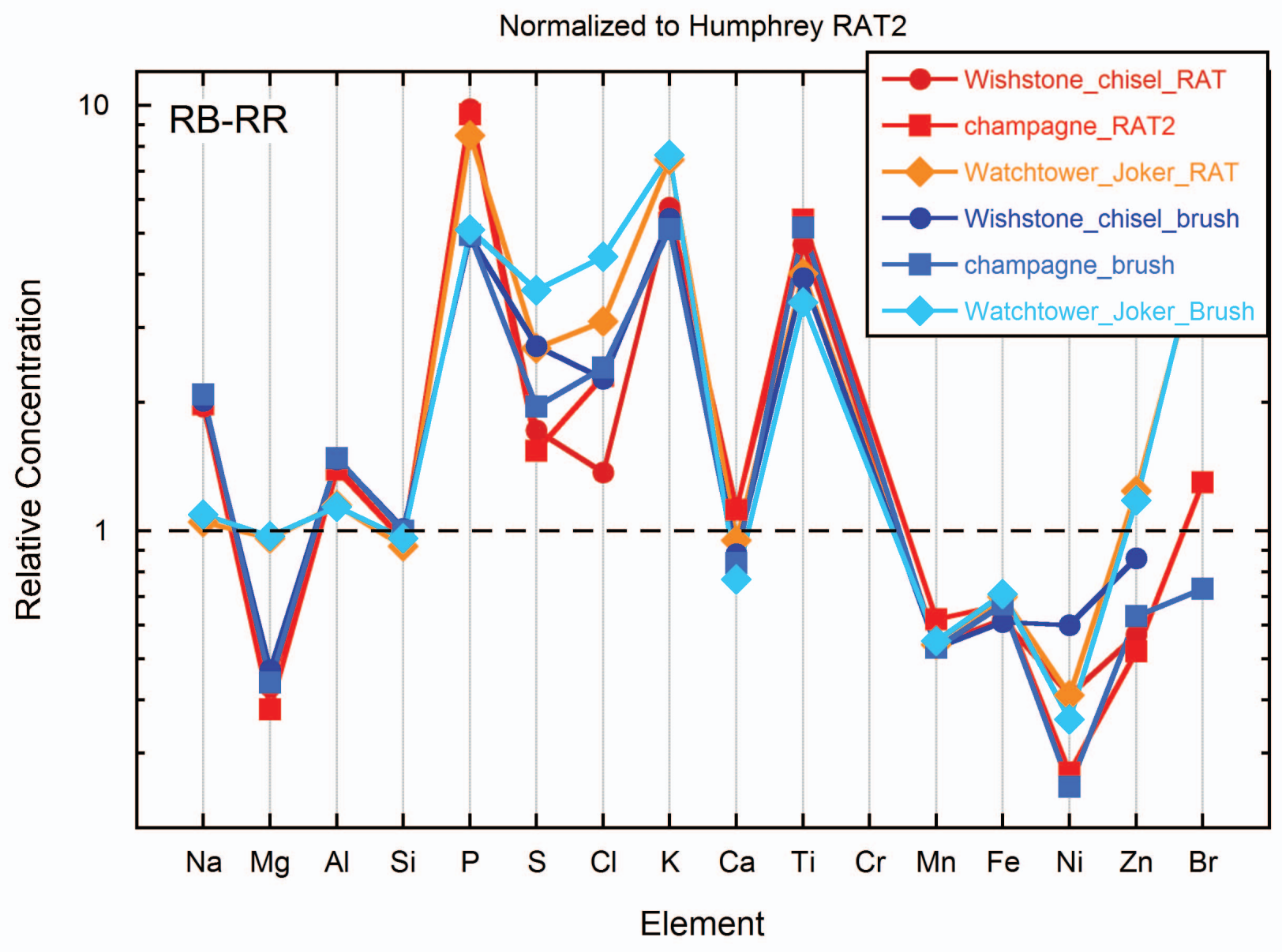
Normalized to Humphrey RAT2
RB-RR
Wishstone_chisel_RAT
champagne_RAT2
Watchtower_Joker_RAT
Wishstone_chisel_brush
champagne_brush
Watchtower_Joker_Brush
Relative Concentration
10
1
Na
Mg
Al
Si
P
S
Cl
K
Ca
Ti
Cr
Mn
Fe
Ni
Zn
Br
Element